



# Photogrammetrie Fernerkundung Geoinformation

Organ der Deutschen Gesellschaft für Photogrammetrie,  
Fernerkundung und Geoinformation (DGPF) e. V.

Jahrgang 2010, Heft 3

Hauptschriftleiter:  
Prof. Dr.-Ing. Helmut Mayer

Schriftleiter:  
Prof. Dr. rer.nat. Carsten Jürgens, Prof. Dipl.-Ing. Thomas P. Kersten,  
Prof. Dr. rer.nat. Lutz Plümer und Dr.-Ing. Eckhardt Seyfert

**Redaktionsbeirat** (Editorial Board): Clement Atzberger, Andrew Frank,  
Christian Heipke, Joachim Hill, Patrick Hostert, Hans-Gerd Maas, Wolfgang  
Reinhardt, Franz Rottensteiner, Jochen Schiewe



E. Schweizerbart'sche Verlagsbuchhandlung  
(Nägele u. Obermiller) Stuttgart 2010



Deutsche Gesellschaft für Photogrammetrie, Fernerkundung  
und Geoinformation (DGPF) e.V.  
Gegründet 1909

---

Die *Deutsche Gesellschaft für Photogrammetrie, Fernerkundung und Geoinformation* (DGPF) e.V. unterstützt als Mitglieds- bzw. Trägergesellschaft die folgenden Dachverbände:



International Society  
for Photogrammetry  
and Remote Sensing

DAGM

Deutsche Arbeits-  
gemeinschaft für  
Mustererkennung e.V.



GeoUnion  
Alfred-Wegener-Stiftung

---

Herausgeber:

© 2010 Deutsche Gesellschaft für Photogrammetrie, Fernerkundung und Geoinformation (DGPF) e.V.  
Präsidentin: Prof. Dr. Cornelia Gläßer, Martin-Luther-Universität Halle-Wittenberg, Institut für Geo-  
wissenschaften, Von-Seckendorff-Platz 4, D-06120 Halle, Tel.: +49(0)345 55-26020  
Geschäftsstelle: Dr. Klaus-Ulrich Komp, c/o EFTAS Fernerkundung Technologietransfer GmbH,  
Oststraße 2–18, D-48145 Münster, e-mail: klaus.komp@eftas.com

Published by:

E. Schweizerbart'sche Verlagsbuchhandlung (Nägele u. Obermiller), Johannesstraße 3A,  
D-70176 Stuttgart. Tel.: 0711 351456-0, Fax: 0711 351456-99, e-mail: mail@schweizerbart.de  
Internet: <http://www.schweizerbart.de>

② Gedruckt auf alterungsbeständigem Papier nach ISO 9706-1994

All rights reserved including translation into foreign languages. This journal or parts thereof may not be reproduced in any form without permission from the publishers.

Die Wiedergabe von Gebrauchsnamen, Handelsnamen, Warenbezeichnungen usw. in dieser Zeitschrift berechtigt auch ohne besondere Kennzeichnung nicht zu der Annahme, dass solche Namen im Sinne der Warenzeichen- und Markenschutz-Gesetzgebung als frei zu betrachten wären und daher von jedermann benutzt werden dürfen.

Verantwortlich für den Inhalt der Beiträge sind die Autoren.

ISSN 1432-8364

Science Citation Index Expanded (also known as SciSearch®) Journal Citation Reports/Science Edition  
Hauptschriftleiter: Prof. Dr.-Ing. Helmut Mayer, Institut für Angewandte Informatik, Universität der  
Bundeswehr München, D-85577 Neubiberg, e-mail: Helmut.Mayer@unibw.de  
Schriftleiter: Prof. Dr. rer.nat. Carsten Jürgens, Ruhr-Universität Bochum, Geographisches Institut,  
Gebäude NA 7/133, D-44780 Bochum, e-mail: carsten.juergens@rub.de, Prof. Dipl.-Ing. Thomas  
P. Kersten, HafenCity Universität Hamburg, Department Geomatik, Hebebrandstr.1, D-22297 Ham-  
burg, e-mail: thomas.kersten@hcu-hamburg.de, Prof. Dr. rer.nat. Lutz Plümér, Universität Bonn,  
Institut für Geodäsie und Geoinformation, Meckenheimer Allee 172, D-53115 Bonn, e-mail:  
Lutz.Pluemler@ikg.uni-bonn.de und Dr.-Ing. Eckhardt Seyfert, Landesvermessung und Geobasis-  
information Brandenburg, Heinrich-Mann-Allee 107, D-14473 Potsdam, e-mail: eckhardt.seyfert@geo-  
basis-bb.de

Erscheinungsweise: 6 Hefte pro Jahrgang.

Bezugspreis im Abonnement: € 191,- pro Jahrgang. Mitglieder der DGPF erhalten die Zeitschrift kosten-  
los. Der Online-Zugang ist im regulären Subskriptionspreis enthalten.

Anzeigenverwaltung: E. Schweizerbart'sche Verlagsbuchhandlung (Nägele u. Obermiller), Johannes-  
straße 3A, D-70176 Stuttgart, Tel.: 0711 351456-0; Fax: 0711 351456-99.

e-mail: mail@schweizerbart.de, Internet: <http://www.schweizerbart.de>

Bernhard Harzer Verlag GmbH, Westmarkstraße 59/59a, D-76227 Karlsruhe, Tel.: 0721 944020, Fax:  
0721 9440230, e-mail: Info@harzer.de, Internet: [www.harzer.de](http://www.harzer.de)

Printed in Germany by Tutte Druckerei GmbH, D-94121 Salzwedel bei Passau

## **PFG – Jahrgang 2010, Heft 3**

### **Inhaltsverzeichnis**

---

#### **Originalbeiträge**

KOPPE, W., LI, F., GNYP, M.L., MIAO, Y., JIA, L., CHEN, X., ZHANG, F. & BARETH, G.: Evaluating Multispectral and Hyperspectral Satellite Remote Sensing Data for Estimating Winter Wheat Growth Parameters at Regional Scale in the North China Plain .....	167
OSKOUEI, M.M.: Independent Component Analysis of Hyperion Data to Map Alteration Zones .....	179
GRÖGER, G. & PLÜMER, L.: Derivation of 3D Indoor Models by Grammars for Route Planning .....	191

---

#### **Berichte und Mitteilungen**

##### **Berichte von Veranstaltungen**

3D – State of the Art: Workshop 3D-Stadtmodelle vom 9.–10. November 2009 in Bonn .....	207
9. Oldenburger 3D-Tage über Optische 3D-Messtechnik – Photogrammetrie – Laserscanning vom 3.–4. Februar 2010 .....	208

##### **Hochschulnachrichten**

Technische Universität Dresden: Habilitation THOMAS LUHMANN .....	213
Westfälische Wilhelms-Universität Münster: Promotion KARL-PETER KRÜGER .....	215

##### **Buchbesprechung**

HOBBIE, D. (Die Entwicklung photogrammetrischer Verfahren und Instrumente bei Carl Zeiss in Oberkochen) .....	216
--	-----

Veranstaltungskalender .....	217
Neuerscheinungen .....	219
Zum Titelbild .....	219
Korporative Mitglieder .....	220

Zusammenfassungen der „Originalbeiträge“ und der Beiträge „Aus Wissenschaft und Technik“ (deutsch und englisch) sind auch verfügbar unter [www.dgpf.de/neu/pfg/ausgaben.htm](http://www.dgpf.de/neu/pfg/ausgaben.htm)





## Evaluating Multispectral and Hyperspectral Satellite Remote Sensing Data for Estimating Winter Wheat Growth Parameters at Regional Scale in the North China Plain

WOLFGANG KOPPE, Köln, FEI LI, Beijing, China, MARTIN L. GNYP, Köln, YUXIN MIAO, Beijing, China, LIANGLIANG JIA, Shijiazhuang, China, XINPING CHEN, FUSUO ZHANG, Beijing, China & GEORG BARETH, Köln

**Keywords:** Hyperion, ALI, vegetation indices, winter wheat, biomass, nitrogen concentration, imaging spectrometry, hyperspectral, multispectral

**Summary:** Timely monitoring of crop growth status at large scale is crucial for improving regional crop management decisions. The main objective of the recent study is a model development to predict and estimate crop parameters, here biomass, plant N concentration and plant height, based on multi- and hyperspectral satellite data. In this contribution, the focus is on relating orbital multispectral (EO-1 ALI) and hyperspectral (EO-1 Hyperion) measurements to winter wheat parameters for regional level applications. The study was conducted in Huimin County, Shandong Province of China in the growing season of 2005/2006 involving three big winter wheat fields managed by different farmers. Winter wheat growth parameters including aboveground biomass, plant N concentration and plant height were collected at different growth stages. Three different predicting models were investigated: traditional vegetation indices calculated from broad and narrow bands, and Normalized Ratio Indices (NRI) calculated from all possible two-band combinations of Hyperion between 400 and 2,500 nm. The results indicated that TVI performed best among the tested vegetation indices using either broad ( $R^2=0.69, 0.32$  and  $0.64$  for biomass, N concentration and plant height, respectively) or narrow ( $R^2=0.71, 0.33$  and  $0.65$  for biomass, N concentration and plant height, respectively) bands. The best performing Normalized Ratio Index (NRI) selected through band combination analysis were significantly better than TVI, achieving  $R^2$  of  $0.83, 0.81$  and  $0.79$  for biomass, plant N concentration and plant height, respectively. The different NRI models use wavebands from the near infrared (NIR) (centered at 874, 732, and 763 nm) and short wave infrared (SWIR) (centered at 1,225 and 1,305 nm) spectrum with varying bandwidth be-

**Zusammenfassung:** Anwendung Multispektraler- und Hyperspektraler Fernerkundung zur Ableitung von Bestandsparametern des Winterweizens in der Nordchinesischen Tiefebene. Methoden und Techniken der Fernerkundung fungieren als ein wichtiges Hilfsmittel im regionalen Umweltmanagement. Ziel der vorliegenden Studie liegt dabei auf der Modelleentwicklung zur Ableitung von Pflanzenparametern für Winterweizen aus multispektralen (EO-1 ALI) und hyperspektralen (EO-1 Hyperion) Bestandsmessungen. Hierfür wurde ein Feldversuch in der Nordchinesischen Tiefebene durchgeführt, wobei Pflanzenparameter zu verschiedenen Wachstumsstadien aufgenommen wurden. Um die aufgenommenen Parameter mit den Fernerkundungsdaten in Beziehung zu setzen, wurden drei verschiedene Modelvarianten untersucht: traditionelle Vegetationsindizes berechnet aus Multispektraldaten, traditionelle Vegetationsindizes berechnet aus Hyperspektraldaten sowie die Berechnung von Normalized Ratio Indices (NRI) basierend auf allen möglichen 2-Band Kombinationen im Spektralbereich zwischen 400 und 2.500 nm.

Für traditionelle Vegetationsindizes (SR, NDVI und SAVI), berechnet aus Multispektral- sowie aus Hyperspektraldaten, wurden geringe statistische Beziehungen zu Pflanzenparametern erzielt. Neben den Standardspektralbereichen (grün, rot, nahes Infrarot) bietet die hohe spektrale Auflösung des Hyperion Sensors jedoch die Möglichkeit, weitere Spektralbereiche mit Pflanzenparametern in Beziehung zu setzen. Aus der Untersuchung aller möglicher 2-Band Kombinationen konnten starke Korrelationen zwischen Pflanzenparametern und Fernerkundungsdaten bei der Kombination von Bändern aus dem nahen Infrarot (NIR) mit Bändern aus dem kurwelligen Infrarot (SWIR) festgestellt werden.

tween 10 and 190 nm. The result of this study suggest that vegetation indices derived from NIR- and SWIR-Hyperion spectrum are better predictors of plant aboveground biomass, nitrogen concentration and plant height than indices derived from only visible spectrum. More studies are needed to further evaluate the results using data from more diverse conditions.

Für die Pflanzenparameter Biomasse, Pflanzestickstoffgehalt und Pflanzenhöhe wurden Korrelationen ( $R^2$ ) von 0,83, 0,81 und 0,79 erzielt. Das Ergebnis der Studie zeigt, dass sich Anwendungsoptimierte Vegetationsindices, berechnet aus schmalen hyperspektralen Bändern des RE, NIR und SWIR, zur Ableitung von Pflanzenparametern eignen und gegenüber Standard Vegetationsindices deutlich bessere Ergebnisse liefern können.

## 1 Introduction

Timely monitoring of crop growth status is important for dynamic in-season site specific crop management, detection of plant vitality, assessment of seasonal production as well as environmental pollution control and yield prediction (MIAO et al. 2009, LAUDIEN & BARETH 2006, ZHAO et al. 2004, HANSEN & SCHJOERING 2003). Traditional techniques for the measurement of accurate crop parameters such as plant aboveground biomass and nitrogen concentration are destructive, extremely cost and labour intensive and not able to provide spatial distributed data on regional level (LU 2006). The estimation of these parameters can be done more efficiently by non-destructive spectral reflectance observations (DAUGHTRY et al. 2000), obtained from field-, airborne- or satellite based sensors. For the linkage of crop parameters with spectral reflectance measurements, a wide range of vegetation indices were developed (ZHAO et al. 2004, HABOUDANE et al. 2004, BROGE & MORTENSEN 2002). Vegetation indices obtained from spectral reflectance measurements are designed to enhance the vegetation cover signal while minimizing the response of various background materials (SCHOWENGERDT 2007). They are mainly based on the difference between low reflection due to strong absorptions by foliar pigments in the red spectrum and high reflection of structural components (cell walls) in the near infrared spectrum (KUMAR et al. 2003, LILLESAND et al. 2004). In the past decades, many attempts have been made to estimate crop parameters at regional level, either directly from remote sensing data or by assimilating remote sensing data into crop models (SCHNEIDER 2003). A lot of earth observation satellites carrying multi-

spectral imaging sensors are available (WOOSTER 2007), providing data that can be used for the calculation of broad band vegetation indices (LU 2006). Vegetation indices calculated from the visible and near infrared bands of multispectral scanners have been used to estimate crop parameters such as standing biomass and grain yield (TUCKER 1979, THENKABAIL et al. 1995, SINGH et al. 2002, DORALSWAMY et al. 2003), leaf area index (LAI) (CLOUTIS et al. 1999) and plant nitrogen content (REYNIERS & VRINDTS 2004). At higher vegetation densities, standard broadband vegetation indices, such as Simple Ratio (SR) or Normalized Difference Vegetation Index (NDVI) are generally less accurate (JONGSCHAAP & SCHOUTEN 2005) and tend to saturate (HABOUDANE et al. 2004, MUTANGA & SKIDMORE 2004), which results in a limited prediction value of crop parameters when LAI exceeds two (HABOUDANE et al. 2004). Improvements could be achieved by using hyperspectral radiometers, which can acquire a continuous electromagnetic spectrum for each pixel between 350 and 2,500 nm (HANSEN & SCHJOERING 2003). The sensitivity of hyperspectral vegetation indices for estimation of crop parameters has already been demonstrated with significant improvements compared to broad bands by several authors during the past several decades (SINCLAIR 1971, FILLELA et al. 1995, STRACHAN et al. 2002). Beyond narrow band standard vegetation indices, imaging spectroscopy provides the opportunity of using more adequate wavebands or waveband combinations to estimate biophysical parameters (CECCATO et al. 2002). According to this, different approaches for index calculation based on all waveband combinations were developed and successfully used for estimation of wheat grain yield (XAVIER et al.

2006), wheat biomass and Nitrogen content (HANSEN & SCHIOERING 2003, THENKABAIL et al. 2000) as well as land cover classification (THENKABAIL et al. 2004). Also, FERWERDA et al. (2005) used waveband selection method successfully for the estimation of leaf nitrogen content across different species. MUTANGA & SKIDMORE (2004) reported that waveband combinations different from the standard NDVI could overcome saturation effects of biomass estimation at full canopy cover.

A lot of studies have been conducted on improving the performance of hyperspectral vegetation indices both on excised leafs and in situ measurements, but there are only a few studies dealing with hyperspectral imaging on regional level (e.g. SMITH et al. 2003, GALVAÑ et al. 2005, DATT et al. 2003). By using high spectral resolution space born radiometers (e.g. Hyperion sensor on Earth Observation-1 satellite), detailed variation in the electromagnetic spectrum between 400 and 2,500 nm can be measured over a wide area (BROGE & LEBLANC 2000), making this approach more efficient for large scale precision crop management.

The objective of this study was to analyse, compare and evaluate satellite based multispectral and hyperspectral images in terms of broad band and narrow band vegetation indices for the estimation of winter wheat above-ground biomass, plant N concentration and plant height. For this research interest, the optical sensors Hyperion and ALI, mounted on Earth Observation-1 satellite were selected, because they can provide multispectral and hyperspectral data simultaneously. Three different types of vegetation indices were calculated to estimate crop parameters: (1) standard broad band vegetation indices derived from multispectral sensor ALI; (2) standard narrow band vegetation indices derived from Hyperion; and, (3) systematic identification of best waveband combinations in the Hyperion reflectance spectrum from 400 to 2,500 nm using Normalized Ratio Indices (NRI) following (THENKABAIL et al. 2000) and (SIMS & GAMON 2002).

## 2 Material and Methods

### Study Area

The research was accomplished in the North China Plain during the winter wheat growing season of 2006. The test fields were located in Huimin County ( $37.3^{\circ}$  latitude,  $117.4^{\circ}$  longitude), Shandong Province. This area is characterized by a continental climate with precipitation maxima between June and September, typical for the warm-temperature subhumid continental monsoon climate. The average temperature is  $12.3^{\circ}\text{C}$  and annual average precipitation sums up to 580 mm. The dominant crop rotation, up to 66 % of the cultivated area, is winter wheat followed by maize enabling two harvests per year. Huimin County was chosen because of the existence of long term field experiments managed by the Dept. of Plant Nutrition (CAU) and availability of collecting ground truth data from selected fields. Three big fields, each of which is about 5 ha and managed by different farmers, were selected for collecting ground truth information. The fields are located in the villages of Xili, Xujia, and Shizhang in Huimin County. Winter wheat in the three villages was sowed from September 17th to October 26th, 2005 and harvested in the beginning of June, 2006. All the fields were managed by the farmers according to their common practices.

### Hyperion and ALI Image Data

Three Hyperion and ALI images were acquired on April 19, May 6 and May 31, 2006. The optical sensors Hyperion and ALI are mounted on the Earth Observing One (EO-1) Satellite that follows the World Reference System-2 (WRS-2) with a 16 day repeat cycle for nadir mode. Both sensors are push broom imaging spectrometers that are capable of cross-track pointing (Earth Observation-1, 2003). The multispectral Advanced Land Imager (ALI) acquires information in nine discrete bands with a spatial resolution of 30 m. An additional panchromatic channel has a resolution of 10 m. The Hyperion hyperspectral sensor collects continuous data with a VNIR and a SWIR spectrometer in the 400–2,400 nm wavelength domain. Each frame taken captures images in a 7.7 km wide and 42 km (resp.

185 km) long area (UNGAR et al. 2003). Similar to the multispectral ALI, Hyperion provides also a spatial resolution of 30 m. EO-1 Hyperion images are radiometric calibrated (Level 1R) and delivered in 16-bit radiance data (PEARLMAN et al. 2003).

### Groundtruth Measurements

Winter wheat canopy spectral reflectance was measured in the field using an ASD FieldSpec® HandHeld Pro optical sensor (Analytical Spectral Devices, Inc., Boulder, CO, USA; [www.asdi.com](http://www.asdi.com)) between 10 am to 2 pm under cloudless conditions. The HandHeld Pro device measures the visible (VIS) and near infrared (NIR) spectrum with 512 channels in the 325–1,075 nm wavelength domain. In the context of this research, the in-Situ spectral measurements were only used for calibrating orbital reflectance data. After field canopy spectral data collection, crop samples were collected for aboveground biomass and plant nitrogen concentration determination on four dates: April 19, April 28, May 12 and May 30, with the corresponding growth stages from shooting to ripening stage. The measurements on April 19 and May 30 matched EO-1 satellite image collection very well; however, no ground measurements could match the EO-1 data acquisition on May 6. Therefore, agronomic measurements on April 28 and May 12 had to be interpolated to coincide with EO-1 acquisition on May 6. Above-

ground biomass was destructively collected by cutting the vegetation on ground level within an area of 100 cm by 30 cm. Then the samples were dried at 70 °C to constant weight. Plant nitrogen concentration was then determined by the Kjeldahl digestion method (Bremner 1960). Around 39 to 45 measurements per field were sampled.

### Satellite Image Pre-processing

Satellite image pre-processing of Hyperion and ALI data included (a) a correction for sensor artifacts, (b) an atmospheric correction as well as (c) a geometric correction. The performed pre-processing steps (LILLESAND et al. 2004, KHURSHID et al. 2006) were aimed to improve the quality of the images for multitemporal data analysis. For correction of sensor artifacts, uncalibrated and corrupted Hyperion bands were eliminated by applying the Flag-Mask that was delivered with the data product. A Flag-Mask indicates detectors which are unresponsive and unreliable (USGS 2007). 158 of the original 242 bands had remained for subsequent desriping (described in DATT et al. 2003). During the desriping process periodic along track stripes in image data, caused by detector errors were removed. Since some of the bands were not repairable, another 17 bands had to be excluded. The desriping and exclusion of image channels was performed with ENVI software (ITT Visual Information Solutions).

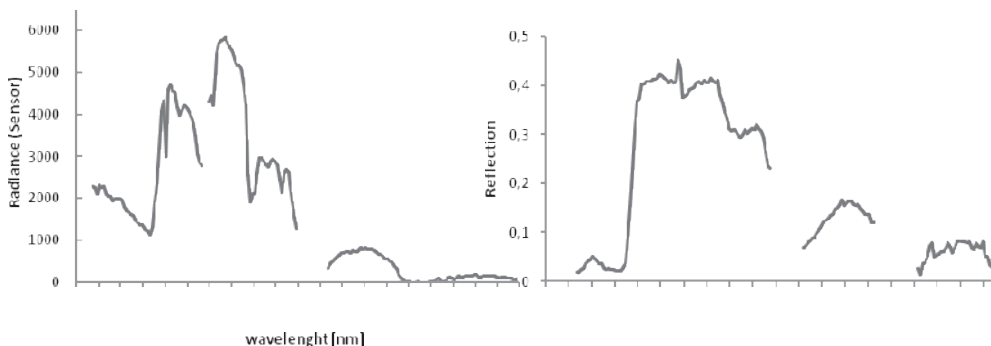


**Fig. 1:** Comparison of single pixel spectra before (a) and after (b) atmospheric correction. Spectra were acquired on April 19, 2006.

For some application using single satellite observations, it is of no importance to atmospherically correct image data (SCHOWENGERDT 2007). However, in the present work, the focus was set on multi-temporal analysis as well as on matching image data to canopy spectral reflectance that was measured using a portable spectroradiometer (Fieldspec® Pro by ASD). The measured at-sensor radiance L of Hyperion and ALI data consists of reflectance from the surface and scattering from the atmosphere. Major sources of distortions of remotely sensed imagery are water vapor and aerosols (CAIRNS et al. 2003). To convert the Hyperion and ALI at-sensor radiance data to surface reflectance data, the MODTRAN-based radiative transfer algorithm implemented in the FLAASH module of ENVI software was used. The radiative transfer algorithm that applies for Lambertian materials, converts the at-sensor radiance L to surface reflectance  $\rho$  on a pixel-by-pixel basis as

$$\rho = \frac{L - L_a}{(L - L_a)S + T_2 \frac{E_s * \cos(\theta_s)}{\pi}} \quad (1)$$

where  $L_a$  is the radiance caused by atmospheric scattering;  $T_2$  is the two-way transmittance; S is the albedo of the atmosphere;  $\theta_s$  is the solar zenith angle and  $E_s$  is the exoatmospheric solar irradiance. The radiative transfer algorithm is described in (BERK et al. 2000).

According to equation (1), atmospheric scattering effects were compensated and a surface reflectance spectrum for each pixel was retrieved. The comparison of single pixel at sensor radiance and surface reflectance from fully developed winter wheat is shown in Fig. 1.

The last step of the Hyperion and ALI pre-processing chain is the geometric correction, which was undertaken to rectify geometric distortions using ground control points (GCPs), sensor parameters and a digital elevation model. For orthorectification process of each scene, 25 GCPs distributed across the area of interest were selected and the image rectification was carried out by bilinear resampling method using ENVI. For evaluation purpose, other 20 independent check points were used, which resulted in overall RMSE of around 0.5 pixels (15 m) for each image.

### Vegetation Index Calculation and Model Development for Crop Parameter Estimation

In this study, the reflectance spectra from multi-temporal Hyperion and ALI data were extracted on a pixel basis (cell size 30 m) on the farmers' fields in the three villages. Pixel based reflectance spectra were then used for the calculation of (1) standard broad band vegetation indices, (2) standard hyperspectral vegetation indices, and (3) narrow band Normalized Ratio Indices (NRI; SCHMIDT & SKIDMORE 2003, SIMS & GAMON 2002). To compare the prediction power of broad band and narrow band crop parameter estimations, the following vegetation indices were calculated: Simple Ratio (SR), Normalized Difference Vegetation Index (NDVI), Soil Adjusted Vegetation Index (SAVI) and Triangular Vegetation Index (TVI). The SR, NDVI and SAVI vegetation indices are based on the difference between strong absorption of solar radiation in the red, caused by chlorophyll pigments and the high leaf cellular reflection in the near infrared. Unlike the Simple Ratio Index, the NDVI is normalized which reduces the effects of variable illuminations and limits the NDVI to values from -1 to 1 (BARET & GYOT 1991). The SAVI is intended to minimize influences due to soil optical properties. The included background factor L depends on vegetation density and requires information about the relationship between soil background and vegetation (HUETE 1988). The TVI was developed by (BROGE & LEBLANC 2000) and is defined additional to red and near infrared reflectance by the magnitude in the green region. The detailed expressions and the notable references of the mentioned Vegetation Indices are provided in Tab. 1.

In addition to standard vegetation indices, a specific waveband selection method suggested by (THENKABAIL et al. 2000) and (SIMS & GAMON 2002) was used to determine best band combinations suitable for crop parameter estimation (see also SCHMIDT & SKIDMORE 2003). The two-band Normalized Ration Index (NRI) is defined as (SIMS & GAMON 2002):

**Tab. 1:** Standard vegetation indices evaluated in this study.

Index	Name	Formula	References
SR	Simple Ratio	$SR = \rho_{NIR} / \rho_R$	(BARET & GUYOT 1991)
NDVI	Normalized Difference Vegetation Index	$NDVI = (\rho_{NIR} - \rho_R) / (\rho_{NIR} + \rho_R)$	(ROUSE et al. 1974)
SAVI	Soil adjusted Vegetation Index	$SAVI = (1 + L)(\rho_{NIR} - \rho_R) / (\rho_{NIR} + \rho_R + L)$	(HUETE 1988)
TVI	Triangular Vegetation Index	$TVI = 0.5 * (120 * (\rho_{NIR} - \rho_{Green}) - 200(\rho_{NIR} - \rho_{Green}))$	(BROGE & LEBLANC 2000)

$$NRI_{(band1, band2)} = \frac{(\rho_{band1} - \rho_{band2})}{(\rho_{band1} + \rho_{band2})} \quad (2)$$

band1  $\geq$  band 2

where  $\rho_{band1}$  and  $\rho_{band2}$  are reflectance of Hyperion narrow bands in the wavelength range between 400 and 2,500 nm. The hyperspectral Hyperion Sensor allows the calculation of a total number of 9,870 ( $141*140/2$ ) possible two-band combinations for each agronomic parameter. A linear regression between each vegetation index and crop parameter was performed.

### 3 Results

#### Variation of Crop Parameters

Due to different farmers' management practices, the investigated fields were different in terms of seeding time, plant density, and nitrogen application rates. As expected, the differences in management practices resulted in a wide range of variation in crop parameters (aboveground biomass, plant nitrogen concentration and plant height). Within-field variation of plant height and aboveground biomass at shooting stage (heading stage) ranged from 31.3 to 51 cm (70.3 to 90 cm), and from 0.28 to 0.79 kg/m<sup>2</sup> (0.72 to 1.55 kg/m<sup>2</sup>), respectively. Plant nitrogen concentration varied from 17.1 to 37.42 g/kg at shooting stage and from 13.1 to 19.5 g/kg at heading stage. The decrease of plant nitrogen concentration during the vegetation period is due to dilution effect.

#### Relationship of Standard Vegetation Indices with Crop Parameters

The relationships of the different vegetation index types (broad band and narrow band) with the three crop parameters showed different results. Best individual R<sup>2</sup> values for broad band and narrow band standard vegetation indices were achieved for TVI (cf. Tab. 2). The narrow band TVI has high coefficient of determination values for aboveground biomass ( $R^2=0,71$ ) and plant height ( $R^2=0,65$ ), but low values for plant nitrogen concentration ( $R^2=0,33$ ). NDVI generally has lower R<sup>2</sup> values than TVI. Narrow band vegetation indices did not improve the relationships significantly compared with broad band vegetation indices. None of the evaluated broad or narrow band vegetation indices performed well for plant nitrogen concentration, with R<sup>2</sup> being less than 0.35 (cf. Tab. 2).

#### Relationship of Narrow Band Normalized Ratio Indices (NRI) with Crop Parameters

A total number of 9,870 narrow band NRIs according to equation (2) were calculated from multi-temporal Hyperion data. Correlation matrices between each agronomic parameter and two-band vegetation indices were constructed. In each correlation matrix, the wavelengths of the two bands were plotted on the x and y axes and the classified coefficients of determination ( $R^2$ ) between crop parameters and all possible two-band vegetation indices were plotted on a color scale (cf. Fig. 2).

The correlation matrices are only displayed below the diagonal because R<sup>2</sup> values are symmetrical. The R<sup>2</sup> values for aboveground biomass and plant nitrogen concentration ranged

**Tab. 2:** Coefficient of determination ( $R^2$ ) between ALI broad band, Hyperion narrow band vegetation indices and measured agronomic parameters.

Sensor	Index	ALI Band / Hyperion wavelength			Coefficient of Determination $R^2$		
		$\Lambda_1$	$\Lambda_2$	$\Lambda_3$	biomass	plant N	pl. height
ALI broad band	SR	Red (4)	NIR (5)		0.35	0.25	0.41
	NDVI	Red (4)	NIR (5)		0.4	0.28	0.43
	SAVI	Red (4)	NIR (5)		0.55	0.21	0.49
	TVI	Red (4)	NIR (5)		0.69	0.32	0.64
Hyperion narrow band	SR	671	803		0.41	0.3	0.41
	NDVI	671	803		0.41	0.29	0.4
	SAVI	671	803		0.58	0.22	0.56
	TVI	671	803	549	0.71	0.33	0.65
Hyperion best waveband combinations	$NRI_1$	874	1225		0.83		
	$NRI_2$	732	1305			0.81	
	$NRI_3$	763	1225				0.79

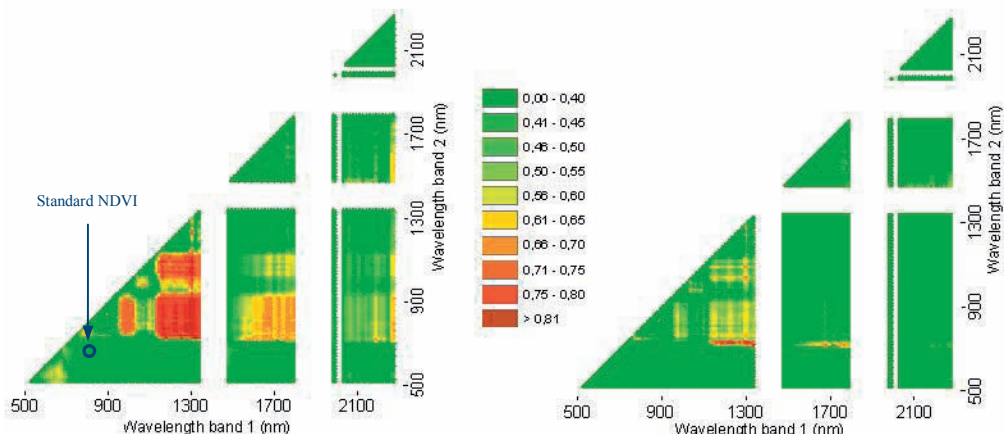


**Fig. 2:** Coefficient of determination ( $R^2$ ) between Hyperion narrow band vegetation indices calculated from all possible two-band combinations according to equation (2) and measured agronomic parameters. (a) Biomass and (b) total nitrogen content.

from 0.08 to 0.83, and several clusters of high  $R^2$  values could be recognized in the two matrix plots (cf. Fig. 2). Wavebands used for broadband NDVI calculation from the red and near infrared spectrum (which match red and nearinfrared ALI bands), are labeled in the matrix plot. This area shows very low correlation coefficients  $R^2$  compared to waveband pairs forming the clusters with high correlation coefficients. Best center wavelengths of

band 1 and band 2 for these patches for aboveground biomass estimation were extracted from the matrices and listed in Tab. 2. Following the same approach, best waveband pairs and bandwidth were determined for the estimation of plant nitrogen concentration (cf. Fig. 2b and Tab. 3). Similar to aboveground biomass, best waveband centers were not located in the R and NIR spectrum. The best values of NRIs for aboveground biomass,

plant N concentration and plant height were 0.83, 0.81 and 0.79, respectively. The selected wavebands were centered at 874, 732 and 763 nm for band 1, and 1,225 and 1,305 nm for band 2 with bandwidth between 10 to 30 nm (cf. Tab. 2).

## 4 Discussion

### Pre-processing of EO-1 Data

For the presented study Hyperion and ALI Level 1R data were used which are radiometrically corrected with no geometric correction applied (USGS 2007). This low level of correction assures no resampling and gives the possibility to bear a complete pre-processing chain to retrieve surface reflectance from at-sensor radiance measured with ALI multispectral and Hyperion hyperspectral sensor. Several authors (BIGGAR et al. 2003, DATT et al. 2003, Coops et al. 2003) pointed out the importance of correction of artefacts or atmospheric effects. A full processing chain for EO-1 Hyperion data was described by (KHURSHID et al. 2006). In comparison to (KHURSHID et al. 2006), the misregistration of VNIR and SWIR wavebands, which include spatial and angular shift, has been solved by a co-registration of the wavebands from the two VNIR and SWIR detectors. Due to the lack of detailed atmospheric information the atmospheric correction was performed with a standard atmosphere implemented in FLAASH (ENVI). The applied atmospheric correction resulted in a good agreement with ASD field data that were taken close to satellite overpass. Similar correction method and observed results were presented by (DATT et al. 2003) as well as by (CHEN & TIAN 2006).

### Standard Vegetation Indices

In the first step of the study three different two-band indices (SR, NDVI, SAVI) and one three-band index (TVI) were compared in order to evaluate the capability of broad band and narrow band standard vegetation indices for crop parameter estimation. The narrow bands of Hyperion Sensor for these indices were centered at green (559 nm), red (681 nm) and near infrared (803 nm) with bandwidth of

10 nm. The corresponding ALI broadband channels were 4, 5 and 6 with a bandwidth between 40 and 80 nm.

Comparing vegetation indices based on different sources (ALI and Hyperion), only a slight improvement of hyperspectral narrow bands was observed for the three measured crop variables compared to broad band indices. Similar results were found by (ZHAO et al. 2007) and (LEE et al. 2004), who tested the ability of different multispectral airborne and orbital sensor data for LAI prediction in an agricultural environment. Also HANSEN & SCHJOERRING (2003) found a slightly improved performance of narrow bands for biomass and nitrogen status of wheat crops. On the contrary, (BROGE & MORTENSEN 2002) and (BROGE & LEBLANC 2000) showed that hyperspectral vegetation indices did not perform better than their simulated multispectral counterparts. Whether broad or narrow bands were used, the standard vegetation indices had limited capability for crop parameter estimation due to canopy closure at high plant densities, which was also observed in the recent study. This saturation effect of standard vegetation indices at high canopy cover is evident for multispectral space based imaging (TUCKER 1977), airborne hyperspectral imaging (OPPELT & MAUSER 2004) and ground-based measurements (MUTANGA & SKIDMORE 2004).

### Narrow Band Normalized Difference Indices

In this study we evaluated the performance of these calculated band ratios that are widely used and readily adaptable in vegetation studies (SCHOWENGERDT 2007, GONG et al. 2003, THENKABAIL et al. 2000). The results in Fig. 2 show, that the two-band combinations respond in a wide range to variations in biomass. High coefficients of determination ( $R^2$ ) between narrow band indices and aboveground biomass are mainly clustered in the red edge, NIR and the SWIR spectra domain. These wavebands are centered in the red edge (720 nm), the NIR peak (874 nm) as well as in the SWIR (1,225 nm and 1,750 nm) with varying spectral range between 10 and 180 nm. Similar findings for biomass estimation are summarized in (THENKABAIL et al. 2004) and (MUTANGA & SKIDMORE 2004). These spectral regions of the

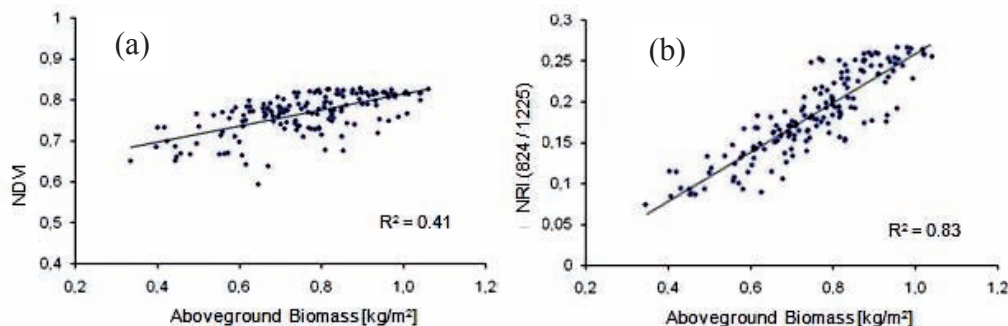


**Fig. 3:** Scatterplot of aboveground biomass against (a) standard narrow band NDVI (671 nm and 803 nm) and (b) best waveband combination from NRI (874 nm and 1,225 nm).

NIR peak and the SWIR in the electromagnetic spectrum are among others sensitive to plant water content (KUMAR et al. 2001), and consequently they have a close relationship to biomass (HUNT 1991). The best waveband combination for estimating aboveground biomass was obtained using wavebands centered at 874 nm and 1,225 nm. Similar approaches in different types of vegetation cover showed, that band combinations from the red edge (ZHAO et al. 2007, MUTANGA & SKIDMORE 2004) as well as NIR and SWIR (MUTANGA & SKIDMORE 2004, XAVIER et al. 2006) had a close relationship to LAI and aboveground biomass and performed much better than spectral bands used in standard vegetation indices.

Analog to biomass, the regression analysis between NRI and plant nitrogen concentration resulted in a wide range of R<sup>2</sup> values. The best correlation was achieved by combining bands from the red edge region (702 to 732 nm) with wavebands centered between 1,138 and 1,332 nm, which is in accordance to findings of (SMITH et al. 2003). In addition to this, several authors showed that the VIS region had a close relationship to plant nitrogen concentration (DAUGHTRY et al. 2000, NGUYEN & LEE 2006). It is well known that canopy spectral reflectance of the VIS (400 to 700 nm) is mainly governed by foliar pigments such as chlorophyll which is induced by plant nitrogen concentration (KUMAR et al. 2003, OPPELT & MAUSER 2004). In addition to the VIS region some authors proved a sensitivity of red edge

(LACAPRA et al. 1996, STRACHAN et al. 2002) as well as NIR (LACAPRA et al. 1996, HANSEN & SCHJOERING 2003) for nitrogen status detection, which is coincident with the best wavebands used for NRI index calculation in our study. Furthermore, the study of (FERWERDA et al. 2005) indicated significant differences in the estimation potential of indices for nitrogen concentration across different species.

## 5 Conclusions

This study compared vegetation indices calculated from multispectral and hyperspectral satellite remote sensing data for estimating winter wheat aboveground biomass, plant nitrogen concentration and plant height in North China Plain, and identified better vegetation indices by systematically evaluating all possible two band combinations using Hyperion satellite hyperspectral remote sensing data from 400 to 2,500 nm. The results indicated that TVI performed best among the tested vegetation indices using either broad (R<sup>2</sup>=0.69, 0.32 and 0.64 for biomass, N concentration and plant height, respectively) or narrow (R<sup>2</sup>=0.71, 0.33 and 0.65 for biomass, N concentration and plant height, respectively) bands. For the evaluated standard vegetation indices, narrow band indices only had slight improvements over corresponding broad band indices. The best performing Normalized Ratio Indices (NRI) selected through band com-

bination analysis were significantly better than TVI, achieving  $R^2$  of 0.83, 0.81 and 0.79 for biomass, plant N concentration and plant height, respectively. They all used wavebands from the near infrared (NIR) (centered at 874, 732, and 763 nm) and short wave infrared (SWIR) (centered at 1,225 and 1,305 nm) spectrum with varying bandwidth between 10 and 190 nm. The results of this study suggest that is important to include SWIR bands in multi-spectral satellite sensors for agricultural crop growth status monitoring. More studies are needed to further evaluate the results using data from more diverse conditions.

We can conclude that narrow band vegetation indices calculated from all possible waveband combination from Hyperion data perform much better for winter wheat parameters estimation on a regional level than standard vegetation indices calculated from red and NIR wavebands. Comparing all three index calculations, it was observed that two-band indices calculated according to Eq. 2 performed much better for estimation of above-ground biomass and total nitrogen content with at least 12 % improvement for above-ground biomass and 48 % for plant nitrogen content for winter wheat in the North China Plain. Because satellite image data were acquired at shooting and heading stage with a canopy closure of almost 100 %, the saturation effect was obvious. This saturation effect is pointed out in a flat slope for regression between standard NDVI and aboveground biomass in Fig. 3. Compared to this, the slope of the regression line is much steeper using bands from the NIR and SWIR for index calculation. The results of band combination showed, that the saturation problem occurred for standard vegetation indices can be overcome by using different combinations for narrow band indices.

## References

- BERK, A., ANDERSON, G.P., ACHARYA, P.K., CHETWYND, J.H., BERNSTEIN, L.S., SHETTLE, E.P., MATTHEW, M.W. & ADLER-GOLDEN, S.M., 2000: MODTRAN4 User's Manual. – Hanscom AFB, MA: Air Force Res. Lab.: 1–93.
- BIGGAR, S.F., THOME, K.J. & WISNIEWSKI, W., 2003: Vicarious Radiometric Calibration of EO-1 Sensors by Reference to High-Reflectance Ground Targets. – *IEEE Transactions on Geoscience and Remote Sensing* **41** (6): 1174–1179.
- BREMNER, J.M., 1960: Determination of nitrogen in soil by the Kjeldahl method. – *Journal of Agricultural Science* **55**: 11–33.
- BROGE, N.H. & LEBLANC, E., 2000: Comparing predicting power and stability of broadband and hyperspectral vegetation indices for estimation of green leaf area index and canopy chlorophyll density. – *Remote Sensing of Environment* **76**: 156–172.
- BROGE, N.H. & MORTENSEN, J.V., 2002: Deriving green crop area index and canopy chlorophyll density of winter wheat from spectral reflectance data. – *Remote Sensing of Environment* **81**: 45–57.
- CAIRNS, B., 2003: SPECIAL ISSUE PAPERS – Atmospheric Correction and its Application to an Analysis of Hyperion Data. – *IEEE Transactions on Geoscience and Remote Sensing* **41** (6): 1232–1245.
- CECCATO, P., GOBRON, N., FLASSE, S., PINTY, B. & TARANTOLA, S., 2002: Designing a spectral index to estimate vegetation water content from remote sensing data: Part 1 Theoretical approach. – *Remote Sensing of Environment* **82**: 188–197.
- CHEN, J. & TIAN, Q., 2006: Estimating canopy chlorophyll and nitrogen concentration of rice from EO-1 Hyperion data. – *Remote Sensing for Agriculture. Proceedings of the SPIE* **6359**.
- COOPS, N.C., SMITH, M.-C., MARTIN, M.E. & OLLINGER, S.V., 2003: Prediction of Eucalypt Foliage Nitrogen Content From Satellite-Derived Hyperspectral Data. – *IEEE Transactions on Geoscience and Remote Sensing* **41** (6): 1338–1346.
- CLOUTIS, E.A., CONNERY, D.R. & DOVER, F.J., 1999: Agricultural crop monitoring using airborne multi-spectral imagery and C-band synthetic aperture radar. – *International Journal of Remote Sensing* **20**: 767–787.
- DATT, B., McVICAR, T.R., VAN NIEL, T.G., JUPP, D.L.B. & PEARLMAN, J.S., 2003: Pre-processing EO-1 Hyperion Hyperspectral Data to Support the Application of Agricultural Indexes. – *IEEE Transactions on Geoscience and Remote Sensing* **41** (6): 1246–1259.
- DAUGHTRY, S.S.T., WALTHALL, C.L., KIM, M.S., DE COLSTOUN, E.B. & McMURTRY, J.E., 2000: Estimating Corn Leaf Chlorophyll Concentration from Leaf and Canopy Reflectance. – *Remote Sensing of Environment* **74**: 229–239.
- FERWERDA, J.G., SKIDMORE, A.K. & MUTANGA, O., 2005: Nitrogen detection with hyperspectral normalized ratio indices across multiple plant

- species. – International Journal of Remote Sensing **26**: 4083–4095.
- GALVÃO, L.S., FORMAGGIO, A.R. & TISOT, D.A., 2005: Discrimination of sugarcane varieties in South-eastern Brazil with EO-1 Hyperion data. – Remote Sensing of Environment **94**: 523–534.
- GONG, P., PU, R., BIGING, G.S. & LARRIEU, M.R., 2003: Estimation of Forest Leaf Area Index Using Vegetation Indices Derived From Hyperion Hyperspectral Data. – IEEE Transactions on Geoscience and Remote Sensing **41** (6): 1355–1362.
- HABOUDANE, D., MILLER, J.R., PATTEY, E., ZARCO-TEJADA, P.J. & STRACHAN, I.B., 2004: Hyperspectral vegetation indices and novel algorithms for predicting green LAI of crop canopies: Modeling and validation in the context of precision agriculture. – Remote Sensing of Environment **90**: 337–352.
- HANSEN, P.M. & SCHJOERRING, J.K., 2003: Reflectance measurement of canopy biomass and nitrogen status in wheat crops using normalized difference vegetation indices and partial least square regression. – Remote Sensing of Environment **86**: 542–553.
- HUETE, A.R., 1988: A soil-adjusted vegetation index (SAVI). – Remote Sensing of Environment **25**: 295–309.
- JONGSCHAAP, R.W.W. & SCHOUTEN, L.S.M., 2005: Predicting wheat production at regional scale by integration of remote sensing data with a simulation model. – Agronomy for sustainable development **25**: 481–489.
- KHURSHID, K., STAENZ, K., SUN, L., NEVILLE, R., WHITE, H.P., BANNARI, A., CHAMPAGNE, C.M. & HITCHCOCK, R., 2006: Preprocessing of EO-1 Hyperion data. – Canadian Journal of Remote Sensing **32**: 84–97.
- KUMAR, L., SCHMIDT, K., DURY, S., & SKIDMORE, A., 2003: Imaging spectrometry and vegetation science. – Imaging Spectrometry, Dordrecht.
- LAUDIEN, R. & BARETH, G., 2006: Multitemporal Hyperspectral Data Analysis for Regional Detection of Plant Diseases by using a Tractor-and an Airborne-based Spectrometer. – Photogrammetrie – Fernerkundung – Geoinformation **3/06**: 217–228.
- LEE, K.-S., COHAN, W.B., KENNEDY, R.E., MAIERSPERGER, T.K. & GOWER, S.T., 2004: Hyperspectral versus multispectral data for estimating leaf area index in four different biomes. – Remote Sensing of Environment **91**: 508–520.
- LI, F., GNYP, M.L., JIA, L., MIAO, Y., YU, Z., KOPPE, W., BARETH, G., CHEN, X. & ZHANG, F., 2008: Estimating N status of winter wheat using a handheld spectrometer in the North China Plain. – Field Crops Research **106**: 77–85.
- LILLESAND, T.M., KIEFER, R.W. & CHIPMAN, J.W., 2004: Remote Sensing and Image Interpretation. – 5<sup>th</sup> Edition. New York, Chichester, Brisbane, Toronto, Singapore.
- LU, D., 2006: The potential and challenge of remote sensing-based biomass estimation. – International Journal of Remote Sensing **27**: 1297–1328.
- MIAO, Y., MULLA, D.J., RANDALL, G.W., VETSCH, J.A. & VINTILA, R., 2009: Combining chlorophyll meter readings and high spatial resolution remote sensing images for in-season site-specific nitrogen management of corn. – Precision Agriculture **10**: 45–62.
- MUTANGA, O. & SKIDMORE, A.K., 2004: Narrow band vegetation indices overcome the saturation problem in biomass estimation. – International Journal of Remote Sensing **25**: 3999–4014.
- NGUYEN, H.T. & LEE, B.-W., 2006: Assessment of rice leaf growth and nitrogen status by hyperspectral canopy reflectance and partial least square regression. – European Journal of Agronomy **24**: 349–356.
- OPPELT, N. & MAUSER, W., 2004: Hyperspectral monitoring of physiological parameters of wheat during a vegetation period using AVIS data. – International Journal of Remote Sensing **25**: 145–159.
- PEARLMAN, J.S., BARRY, P.S., SEGAL, C.C., SHEPANSKI, J., BEISO, D. & CARMAN, S.L., 2003: Hyperion, a Space-Based Imaging Spectrometer. – IEEE Transactions on Geoscience and Remote Sensing **41** (6): 1160–1173.
- REYNIERS, M. & VRINDTS, E., 2006: Measuring wheat nitrogen status from space and ground-based platform. – International Journal of Remote Sensing **27**: 549–567.
- ROUSE, J.W., HAAS, R.H., SCHELL, J.A., DEERING, D.W. & HARLAN, J.C., 1974: Monitoring the vernal advancements and retrogradation of natural vegetation. – NASA/GSFC, Final Report, Greenbelt, USA, 1–137.
- SERRANO, L., FILELLA, I. & PEÑUELAS, J., 2000: Remote sensing of biomass and yield of winter wheat under different nitrogen supplies. – Crop Science **40**: 723–731.
- SCHMIDT, K.S. & SKIDMORE, A.K., 2003: Spectral discrimination of vegetation types in a coastal wetland. – Remote Sensing of Environment **85**: 92–108.
- SCHNEIDER, K., 2003: Assimilating remote sensing data into a land surface process model. – International Journal of Remote Sensing **24**: 2959–2980.
- SCHOWENGERDT, R.A., 2007: Remote sensing: models and methods for image processing. – 3<sup>rd</sup> ed., Elsevier Academic Press, Amsterdam.

- SIMS, D. A. & GAMON, J.A., 2002: Relationships between leaf pigment content and spectral reflectance across a wide range of species, leaf structures and development stages. – *Remote Sensing of Environment* **81**: 337–354.
- SMITH, M.-L., MARTIN, M.E., PLOURDE, L. & OLLINGER, V., 2003: Analysis of Hyperspectral Data for estimation of Temperate Forest Canopy Nitrogen Concentration: Comparison Between an Airborne (AVIRIS) and a Spaceborne (Hyperion) Sensor. – *IEEE Transactions on Geoscience and Remote Sensing* **41** (6): 1332–1337.
- STRACHAN, I.B., PATTEY, E. & BOISVERT, J.B., 2002: Impact of nitrogen environmental conditions on corn as detected by hyperspectral reflectance. – *Remote Sensing of Environment* **80**: 213–224.
- THENKABAIL, P.S., ENCLONA, E.A., ASHTON, M.S. & VAN DER MEER, B., 2004. Accuracy assessment of hyperspectral waveband performance for vegetation analysis application. – *Remote Sensing of Environment* **91**: 354–376.
- THENKABAIL, P.S., SMITH, R.B. & DE PAUW, E., 2000: Hyperspectral vegetation indices and their relationships with agricultural crop characteristics. – *Remote Sensing of Environment* **71**: 158–182.
- TUCKER, C.J., 1979: Red and Photographic Infrared Linear Combinations for Monitoring Vegetation. – *Remote Sensing of Environment* **8**: 127–150.
- USGS, 2007: EO-1 User's Guide, [eol.usgs.gov/userGuide/index.php](http://eol.usgs.gov/userGuide/index.php).
- WOOSTER, M., 2007: Remote sensing: sensors and systems. – *Progress in Physical Geography* **31**: 95–100.
- XAVIER, A.C., RUDORFF, B.F.T., MOREIRA, M.A., ALVARENGA, B.S., DE FREITAS, J.G. & SALOMON, M.V., 2006: Hyperspectral field reflectance measurements to estimate wheat grain yield and plant height. – *Science Agriculture* **63**: 130–138.
- ZHAO, D., LI, J. & QI, J., 2004: Hyperspectral characteristic analysis of a developing cotton canopy under different nitrogen treatments. – *Agronomie* **24**: 463–471.
- ZHAO, D., HUANG, L., LI, J. & QI, J., 2007: A comparative analysis of broadband and narrowband derived vegetation indices in predicting LAI and CCD of a cotton canopy. – *ISPRS Journal of Photogrammetry & Remote Sensing* **62**: 25–33.

#### Addresses of the Authors:

WOLFGANG KOPPE, Institute of Geography, GIS & RS Group, University of Cologne, D-50923 Köln, Germany and Infoterra GmbH (EADS Astrium), D-88039 Friedrichshafen, Germany, Tel.: +49-7545-84226, e-mail: wolfgang.koppe@infoterra-global.com

DR. FEI LI, College of Resources and Environmental Sciences, China Agricultural University, 100094, Beijing, China and College of Ecology and Environmental Science, Inner Mongolia Agricultural University, 010019, Hohhot, China. Tel.: +86-471-4307376, e-mail: cau\_lifei@163.com

MARTIN GNYP & Prof. Dr. GEORG BARETH, Institute of Geography, GIS & RS Group, University of Cologne, D-50923 Köln, Germany, Tel.: +49-221-470-6620, -6552, Fax: +49-221-470-1638, e-mail: mgnyp1@uni-koeln.de, g.bareth@uni-koeln.de

DR. YUXIN MIAO, Agro-Informatics and Sustainable Development Group, College of Resources and Environmental Sciences, China Agricultural University, Beijing 100193, China, e-mail: ymiao@cau.edu.cn and Resources & Environment, Hebei Academy of Agriculture and Forestry Sciences, 050051, Shijiazhuang, China, e-mail: jiall@cau.edu.cn

Prof. Dr. XINPING CHEN & Prof. Dr. FUSUO ZHANG, Department of Plant Nutrition, College of Resources & Environmental Sciences, China Agricultural University, 100094, Beijing, China, e-mail: chenxp@cau.edu.cn, zhangfs@cau.edu.cn

Manuskript eingereicht: Oktober 2009

Angenommen: Dezember 2009



# Independent Component Analysis of Hyperion Data to Map Alteration Zones

MAJID M. OSKOUEI, Tabriz, Iran

**Keywords:** Remote Sensing, ICA, Hyperspectral, Hyperion, Mineral detection, Mapping

**Summary:** We present an improved method for independent component analysis aiming to detect minerals in the Erongo complex, Namibia. We evaluate independent component analysis (ICA) to detect and map alteration halos in Erongo Namibia using the Hyperion dataset. Detailed surveys and investigations are possible given the capability of the hyperspectral sensors to render a great deal of spectral information by observing the surface of earth. In terms of mineral detection, however, there are particular challenges. In this research, we used two methods to achieve an independent components (ICs) map. The first method computes the virtual dimensionality (VD) of a dataset, prioritises calculated ICs, and finally picks up only a certain number of ICs. This number is equal to the calculated VD. Since some ICs share extreme pixels, the final extremes from this method are less than the VD. The presented modified method differs slightly from the first one. In this method, extreme pixels for all ICs are determined, and all ICs with the same extreme pixels are considered equal. Prioritisation of IC bands takes place afterward. The results demonstrate that the second method performs better because in addition to its ability to map more end-members, the mapped zones match lithological structures better. The dataset is atmospherically corrected by ACORN, and data quality assessment is performed to discriminate bad bands before ICA. To determine each extreme pixel mineralogical, spectral feature fitting (SFF) algorithm was used in the SWIR range of electromagnetic wavelength by comparing to USGS mineral spectral library.

**Zusammenfassung:** Analyse unabhängiger Komponenten von Hyperion Daten zur Kartierung von Verwitterungszonen in Erongo, Namibia. Wir präsentieren ein verbessertes Verfahren für die Analyse unabhängiger Komponenten (ICA) mit dem Ziel der Mineral-Erkennung im Erongo Komplex. Detail- Untersuchungen sind unter Verwendung von Hyperspektral-Sensoren möglich, weil diese Sensoren eine große Leistungsfähigkeit in der Wiedergabe der Spektralinformation der Erdoberfläche besitzen. Bei der Mineral-Erkennung gibt es jedoch besondere Herausforderungen. In dieser Untersuchung wurden zwei Methoden zur Erzeugung einer unabhängigen Komponenten (IC) Karte berücksichtigt. Die erste Methode berechnet die virtuelle Dimensionalität (VD) des Datensatzes, priorisiert berechnete ICs, und verwendet schließlich nur eine bestimmte Anzahl von ICs. Diese Anzahl entspricht der berechneten VD. Da sich einige ICs extreme Pixel teilen, sind die endgültigen Extrema bei dieser Methode weniger als bei der VD. Die vorgestellte Methode unterscheidet sich ein wenig von der ersten. Bei ihr werden extreme Pixel für alle ICs bestimmt, und alle ICs mit den gleichen extremen Pixeln werden als gleich angesehen. Die Priorisierung von ICs Bands erfolgt später. Die Ergebnisse zeigen, dass die zweite Methode eine höhere Leistungsfähigkeit besitzt, weil zusätzlich zu der Fähigkeit, mehr Endmember zu kartieren, die zugeordneten Zonen besser zu den lithologischen Strukturen passen. Der Datensatz wird atmosphärisch mit ACORN verbessert und es wurde eine Bewertung der Datenqualität durchgeführt, um schlechte Bänder vor der ICA zu unterscheiden. Für die Detektion von Mineralien wird in jedem extremen Pixel ein spektraler Merkmalsanpassung (SFF) Algorithmus im SWIR Band verwendet, indem mit der USGS Mineral-Bibliothek verglichen wird.

## 1 Introduction

Independent Component Analysis (ICA) has been widely used in various blind source separations. Its application to linear spectral mixture analysis in remote sensing and image processing has shown promising results (BAYLISS et al. 1997, CHIANG et al. 2000, LENNON et al. 2001, BOTCHKO et al. 2003, WANG & CHANG 2006a, DU et al. 2006). Independent Component Analysis addresses the problem of determining the factors that contribute independently (in a statistical sense) to observed data from a set of sensors. So far, considering the linear mixture model, in contrast to other approaches, ICA assumes that the abundance fractions that are commonly assumed to be unknown and non-random constants are now random parameters and statistically independent signal sources. In addition, one signal source at the most is allowed to be Gaussian (VARSHNEY & ARORA 2004). These two assumptions should be closely considered in the unmixing procedure when violating of them could result in estimation errors.

ICA is known as a blind source separation, so it is possible to achieve estimation for end-members themselves. If we assume that observations or  $R$ s are noise-free ( $R=aE$ ), then there is a matrix  $W$

$$\text{where } E = WR \quad (1)$$

With regard to the ICA concept (independent components), the matrix  $W$  can be determined by solving an optimisation problem that aims to minimise mutual information between components (VARSHNEY & ARORA 2004, HYVÄRINEN 1999).

It is important in practice to make learning faster and more reliable. This can be achieved using fixed-point iteration algorithms. In these algorithms, the computations are made in batch (or block) mode, i.e., a large number of data points are used in a single step of the algorithm. In other respects, however, these algorithms may be considered neural. In particular, they are parallel, distributed, computationally simple, and require little memory space. HYVÄRINEN (1999) showed that fixed-point algorithms have very appealing convergence properties, making them an interesting alternative to adaptive learning rules

in environments where fast real-time adaptation is not necessary. Note that their basic ICA algorithms require a preliminary spherling or whitening of the data  $R$ . Spherling means that the original observed variable, e.g.,  $v$ , is linearly transformed to a variable  $R = Qv$  such that the correlation matrix of  $R$  equals unity:  $E\{RR^T\} = I$ .

### 1.1 Study Area

The study area is located in north-western Namibia and includes the Erongo Complex with a diameter of approximately 35 km; this is one of the largest Cretaceous anorogenic complexes in that country. The centre of the complex is located at approximately 21°40' S and 15°38' E (cf. Fig. 1).

This represents the eroded core of a caldera structure with peripheral and central granitic intrusions. Surrounding the outer granitic intrusions of the Erongo Complex is a ring dike of olivine dolerite that locally reaches some 200 m in thickness and has a radius of 32 km. The ring dike weathers easily and is therefore highly eroded. However, it can be easily identified in aeromagnetic data and satellite images.

The central part of the Erongo complex consists of a layered sequence of volcanic rocks that form prominent cliffs rising several hundred meters above the surrounding basement. The basement rocks consist of mica schists and meta-greywackes of the Kuiseb Formation and various intrusions of granites. In the southeast, the rocks of the Erongo Complex overlie the Triassic Lions Head Formation, which consists of conglomerates, gritstone, arkose with interbedded siltstone and mudstone, and quartz arenite (SCHNEIDER & SCHNEIDER 2004).

### 1.2 Pre-processing

There are some essential processes that must be done on the data before main processing concerning on the sensor type and its technical specifications. The pre-processing includes algorithms to correct probable errors that occur during image acquisition. Vertical destriping, georeferencing, atmospheric correction,

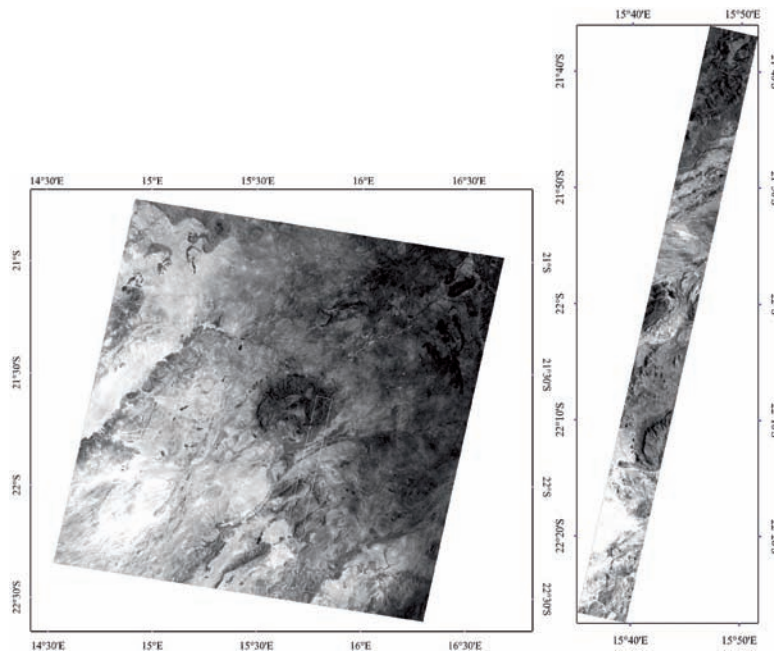


**Fig. 1:** ETM scene of the Erongo complex and location of the Hyperion scene (left) in addition to Hyperion band 28 (right).

and spectral profile enhancement (or polishing) are the corrections that were performed on the Hyperion data.

Vertical stripes usually occur in several columns with constant Digital Number (DN) because of technical failure in the functionality of some detectors and they were removed by averaging the neighbouring columns.

Georeferencing of the data is performed just before producing final map to prevent possible errors that resampling and approximating make in the data and will therefore affect functionality of other processing tasks. The Hyperion data was registered with the use of the ETM image of Erongo that had been supplied georeferenced.

The smile effect (line curvature) on the Hyperion data is an across track shift from a centre wavelength because of changes in dispersion angle. This is negligible in the SWIR range of the spectra (less than 1 nm), but variables in the VNIR are about 30 % and should be rectified. In this research the smile effect was corrected by ACORN using prior the launch parameters measured by TRW (a company contracted by NASA to build Hyperion).

A variety of packages for atmospheric correction have been developed, including ATREM, FLAASH, ATCOR, ACORN, and the atmospheric correction module in the GEOMATICA platform. All of these use the MODTRAN radiative transfer algorithm, however, and some of them, like FLAASH and ACORN; have options to share the empirical experience of the user.

According to some previous studies about different algorithms for atmospheric correction, ACORN has proven its reliability. Its only drawback is that applying this method requires a great deal of knowledge about hyperspectral remote sensing (CHANG & DU 2004). ACORN offers different algorithms for atmospheric correction of various sensors (modes 1 to 7) and mod 1 is planned for hyperspectral data. We therefore used ACORN mode 1 for the atmospheric correction of the dataset.

ACORN offers a range of strategies for atmospheric correction. These include both empirical and radiative transfer code based methods for atmospheric correction of both hyperspectral and multispectral datasets.

ACORN also offers several artefact suppression options, as well as single spectrum enhancement options to improve atmospheric correction results. Radiative transfer atmospheric correction of calibrated data uses both the calibrated data and additional specified parameters to derive and model the absorption and scattering characteristics of the atmosphere. These modelled atmospheric characteristics are then used to invert the radiance to apparent surface reflectance.

Available artefacts on ACORN are divided into three types. Type 1 corrects for any mismatch in the spectral calibration of the hyperspectral data and the spectral radiative transfer calculations. It suppresses the artefacts located near the strong atmospheric absorption features at 760, 940, 1150, and 2000 nm. Type 2 identifies and suppresses other small artefacts located across the spectral range due to errors in the absolute radiometric calibration and/or errors in the radiative transfer calculations. The spectrum across the 1,400 and 1,900 nm water vapour bands often produces noisy reflectance results because of the low radiance values recorded in these regions. Type 3 assesses the signal levels of the calibrated radiance and suppresses the lowest signal portions where erroneous reflectance calculations may occur. The result is that the lowest signal portions of the spectrum are set to zero on the apparent surface reflectance output. These artefacts do not manipulate absorption features on the spectral profiles. Fig. 2 il-

lustrates the spectral profiles of a pixel before and after atmospheric correction. All three artefact suppressions were applied.

After applying atmospheric correction and artefact suppressions available in ACORN, some additional tasks like bad band determination and polishing are done to improve the spectral profile quality. This process smoothen noisy fluctuations on spectral profile and small absorption features are probably eliminated.

Briefly, bad bands refer to some bands in the dataset that contain very little or no extractable information. The quality of digital remote sensing data is directly related to the level of the signal to system noise ratio (SNR). Theoretically, the SNR ratio for Hyperion is 190 to 40 as the wavelength increases (PEARLMAN et al. 2000). One common approach to determining an approximate SNR for remote sensing data is to use a mean/standard deviation method. This approach requires defining a spectrally homogeneous area (an area with minimum intrinsic variance), calculating the average spectrum for that area, and determining the spectrally distributed standard deviation for the average spectrum. MANOLAKIS et al. (2003) conducted a survey by analysing approximately 14 Hyperion scenes from around the world using the mean/standard deviation SNR method and showed that there is a strong relationship between the acquisition time of the year (because of the effect of illumination to observation geometries) and the SNR of the Hyperion data. The calculated SNRs for Hy-

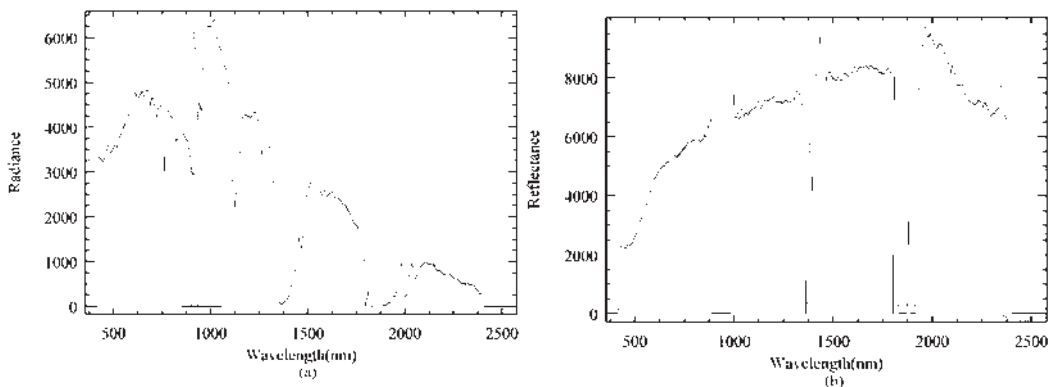


**Fig. 2:** Spectral profile of a pixel before (a) and after (b) atmospheric correction by ACORN; bad bands are marked by dotted ellipses.

perion SWIR data are higher in the summer and lowest in the winter. This has a direct effect on spectral mineral mapping, with lower SWIR SNRs resulting in the extraction of less detail (MANOLAKIS et al. 2003). Fig. 3 illustrates the signal to noise ratio calculated for our Hyperion data by the aforementioned method. According to this plot, uncalibrated channels (channels 1–8 and 222–242) in addition to those affected strongly by water vapour absorption (940 nm, 1,400 nm, 1,900 nm) have zero SNR. These channels are listed in the list of bad bands for the following processing tasks. In addition, the bands that possess lower SNR ratios compared to the nearby channels are also considered to be bad bands.

The effect of an additive noise process,  $n_a$ , on an image digital number (DN) at the  $i^{\text{th}}$  and  $j^{\text{th}}$  pixel can then be modelled as the summation of the true signal,  $S$ , with the noise, as shown by Tu et al. (1998):

$$DN(i, j) = S(i, j) + n_a(i, j) \quad (2)$$

If the noise proportion in the above equation is significant, the DNs almost equal the noise amount and the band will be labelled as bad. We used up only good bands (subset 166 good bands of total 242 bands) to avoid any possible mistakes during pre-processing and subsequent steps. As a final pre-processing task, the data were polished using a geostatistical algorithm presented by the author (OSKOUEI & BUSCH 2008).

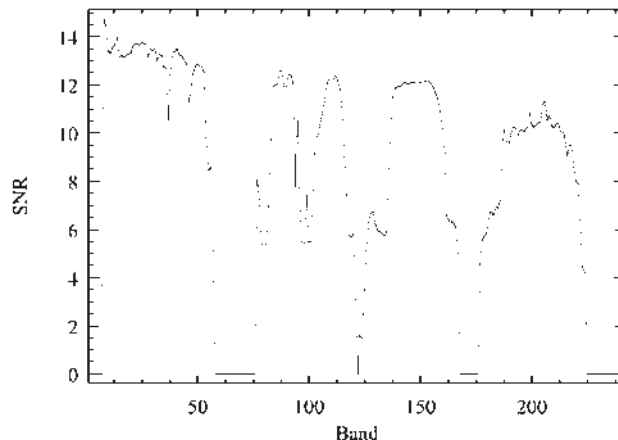


**Fig. 3:** Signal to noise ratio calculated for Hyperion data by the mean/deviation method.

## 2 Independent Components Analysis

Determining the virtual dimensionality (VD) of a dataset is essential to perform a successful ICA. This is also known as the number of detectable endmembers. The VD was computed using the HARSANYI, FARRAND, and CHANG (HFC) method presented by HARSANYI et al. (1993), and then the Fast fixed-point algorithm for Independent Component Analysis (FastICA) programme was applied to calculate independent components (ICs). Since this program does not prioritise the output ICs, a prioritisation step is also necessary after achieving the ICs. Finally, the abundances of the ICs were calculated for mapping purposes.

### 2.1 Virtual Dimensionality of the Data

The HFC method is presented by HARSANYI et al. (1993) and uses Neyman-Pearson detection theory to estimate the number of endmembers. This idea is described in CHANG & DU (2004) and NASH & JOHNSON (2002). According to CHANG & DU (2004), the eigenvalues generated by the sample correlation matrix and the sample covariance matrix are denoted by correlation eigenvalues and covariance eigenvalues, respectively. Since the component dimensionality is equal to the total number of eigenvalues, each eigenvalue specifies a component dimension and provides an

indication of the significance of that particular component in terms of variance. If there is no signal source contained in a particular component, the corresponding correlation eigenvalue and covariance eigenvalue in this component should reflect only the noise energy, in which case the correlation eigenvalue and covariance eigenvalue are equal. This provides us with a basis from which we can formulate the difference between the correlation eigenvalue and its corresponding covariance eigenvalue as a binary composite hypothesis testing problem. The null hypothesis represents the case of zero difference, while the alternative hypothesis is the case in which the difference is greater than zero. When the Neyman-Pearson test is applied to each pair of correlation eigenvalues and its corresponding covariance eigenvalue, the number of times the test fails indicates how many signal sources are present in the image. In other words, a failure of the Neyman-Pearson test in a component indicates the truth of the alternative hypothesis, which implies that there is a signal source in this particular component. Using this approach, we can estimate the virtual dimensionality with the receiver operating characteristic analysis to evaluate the effectiveness of the decision. The virtual dimensionality of the image was calculated using various false alarm probabilities (HARSANYI et al. 1993); these are listed in Tab. 1.

Decreasing the false alarm probability ( $P_{fa}$ ) will increase the threshold amount used to compare the correlation and covariance eigenvalues, but after achieving a certain magnitude, it does not have a significant effect on the threshold. Therefore, as mentioned by the innovators of the method,  $10^{-4}$  seems to be a reasonable value and consequently the virtual dimensionality of the data is 37.

## 2.2 Prioritisation

After determining the number of endmembers by HFC (37 endmembers), the FastICA program (HYVÄRINEN 1999, HYVÄRINEN & OJA 2000) was used to compute the demixing matrix. It was not possible to load the image in MATLAB because of the large size of the Hyperion dataset. According to HYVÄRINEN (1999), we therefore resized them by averaging while producing the two dimensional matrix from the Hyperion cube. The averages can be estimated using a smaller sample, whose size may have a considerable effect on the accuracy of the final estimates. The sample points should be chosen separately at every iteration. If the convergence is not satisfactory, one may then increase the sample size (HYVÄRINEN 1999).

The rows of the matrix are equal to the channel number (166), and each row consists of observations for one band. The method presented by WANG & CHANG (2006b) has been used to perform the priority task. They calculated a high order statistical formula as a score for each independent component obtained by FastICA:

$$ps(IC_i) = \frac{(k_i^3)^2}{12} + \frac{(k_i^4 - 3)^2}{48} \quad (3)$$

where  $k_i^3 = \frac{\sum_{n=1}^{MN} (z_n^i)^3}{MN}$ ,  $k_i^4 = \frac{\sum_{n=1}^{MN} (z_n^i)^4}{MN}$  and

$z_n^i$  is the DN of pixel  $n$  in IC  $i$

Previous work, e. g., (WANG & CHANG 2006a), suggested extracting twice the VD, but we ran the ICA to extract all possible ICs (166 ICs), and the prioritisation algorithm based on formula (3) was used to order ICs. Tab. 2 illustrates the first 37 ICs in priority order.

**Tab. 1:** VDs calculated by the HFC method for different false alarm probabilities ( $P_{fa}$ ).

$P_{fa}$	$10^{-1}$	$10^{-2}$	$10^{-3}$	$10^{-4}$	$10^{-5}$
VD	43	38	37	37	37

**Tab. 2:** First 37 prior ICs.

18	2	5	1	4	7	6	11	13	16	3	20	19	8	33	39	32	15	35
24	17	50	10	12	22	29	28	31	21	23	41	53	36	9	26	40	30	

The results imply that running FastICA for only 74 ICs (twice the VD calculated by HFC) was enough. After this the demixing ( $W$ ) and whitening matrices obtained from FastICA were multiplied by original data to obtain IC images according to formula (1) and the above 37 priority channels were picked for later processes. The method for normalising the IC abundances introduced by ZHENG et al. (2006) and WANG & CHANG (2006b) was also applied. According to their formula for each endmember pixel  $e_i$ , let  $IC_i$  be the IC from which  $e_i$  was extracted and  $|IC_i(r)|$  denote the value of each pixel  $r$  in  $IC_i$ . We normalize the absolute value of  $IC_i(r)$ ,  $|IC_i(r)|$  with respect to  $|e_i|$ , the absolute value of  $e_i$  and define its corresponding abundance fraction  $a_{IC_i}(r)$  by

$$a_{IC_i}(r) = \frac{|IC_i(r)| - \min_r |IC_i(r)|}{|e_i| - \min_r |IC_i(r)|} \quad (4)$$

$e_i$  is the maximum of  $|IC_i(r)|$  over all the image pixels in the  $IC_i$

In each channel of this image, the location of any pixel that has a maximum amount for the appropriate IC was noted. Knowing the locations of these pixels helps us to obtain a preliminary evaluation for the independent components and their similarities. In addition, the image of each IC was surveyed visually to recognise ICs that are related to backgrounds. The result demonstrates that some of the IC images have the same extreme pixel, which means that their maximum amount occurred in the same pixels, like ICs 1,4,5,7,10–11, 14–16,18–21,23–35; ICs 2,22,36; and ICs 6,9. It clearly does not mean that they are completely equal ICs, but we can conclude that they are very similar; on the other hand, we cannot distinguish their differences by this method as our only tool to obtain information about them is their spectral profiles.

### 2.3 Mapping Independent Components

The spectral profiles of those extreme pixels are shown in Fig. 4(a). The spectral angle mapper (SAM) was applied to map the distributions of ICs. In the map produced by this method, only 6 ICs show considerable distributions. Studying each of the IC abundances map separately could help one to obtain valuable information about the mineralogy in the region, but preparing a comprehensive map using by them is not really helpful (Fig. 5(b)).

### 2.4 Stepwise Algorithm

The outcomes of the last procedure imply that some useful endmembers are ignored during the process of prioritisation. This is because of the close similarity between some prioritised ICs that share in extreme pixels and prevent us from detecting other purest pixels. The stepwise algorithm presented here yields an exact solution for this problem. Since the ICs with the same extreme pixels cannot be discriminated, they will be considered as one. To do this practically, the extreme pixels of all possible ICs (166 ICs) should be determined and then the ICs are categorised based on their extreme pixels (ICs with the same extreme pixel in one group). Finally the IC with the best priority score represents its group and distributions of these representative ICs are mapped on the scene. The stepwise process of this method is summarised as follows:

- 1) run FastICA for extracting all possible ICs
- 2) change IC images to abundances map according to formula (4)
- 3) find the maxima for each IC (extreme pixels)
- 4) group the ICs with the same extremes
- 5) prioritisation
- 6) select one IC for each group based on their priority score

- 7) classify the dataset by SAM based on the extremes' spectral profiles
- 8) match the spectral profile to the reference data spectra

The application of this algorithm produced 24 prioritised from 166 primary ICs, as illustrated in Tab. 3. Classification of the scene is done by SAM using the spectral profiles of the extreme pixels as profiles of ICs. The resulting map (cf. Fig. 5(c)) shows a considerable distribution for 8 ICs. To identify the mineralogy of each independent component, the spectral

profiles of extreme pixels were compared to the USGS mineral spectral library, which is resampled for the Hyperion wavelengths. The spectral feature fitting (SFF) method was used to perform that task in the short wave infrared region of the spectra because most differences between the endmember profiles are distinguishable in the range of 1971 to 2365  $\mu\text{m}$  according to Fig. 4(b). Several minerals from the SFF lookup table were selected considering their matching scores as indicative of alteration minerals. Tab. 4 illustrates selected minerals for each endmember.

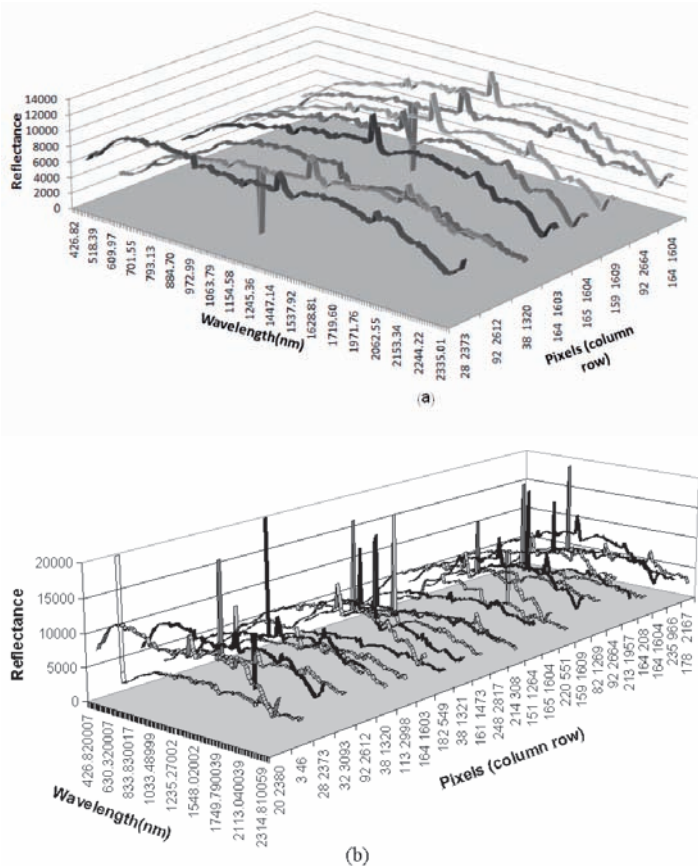


**Fig. 4:** Spectral profiles of extreme pixels: (a) Ordinary method and (b) Stepwise algorithm.

**Tab. 3:** Extreme pixels of 24 different ICs.

priority	IC	sample	line	priority	IC	sample	line
1	18	20	2380	13	59	214	308
2	2	3	46	14	79	151	1264
3	5	28	2373	15	93	165	1604
4	7	32	3093	16	66	220	551
5	11	92	2612	17	102	159	1609
6	20	38	1320	18	114	82	1269
7	19	113	2998	19	134	92	2664
8	32	164	1603	20	139	213	1957
9	30	182	549	21	152	164	208
10	42	38	1321	22	158	164	1604
11	54	161	1473	23	155	235	966
12	73	248	2817	24	163	178	2167

**Tab. 4:** Minerals that show a high match to 8 mapped ICs.

IC	minerals
5	almandine1,hematitea,almandine3,augite3diposide3
11	ammonioillite,buddingtonite2,mascagnite,buddingtonite1,alunite2
20	ammoniojarosite,buddingtonite2,mascagnite2,buddingtonite1,hypsthen2
30	axinite,sphalerite4,5,augite3,1,mascagnite1
66	vegetation, mascagnite1,2,galena2, a-jarosite
102	axinite,augite3
134	rivadavite,alunite2,ulexite2alunite6,4,ulexitel,a-illite,orthoclase,a-smectite
155	a-jarosite,mascagnite2,buddingtonite2,mascagnite1,buddingtonite1,a-chlorite, sphalerite4,acmite, sphalerite5, howlite,pectolite1

### 3 Conclusions

Independent component analysis on the Hyperion data of Erongo led us to present a modified algorithm in this study, as a previous method (WANG & CHANG 2006) was able to detect all possible ICs. Since some ICs share in extreme pixels, only eight ICs were detected by their method. The Hyperion scene is then classified by a spectral angle mapper using the spectral profiles of eight extreme pixels as endmembers. This classifier revealed that only six of them show considerable distribution on the study scene.

The presented method differs from theirs, as in this method extreme pixels for all 166 ICs are determined and all ICs with the same extreme pixels are considered equal. Prioritisation of the IC bands takes place afterward. Therefore, by this method 24 different extreme pixels were recognised, and like the first method, a spectral angle mapper was used for classification. The maps produced by these two methods demonstrate that the second algorithm performs better, because in addition to its ability to map more endmembers, the mapped zones match lithological structures better (Fig. 5 (a) and (b)).

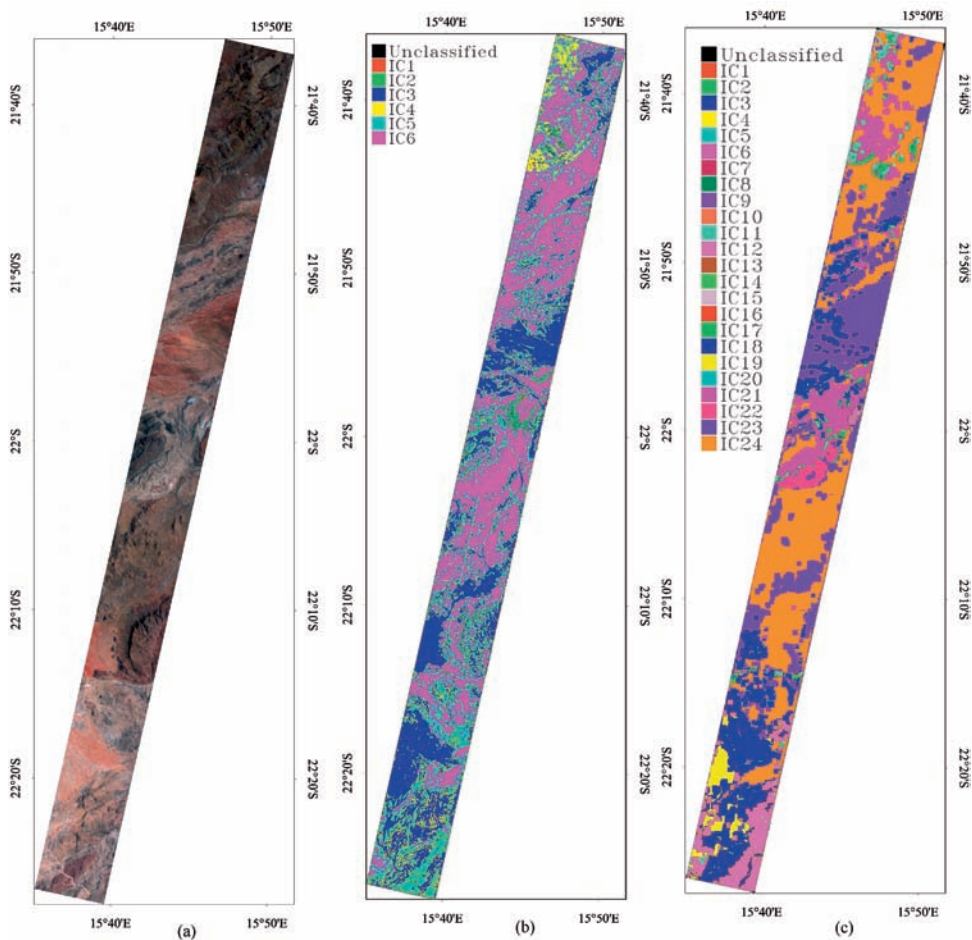


**Fig. 5:** RGB image of Hyperion data (a), ICs distribution map by the Chang method (b) and by the method presented here (c).

## References

- BAYLISS, J.D., GUALTIERI, J.A. & CROMP, R.F., 1998: Analysing hyperspectral data with independent component analysis. – SPIE International Conference, Washington, DC, 133–143.
- BOTCHKO, V., BERINA, E., KOROKAYA, Z., PARKKINEN, J. & JAASKELAINEN, T., 2003: Independent component analysis in spectral images. – 4th International Symposium on Independent Component Analysis and Blind Signal Separation, Nara, Japan, 203–207.
- CHANG, C.I. & DU, Q., 2004: Estimation of number of spectrally distinct signal sources in hyperspectral imagery. – IEEE Transactions on Geoscience and Remote Sensing **42** (3): 608–619.
- CHIANG, S.S., CHANG, C.I. & GINSBERG, I.W., 2000: Unsupervised hyperspectral image analysis using independent component analysis. – IEEE International Geoscience and Remote Sensing Symposium, 3136–3138.
- DU, Q., KOPRIVA, I. & SZU, H., 2006: Independent component analysis for hyperspectral remote sensing imagery classification. – Optical Engineering **45** (1): 17008.
- HARSANYI, J.C., FARRAND, W. & CHANG, C.I., 1993: Determining the number and identity of spectral endmembers: An integrated approach using Neyman-Pearson eigenthresholding and iterative constrained RMS error minimiza-

- tion. – 9th Thematic Conference on Geologic Remote Sensing, Pasadena, California, USA.
- HYVÄRINEN, A., 1999: Fast and Robust Fixed-Point Algorithms for Independent Component Analysis. – IEEE Transactions on Neural Networks **10** (3): 626–634.
- HYVÄRINEN, A. & OJA, E., 2000: Independent Component Analysis: Algorithms and Applications. – IEEE Transactions on Neural Networks **13** (4–5): 411–430.
- LENNON, M., MOUCHOT, M., MERCIER, G. & HÜBERT-MOY, L., 2001: Spectral unmixing of hyperspectral images with the independent component analysis and wavelet packets. – IEEE International Geoscience and Remote Sensing Symposium.
- MANOLAKIS, D., MARDEN, D. & SHAW, G.A., 2003: Hyperspectral Image Processing for Automatic Target Detection Applications. – Lincoln Laboratory Journal **14** (1): 79–166.
- NASH, G.D. & JOHNSON, J.W., 2002: Soil mineralogy anomaly detection in Dixie Valley, Nevada using hyperspectral data. – Twenty-Seventh Workshop on Geothermal Reservoir Engineering, Stanford University.
- OSKOUEI, M.M. & BUSCH, W., 2008: A geostatistically based preprocessing algorithm for hyperspectral data analysis. – GIScience & Remote Sensing **45** (3): 356–368.
- PEARLMAN, J., SEGAL, C., LIAO, L., CARMAN, S., FOLKMAN, M., BROWNE, B., ONG, L. & UNGAR, S., 2000: Development and operations of the eo-1 hyperion imaging spectrometer. – SPIE Conference on Earth Observing Systems **4135**: 243–254.
- SCHNEIDER, G.I.C. & SCHNEIDER, M.B., 2004: Gondwanaland Geopark. (Windhoek Cluster Office), Namibia.
- TU, T.M., CHEN, C.H., WU, J.L. & CHANG, C.I., 1998: A fast two-stage classification method for high dimensional remote sensing data. – IEEE Transactions on Geoscience and Remote Sensing **36**: 182–191.
- VARSHNEY, P.K. & ARORA, M.K., 2004: Advanced image processing techniques for remotely sensed hyperspectral data. – Springer, Berlin.
- WANG, J. & CHANG, C.I., 2006: Applications of independent component analysis (ICA) in endmember extraction and abundance quantification for hyperspectral imagery. – IEEE Transactions on Geoscience and Remote Sensing **44** (9): 2601–2616.
- WANG, J. & CHANG, C.I., 2006: Independent Component Analysis-Based Dimensionality Reduction with Applications in Hyperspectral Image Analysis. – IEEE Transactions on Geoscience and Remote Sensing **44** (6): 1586–1600.
- ZHENG, C.H., HUANG, D.S., SUN, Z.L., LYU, M.R. & LOK, T.M., 2006: Nonnegative independent component analysis based on minimizing mutual information technique. – Neuro Computing **69**: 878–883.

Address of the Author:

Dr. MAJID MOHAMMADY OSKOUEI, Faculty of Mining Engineering, Sahand University of Technology, Tabriz, Iran; Tel: +98(0)4123459-299, Fax: -299, e-mail: moskouei@yahoo.com

Manuskript eingereicht: Juni 2009

Angenommen: Dezember 2009



# Derivation of 3D Indoor Models by Grammars for Route Planning

GERHARD GRÖGER & LUTZ PLÜMER, Bonn

**Keywords:** 3D city models, spatial grammars, CityGML, indoor route planning

**Summary:** This paper presents a method to generate three-dimensional indoor building models and corresponding route graphs which are suitable for indoor route planning. The concept of attributed grammars is adapted to generate the indoor model which meets the two essential preconditions for the automatic derivation of connectivity information for route graphs: consistency, which enables the identification of neighbouring spaces, and the representation of semantics. The first precondition is met by implementing a model that has been developed earlier and which provably assures consistency between geometry and topology. This gives a contrast to earlier approaches for generating buildings by grammars. Topology is represented by constraints generated by the grammar rules and is maintained by constraint reasoning methods. Semantic aspects being relevant for deriving the connectivity relation between spaces are represented according to *CityGML*. The generation of the indoor model by grammar rules requires only a small number of observations, and the derivation of the route graph from the indoor model is accomplished automatically.

**Zusammenfassung:** Herleitung dreidimensionaler Innenraummodelle mit Grammatiken zur Planung von Wegen. Dieser Artikel beschreibt ein Verfahren zur Herleitung dreidimensionaler Innenraummodelle für Gebäude und der zugehörigen routingfähigen Graphen, die für die Planung von Wegen in Gebäuden geeignet sind. Das Konzept der attribuierten Grammatiken wird für die Erzeugung des Innenraummodells angepasst. Dieses Modell erfüllt die beiden entscheidenden Bedingungen zur Herleitung der Erreichbarkeitsinformationen für den routingfähigen Graphen: Konsistenz, die die Detektion benachbarter Räume ermöglicht, und die Repräsentation der Semantik. Die erstgenannte Bedingung ist durch die Nutzung eines bereits früher entwickelten Modells erfüllt, das die Konsistenz zwischen Geometrie und Topologie nachweisbar sicher stellt, im Gegensatz zu bisherigen Ansätzen zur Erzeugung von Gebäudemodellen mit Grammatiken. Die Topologie wird durch Constraints repräsentiert und durch Schlussfolgerungsmechanismen konsistent gehalten. Semantische Aspekte, die für die Herleitung der Erreichbarkeitsrelation zwischen Räumen relevant sind, werden in Anlehnung an *CityGML* repräsentiert. Die Erzeugung des Innenraummodells erfordert nur eine kleine Menge an Beobachtungen, und der routingfähige Graph wird automatisch aus dem Innenraummodell hergeleitet.

## 1 Introduction

Navigation and route planning are important applications in geo-information science. Whereas systems for outdoor navigation – car navigation, pedestrian navigation, etc. – are widely used nowadays, indoor navigation is still an active research area, e.g., PU &

ZLATANOVA (2005) or BECKER et al. (2009). Indoor navigation is more difficult, mainly for two reasons: First, positioning as prerequisite for navigation is more difficult indoor, since positioning systems like GPS which are used outdoor very successfully do not work indoor. Second, the spatial data required for navigation and route planning is mostly not available

for indoor scenarios (e. g., BECKER et al. 2009). This paper deals with the second problem.

For all route planning problems, indoor in rooms, floors and staircases as well as outdoor on streets, paths and places, a structure which represents connectivity and reachability explicitly as graph is an essential prerequisite. Such structures are called *route graphs*. In an outdoor environment, the edges of the graph typically represent street or path segments, and the nodes crossings or junctions where the segments meet. In an indoor environment, (parts of) rooms, hallways or staircases are modeled by nodes, while edges represent the reachability between the corresponding objects. In addition, route graphs store information relevant for route planning, like segment length, travel time for a segment, or constraints when a segment may be passed only in one direction, e. g., in a one-way street, or may not be passed by specific individuals, e. g., by handicapped persons, or by huge vehicles like trucks. Well known path finding methods like the algorithm of DIJKSTRA (1959) or its more efficient extensions, e. g., the *A\** algorithm (NORVIG & RUSSELL 2003), may be employed to derive optimal paths from route graphs.

In order to automatically derive route graphs from indoor building models, those models must meet two demands: First, *adjacency*, the immediate neighborhood between rooms, floors or stair cases, must be represented correctly, since adjacency is one precondition for the derivation of an edge of the route graph representing the reachability between rooms. The correctness of the adjacency relation is guaranteed only if the building model is geometrical-topologically consistent (GRÖGER & PLÜMER 2010).

Whereas adjacency is a *necessary* condition for reachability between two rooms or between indoor and outdoor, it is not a *sufficient* one: Two adjacent rooms are in a reachability relation, only if an opening or a door connects both. Hence, the adequate representation of *semantics* of the components of the building model is crucial for the derivation of route graphs. A model representing the semantics of buildings and indoor components is *CityGML* (GRÖGER et al. 2008, KOLBE et al. 2008), which addresses the aspect of indoor modeling, but does not solve the problem of geometric-topo-

logical consistency. This is not the intention CityGML was developed for, since it claims to model spatial base data regardless of specific applications. Consistency as aspect of data quality (GUPTILL & MORRISON 1995) is defined as ‘suitability for a specific purpose’ (ISO TC 211 2002), hence it often can be defined only in the context of a specific application.

A model guaranteeing the geometric-topological consistency provably, particularly for buildings and their interior structures, is defined in GRÖGER & PLÜMER (2010), see also Section 3. Methodically, this model is one essential base of the concepts presented in this paper.

The generation of 3D city and building models is also the intension of *spatial grammars*, particularly of *split grammars* (WONKA et al. 2003, MÜLLER et al. 2006). These constitute the second methodological base of the concepts presented in this paper. Split grammars model buildings by regular geometrical objects like cubes, but the problem of geometric-topological consistency is not addressed: these approaches do not claim to assure consistency. Penetrations of solids are not excluded explicitly, and in fact occur by rule applications.

The main contribution of this paper is a method to generate geometric-topological consistent indoor models, which allow for the derivation of route graphs. We show that the split grammars presented by WONKA et al. (2003) and MÜLLER et al. (2006) can be rephrased as attributed grammars and extend these approaches by providing an explicit representation of topology and by guaranteeing consistency. Our rules are a special case of the transaction rules in GRÖGER & PLÜMER (2009) and GRÖGER (2006).

For consistency, route planning is used as a benchmark: it poses a big challenge, since an existing path must be identified by the method, and since a derived path must in fact be passable. This paper links the topics geometry, topology and semantics: geometry and topology produce the route graph, which is the base for escape route planning. However, this structure is not sufficient, since semantics must be considered in addition.

The rest of this paper is organized as follows: In Section 2, related approaches to in-

door route planning as well as on the use of formal grammars for the derivation of 3D models are recapitulated. Section 3 introduces a geometric-topological 3D model for buildings, which is suited for the derivation of indoor models and for the representation of indoor reachability due to its consistency. The semantic aspects of indoor models are discussed in the Section 4 by introducing City-GML, which enables the representation of objects classes that are relevant for indoor route planning. Section 5 presents a grammar which generates geometric-topologically consistent, semantic indoor models from a minimal set of observations. The derivation of route graphs is supported by that model. The paper ends with concluding remarks and a discussion of open questions and future work.

## 2 Related Work

The problem of representing and deriving route graphs which are suitable for planning routes in buildings has been in discussion for about two decades, e.g., CHALMET et al. (1982), HOPPE & TARDOS (1995), LEE (2001), or PU & ZLATANOVA (2005), but has only partially been solved. LEE & KWAN (2005) introduce a graph called *Combinatorial Data Model (CDM)*, whose nodes represent rooms, while the edges describe the reachability relation between rooms. This relation is defined by the concept of Poincaré Duality (HATCHER 2001), which is based on the topological ‘meets’ relation provided by Egenhofer’s 4-intersection model (EGENHOFER & HERRING 1991). The embedding of the CDM in 3D space, called *Geometric Network Model (GNM)*, in addition enables the representation of metrical properties and multiple routes between two rooms. These approaches focus on the representation of graphs, but do not solve the problem of deriving those graphs from 3D models of the interior of buildings.

LEE & ZLATANOVA (2009) and MEIJERS et al. (2005) extend the GNM concept geometrical-  
ly by considering paths composed of edges, which are derived by a median axis transformation from ground plans of rooms or storeys. Such a graph embedded in the 2D plane is derived for each floor of a building, and these

plans are then linked by employing 2D overlay methods. These approaches define graphs suitable for route planning and its derivation from 2D floor plans, but do not provide any procedure how to derive such graphs from a 3D building model automatically and effectively. A pragmatic approach to tackle this problem (MEIJERS et al. 2005) is based on a procedure (VAN TREECK & RANK 2004) to correct geometric-topological errors (e.g., mutually penetrating faces, gaps between faces or neighboring solids) by merging polygons, line segments or points, which have a distance smaller than a certain threshold. This method, which generalizes 2D methods used in commercial GIS like *ArcInfo*, however, lacks a method to check whether the resulting structure is consistent.

In procedures to derive route graphs from indoor models, semantics is considered only in a few approaches. MEIJERS et al. (2005) classify vertical polygons separating two rooms according to its reachability function. They differentiate between ‘always passable’, ‘only with key passable’, ‘only in emergency case passable’, ‘bidirectional’ or ‘unidirectional passable’. ANAGNOSTOPOULOS et al. (2005) define an indoor ontology and extend the nodes and edges of route graphs by corresponding labels. A procedure to generate labeled graphs from 2D ground plans is drafted roughly.

LORENZ et al. (2006) propose the decomposition of rooms into *cells* to reflect that parts of a room differ with regard to reachability. Each cell is represented by a node in the route graph. This approach is restricted to a 2D representation of rooms and cells, and no procedure to automatically derive cells from rooms is given. BECKER et al. (2009) extend the GNM concept of LEE & KWAN (2005) as well as the cell decomposition by defining distinct models, called layers, for orthogonal indoor aspects with regard to escape route planning (room topography/topology, sensor transmission ranges). Each layer is represented separately, both as 3D model and corresponding graph. The spatial interaction of cells from different layers is represented explicitly by links between the corresponding nodes.

For deriving models of buildings, particularly for facades, outer hulls or interior structures, *formal grammars* (CHOMSKY 1959) play

a crucial role. In a spatial context, the special case of a *context free* or *type 2 grammar* is relevant. Such a grammar  $G = (T, N, S, P)$  is composed of five components:  $T$  is the set of *terminal symbols*,  $N$  the set of *non terminal symbols* ( $T \cap N = \emptyset$ ),  $S \in N$  is the *start symbol* and  $P$  is the set of *rules*. The elements of  $P$  have the structure  $A \rightarrow X$ , where  $A$  is a non terminal and  $X$  is a sequence (a string) of terminal and non-terminal symbols. The *language* generated by the grammar is the set of strings which consists of terminal symbols only, and which is obtained by subsequent applications of rules – replacement of a non-terminal  $A$  by the right-hand-side  $X$  of the corresponding rule – starting with  $S$ . In an *attribute grammar* (ALBLAS & MELICHAR 1991), a set of attributes is attached to the terminal as well as to the non terminal symbols. The value of an attribute is computed by a *semantic rule*, accompanying a grammar rule from  $P$ . If an attribute value attached to a (terminal or non-terminal) symbol on the right-hand-side of a grammar rule is computed by the values of the attributes on the left-hand-side, the attribute is called *inherited*. Vice versa, it is called *synthesized*, if a value attached to a left-hand-side symbol is derived from a value of a right-hand-symbol.

A grammar for the generation of spatial objects, called *shape grammar*, was developed by STINY & GIPS (1972) for architectural purposes. Such grammars operate on a purely geometrical level, not on a symbolical level of non-terminals, complicating the design of the rules. The *split grammars* presented by WONKA et al. (2003) can be interpreted as attribute grammars, which are used to generate building facades. The appearance of the facades and the design process are controlled by attributes attached to terminal or non terminal symbols. MÜLLER et al. (2006) extend this approach by generating the complete outer hull of buildings. Their grammar, which is called *CGA Shape*, contains rules which split a geometry shape, e.g., a polygon, into a sequence of polygons, according to a given ratio. An example for a split rule is given by

$$fac \rightarrow Subdiv('Y', 3.5, 0.3, 3, 3, 3) \{floor | ledge | floor | floor | floor\}$$

which splits the non terminal polygon *fac* into five parts along the y-axis, each having the length 3.5, 0.3, 3, 3, or 3, and the type *floor*, *ledge*, *floor*, *floor* or *floor*, respectively. To avoid occlusions of doors or windows by other parts of the building, a geometrical occlusion test is provided. Symmetry of the facades is achieved by introducing *snap lines*. The aim of the grammar of MÜLLER et al. (2006) is the generation of artificial spatial objects for movies or computer games, not the reconstruction of existing urban objects. The approach focuses on the generation of facades, not on interior building structures. The consistency of these models, however, is not intended by the grammar and achieved at most incidentally: there is no concept of sharing of common walls, and penetrations of objects are not prohibited. For the purpose of reconstruction, grammars are used by BRENNER & RIPPERDA (2006) and by MÜLLER et al. (2007) for facades, by DÖRSCHLAG et al. (2008) for buildings with detailed roof structures, and by SCHMITT-WILKEN et al. (2007) for different types of stairs.

### 3 3D Models Being Geometric-topologically Consistent

An essential prerequisite for the automatic derivation of route graphs from interior building models is consistency, particularly with regard to the neighborhood between rooms, but also between the outer hull and the interior of the building. Two neighboring rooms (solids) are not allowed to penetrate mutually, and gaps separating both solids are prohibited as well. The first requirement may be met by sharing common faces, while the second is guaranteed by a complete covering of the building's interior by solids. Both requirements constitute a *three-dimensional tessellation* of the interior of a building.

A model which meets both requirements and therefore is geometrical-topologically consistent is defined in GRÖGER & PLÜMER (2010). It is based on the concept of *cell complexes* (HATCHER 2001), which essentially requires that nodes, edges, faces and solids are either pair-wise disjoint or touch in their common boundaries. In the latter case, both touch

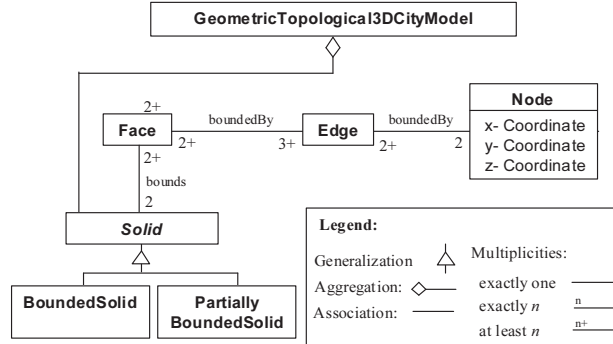


**Fig. 1:** UML-Diagram of the geometric-topological 3D model of GRÖGER & PLÜMER (2010).

in a common face, edge or node. To be more specific, when two solids touch, then they touch in a common face, if two faces touch, they touch in a common edge, and if two edges touch, they touch in a common node. A second condition is that 3D space is completely covered by solids, without any voids or hollow spaces not occupied by solids. Hence, two special solids are introduced: a solid representing the air space (which is bounded partially by the terrain and is not bounded from above) and one representing the earth's mass (which is bounded partially by the terrain and is not bounded from below). Hence, solids constitute a complete coverage of 3D space. An UML class diagram (BOOCH et al. 2005) of the model is depicted in Fig. 1. The model described so far defines consistency from a mathematical point of view. However, it does not provide a method to effectively and efficiently check whether a data set meets these requirements: It is not effective, since the complete covering by solids is not immediately checkable, and not efficient since the pair-wise test for penetrations or intersections is very expensive from a computational point of view. In GRÖGER (2006) and GRÖGER & PLÜMER (2010), this problem is solved by introducing so-called *axioms*, which are provably equivalent to the mathematical model described above, while being effectively and efficiently implementable. The pair-wise checking of penetrations and intersections is restricted locally to faces and edges in the boundary of a solid, hence avoiding the pair-wise consideration of all faces and edges.

## 4 Representation of Semantics

The geometrical-topological model presented in the last section is the base for defining semantic objects (often called *features*) which are relevant for modeling indoor structures and for route planning. A semantically very rich model for cities and urban objects is *City-GML* (GRÖGER et al. 2008, KOLBE et al. 2005, 2008), which is based on the *Geography Markup Language GML 3* (LAKE et al. 2004). GML is designed and widely used for data exchange in spatial data infrastructures.

CityGML defines specific levels of detail (LoD), which differ with regard to semantic and geometric resolution. The most detailed LoD4 enables the modeling of the outer hull and of interior structures of buildings. The corresponding UML diagram is given in Fig. 2. A building is defined geometrically by its outer hull (*Solid*), external constructions like balconies and dormers (*BuildingInstallations*), and *Rooms*, which may contain immovable installations (*BuildingInstallations*) like stairs or pillars, or mobile objects (*BuildingFurnitures*) like desks or chairs. Rooms are represented geometrically by solids, and are bounded by thematic surfaces (*InteriorWallSurface*, *CeilingSurface*, *FloorSurface*), which may contain *Openings*. i. e., *Doors* and *Windows*.

Hence, CityGML meets the basic semantic requirements of indoor modeling for route planning. For special cases, e. g., planning of escape routes, more detailed semantic specifications of features are needed, e. g., the repre-

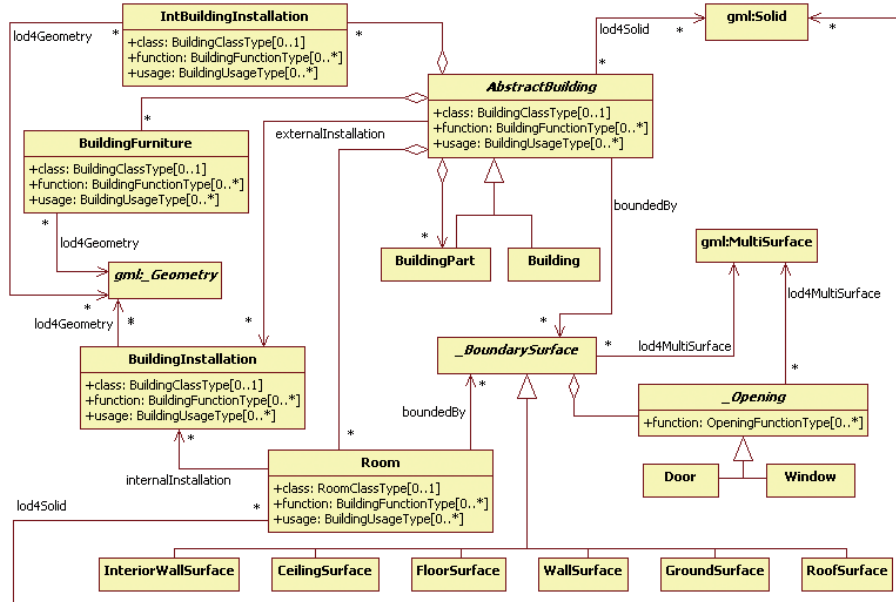


**Fig. 2:** Modeling of buildings and its internal structures in *CityGML* (GRÖGER et al. 2008). The UML diagram depicts the most detailed Level-of-Detail 4.

sentation of fire protection classifications of doors, or of the side to which a door may be opened. These requirements can be included by the object-oriented concept of *Application Domain Extensions*, which is provided by CityGML to extend the model in a seamless and consistent way.

In the UML diagram, the spatial representation of features is given by geometric objects viz. *Solids*, *MultiSurfaces*, or *Geometries*. Additionally, these objects may be defined by corresponding topological primitives provided by GML – nodes, edges, faces, and topological solids. These data types cover the ones of the model described in the last section. Hence, CityGML is suitable for representing the geometric-topological model described in Section 3 and will be used to represent and provide the building model derived by the grammar.

To summarize the related approaches presented so far, a model representing geometry and topology in a consistent way is available, and semantics is provided by CityGML. What is missing is a method to derive consistent, semantic building models, which are a suitable base to derive route graphs for indoor route planning, and a method to automatically de-

rive such graphs from indoor models. Approaches to cope with both tasks will be provided in the following sections.

## 5 A Grammar for the Generation of Interior Building Models

In this section, an attribute grammar for the construction of building models with interior structures is presented. This grammar generates models which firstly are geometrical-topologically consistent (cf. Section 3), which secondly include the semantics which are mandatory to compute routes (cf. Section 4) and which thirdly require only a few observations to be generated, starting with the exterior hull of a building. In contrast to the grammar presented by MÜLLER et al. (2006), our approach guarantees consistency.

When grammar rules are applied in order to construct buildings by splitting objects, as in, e.g., MÜLLER et al. (2006), the context of rule applications and the ‘knowledge’ is local, restricted to the object which is split. In contrast, concepts of consistency and reachability are more global, and therefore require informa-

tion about objects which are close spatially, but ‘remote’ from a grammar derivation point on view. When a box  $B$  is split, for example, the inserted separating face is prohibited to interact with a door which has been inserted in a wall of a box adjacent to  $B$  by a previous rule application. This interaction would yield an error with regard to reachability and consistency. We solve this problem of combining local rules and global concepts of topology and reachability by introducing a global *constraint store*, which contains constraints providing the knowledge to prevent such error cases where a door and a wall interact in an inconsistent way. These constraints are generated by rule applications and explicitly formalize the concepts of adjacency, reachability and semantics.

### 5.1 Representation of Geometry and Topology by Constraints

The restriction of the geometry to boxes enables a simple representation of the model presented in Section 3. In Section 5.5, we will discuss how irregularly shaped buildings and rooms can be generated by aggregating boxes. We assume that the sides of the box are parallel to the axes of the coordinate systems; an affine transformation can be applied afterwards to transform the model to its location in geographic or geodetic space. Such a box can geometrically be represented uniquely by two corner points  $P_1 \in \mathbb{R}^3$  and  $P_2 \in \mathbb{R}^3$ , such that the absolute values of the three components of the difference  $P_1 - P_2$  are equal to the three side lengths the box.

Topology is represented explicitly by *constraints* stating relationships between faces. We consider the following three types of constraints:

- *Equality constraints*

When two boxes share a common face, or when a wall surface shares a face with a box, the two corresponding faces  $F_1$  and  $F_2$  are identical, i. e., they denote the same face. This is stated by an equality constraint

$$\text{equals}(F_1, F_2).$$

- *Aggregation constraints*

When a box is split, the bounding faces are split accordingly. The relation of the original face (say,  $F$ ) to the two resulting disaggregated faces (namely,  $F_1$  and  $F_2$ ) which have been split is stated explicitly by a ternary aggregation constraint

$$\text{aggr}(F, F_1, F_2).$$

The meaning of that constraint is that face  $F$  is the aggregation of faces  $F_1$  and  $F_2$ , or vice versa, that the interiors of  $F_1$  and  $F_2$  are disjoint and that the union of  $F_1$  and  $F_2$  yields  $F$ .

- *Containment constraints*

When an opening (face  $F_1$ ) is inserted into a wall (face  $F_2$ ), this relation is explicitly represented by a containment constraint

$$\text{inside}(F_1, F_2).$$

The face  $F_1$  is contained in  $F_2$ , i. e., the point set representing  $F_1$  is a subset of the point set representing  $F_2$ . Note that the boundaries of  $F_1$  and  $F_2$  do not have to be disjoint.

All constraints are generated by the applications of grammar rules and are collected in the constraint store. By applying geometrical constraint solving and reasoning methods to this set of constraints and the box geometry, topology can be derived. This kind of topological reasoning is similar to the approach presented in EGENHOFER (1991).

The constraints considered in this paper differ from the binary relations of the 4-intersection model (EGENHOFER & FRANZOSA 1991) and its 3D extensions (ZLATANOVA 2000): whereas the *equals* relation is the same, our *inside* denotes Egenhofer’s relation *inside* as well as *coveredBy*. The aggregation constraint goes beyond the relations of the 4-intersection model, since it states that one face is equal to the disjoint union of two other faces.

### 5.2 Symbols and Attributes

The components of the grammar  $G = (N, T, S, P)$  for the construction of building models are defined as follows: The set  $N$  of non-terminal

symbols<sup>1</sup> is  $\{S, Box, Rectangle\}$ , where  $S$  is the start symbol, and the set  $T$  of terminal symbols is  $\{box, rectangle, internalDoor, externalDoor, window\}$ . The non-terminal symbol  $Box$ , which represents either a building, a storey, a part of a storey or a room, has the following attributes:

- The geometry of a  $Box$  is given by two corner points  $P_1, P_2 \in \mathbb{R}^3$ , as introduced above.
- The six rectangular faces bounding the  $Box$  are specified implicitly by six attributes  $F_1, \dots, F_6$  of type  $rectangle$ . Each  $F_i$  is characterized by two Boolean values  $OuterFace$  resp.  $VerticalSeparatingFace$ , which are *true* if and only if the rectangle is in the outer hull of the buildings resp. is a vertical rectangle separating rooms. Both values are used to denote potential positions for windows and (internal and external) doors. By a naming schema (cf. the presentation of rule R1), the six faces  $F_1, \dots, F_6$  are uniquely assigned to the six bounding faces of a box. Hence, the geometry of each of the  $F_i$  can be derived anytime from the corresponding box geometry.
- The thematic classification of a box is denoted by a  $Type$  attribute. Possible values are  $\{Building, BuildingPart, Storey, StoreyPart, Room, Hall, Staircase\}$ .

The attributes of a terminal  $box$  symbol are identical to the attributes of non terminal  $Box$ . A non-terminal  $Rectangle$  represents a thematic surface, e.g., a wall or a roof surface. Its attributes are a  $Type$  with potential values  $\{Wall, Ceiling, Floor\}$  and a geometry  $Geom$  which represents the extent of the surface by two points  $P_1, P_2 \in \mathbb{R}^3$ . Again, the attributes of the terminal  $rectangle$  symbol are the same. The terminal symbols  $internalDoor$ ,  $externalDoor$  and  $window$  have only a  $Geom$  attribute which is defined accordingly.

### 5.3 Rules

The grammar rules are enhanced by parameters, whose values are instantiated when the rule is applied. These values typically emerge from observations and are denoted in brackets, following the left hand non-terminal symbol. According to the concept of *guarded horn clauses* (UEDA 1985), a rule may have a precondition or *guard*, which prevents rule applications yielding an inconsistent state. In general, a rule can only be applied if the guard, which is a Boolean expression, yields true. This concept is also used in the *CGA shape grammar* of MÜLLER et al. (2006).

Now the set  $P$  of grammar rules which consists of the rules R1 to R8 is introduced:

**R1:**  $Box (Direction, Ratio, Type_1, Type_2): Pre \rightarrow Box^1 Box^2$

This rule splits a box, denoted by the non-terminal  $Box$ , in two boxes, namely  $Box^1$  and  $Box^2$ , if the guard  $Pre$  holds true; this will be explained later. The three non-terminals  $Box$  denote the same symbol but differ with regard to the attribute values; hence they are differentiated by superscript indices.  $Direction$ ,  $Ratio$ ,  $Type_1$  and  $Type_2$  are parameters. The direction of the split, either along the x-, the y- or the z-axis, is denoted by a parameter, as well as the split  $Ratio$  in the range  $0 < Ratio < 1$ . The thematic classifications of the resulting boxes are given by two parameters  $Type_1$  und  $Type_2$ . In the following, the case  $Direction = 'x'$  is considered only; the other cases are defined accordingly. The geometrical aspect of rule R1 is implemented by a semantic rule  $S_1^1$ , which uses a procedure *split* to compute the corner points of both new boxes  $Box^1$  and  $Box^2$ :

**$S_1^1:$**   $(Box^1, Box^2) = split(Box, Direction, Ratio)$

The result of this rule is the computation of the corner points of the new boxes. Hence,  $P_1$  and  $P_2$  are inherited attributes. The calculations are carried out by the following constraints, which are added to the constraint store (again, the case  $Direction = 'x'$  is considered):

<sup>1</sup> As usual, non-terminal symbols start with an upper-case letter and terminals with a lower-case letter.

- $\text{Box}^1.P_1 = \text{Box}.P_1$
- $\text{Box}^2.P_2 = \text{Box}.P_2$
- $\text{Box}^1.P_2 = (\text{Box}.P_1.x + |\text{Box}.P_2.x - \text{Box}.P_1.x| * \text{Ratio}, \text{Box}.P_2.y, \text{Box}.P_2.z)$
- $\text{Box}^2.P_1 = (\text{Box}.P_1.x + |\text{Box}.P_2.x - \text{Box}.P_1.x| * \text{Ratio}, \text{Box}.P_1.y, \text{Box}.P_1.z)$

A second semantic rule accompanying the grammar rule R1 generates the following seven constraints and adds them to the constraint store:

- $C_1^1: \text{equals}(\text{Box}^1.F_1, \text{Box}.F_1)$
- $C_1^2: \text{equals}(\text{Box}^2.F_3, \text{Box}.F_3)$
- $C_1^3: \text{equals}(\text{Box}^1.F_3, \text{Box}^2.F_1)$
- $C_1^4: \text{aggr}(\text{Box}.F_2, \text{Box}^1.F_2, \text{Box}^2.F_2)$
- $C_1^5: \text{aggr}(\text{Box}.F_5, \text{Box}^1.F_5, \text{Box}^2.F_5)$
- $C_1^6: \text{aggr}(\text{Box}.F_6, \text{Box}^1.F_6, \text{Box}^2.F_6)$
- $C_1^7: \text{aggr}(\text{Box}.F_4, \text{Box}^1.F_4, \text{Box}^2.F_4)$

These equations completely specify the topological relations between the faces bounding the origin  $\text{Box}$  and the faces bounding the boxes  $\text{Box}^1$  and  $\text{Box}^2$ . Fig. 3 illustrates these relations between faces by giving an example of the application of rule R1. If the common face  $\text{Box}^1.F_3$  is vertical, the attribute *VerticalSeparatingFace* is set to *true*.

The precondition for splitting a box by rule R1 is that the inserted face which separates  $\text{Box}^1$  from  $\text{Box}^2$  does not split or affect an existing opening, viz. an internal or external door, or a window. This is prevented by the guard *Pre* of R1, which operates as follows:

First, all openings in face  $\text{Box}.F_4$  or in face  $\text{Box}.F_2$  – the faces affected by the face to be inserted – are determined. Note that an opening is related to a wall by the relation *inside* (cf. the discussion of rule R4 below), and that a wall is related to the corresponding face of a box by an *equals*-constraint (cf. rule R3 below). The procedure *collectOpenings*, the pseudo code of which is given now, returns a list of all openings in a face  $F$ :

```

Procedure List(Openings)
  collectOpenings(rectangle F)
    //First case: F has not been split (***
     denotes an arbitrary value)
    if there is no constraint aggr( $F, *, *$ )
      then return all openings o with
        equals( $F, W$ ) and inside( $o, W$ )
      else //second case: F has been split:
        recursive calls for both faces
        select  $F', F''$  with aggr( $F, F', F''$ )
        return collectOpenings( $F') \cup$ 
          collectOpenings( $F''$ )

```

For the set of openings collected by the procedure, it has to be assured that all are disjoint to the face  $\text{Box}^1.F_3$  resp.  $\text{Box}^2.F_1$  inserted by rule R1. Equivalently, all openings have to have the relation *inside* to either  $\text{Box}^1.F_4$ ,  $\text{Box}^1.F_2$ ,  $\text{Box}^2.F_4$  or  $\text{Box}^2.F_2$  (cf. Fig.3). This topological relation can be checked by implementing a corresponding predicate *inside* and then by analyzing the constraint store.

Now all prerequisites for the implementation of the precondition *Pre* of rule R1 have

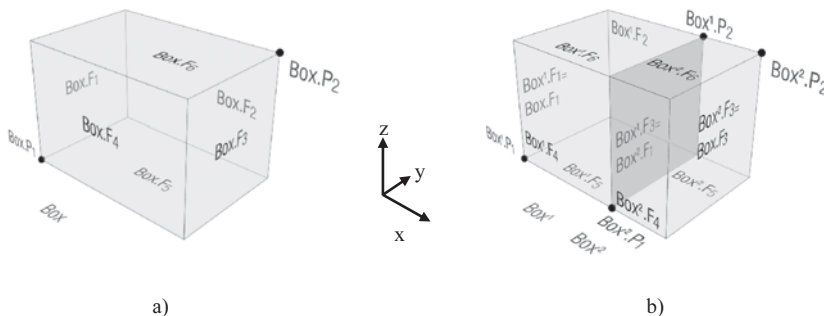


**Fig. 3:** Example for the application of rule R1. a) box before and b) after rule application with values *Direction* = ,*x'* and *Ratio* = 0.7. The rectangle shared by  $\text{Box}^1$  and  $\text{Box}^2$  is depicted in grey color.

been introduced. It is as follows (again in pseudo code):

```
Pre: List(Openings) LO = collectOpenings(Box.F2) ∪ collectOpenings(Box.F4);
      if for all openings o in LO either
        inside(o, Box1.F4) or inside(o, Box1.F2)
        or inside(o, Box2.F4) or inside(o, Box2.F2)
      then return true;
      else return false;
```

Note that a non-terminal symbol that has been replaced by a rule application and does not occur on the right-hand side of the rule is not deleted as in standard grammars, but is labeled as non-replaceable. Particularly, all attributes are still available, since they are required to reconstruct topology and geometry.

The next rule is applied to a non-terminal *Box* symbol if it is not intended to split it any further or to derive any wall symbol from its boundary; it becomes a terminal *box* symbol. The rule is applicable only if the type of the *Box* is allowed in terminal boxes, i. e., if the type is *Room*, *Hall* or *Staircase*. This is assured by a precondition:

```
R2: Box: Box.Type ∈ {Room, Hall,
                      Staircase} → box
```

The attribute values of *box* are obtained by copying the values of *Box*.

The third rule takes one of the six faces bounding a box and designates it explicitly as semantic surface object, viz. a wall, a ceiling or a ground surface, according to CityGML. One purpose of the rule is to construct a rectangle in which an opening, i. e., a door or a window, can be inserted afterwards. The geometry of the rectangle is given by a variable *Index* ( $1 \leq \text{Index} \leq 6$ ), which refers to the numbering of boxes' faces (see Fig. 3).

```
R3: Box (Index, Type): Type ∈ {Wall,
                                 Ceiling, Floor} → Box Rectangle
```

The following constraints are added to the constraint store by rule R3:

```
C31: equals(Rectangle.Geom, Box.
           FIndex)
```

and the attribute *Rectangle.Type* is set to the value of *Type*.

The next rule inserts a rectangular opening into a rectangle derived by rule R3. The geometry of an opening is specified by two points  $P_1, P_2 \in \mathbb{R}^3$ :

```
R4: Rectangle (P1, P2): Pre → Rectangle
      interiorDoor
```

The geometry of the terminal *interiorDoor* is derived from the opposite corner points  $P_1$  and  $P_2$ . Four preconditions, the conjunction of which is denoted by *Pre*, have to be fulfilled before R4 can be applied: 1) The geometry of the *interiorDoor* has to be disjoint to other openings, 2) the geometry of the *interiorDoor* has to be disjoint to the boundary of other faces, 3) the *Rectangle* has to be vertical (*Rectangle.VerticalSeparatingFace = true*), and 4) both points  $P_1$  and  $P_2$  have to be inside the *Rectangle*. The first precondition is similar to the one introduced in R1 and can be implemented accordingly by using the procedure *collectOpenings*. The second one again is similar to the one of R1 which avoids conflicts between walls and openings.

The rule R4 adds a single constraint to the store, which states that the opening is inside the wall face:

```
C41: inside(interiorDoor.Geom,
           Rectangle.Geom)
```

In a similar fashion, rules for inserting exterior doors and windows are provided, which differ only with regard to the third precondition: it is replaced by *Rectangle.OuterFace = true*. Exterior doors are inserted by the rule

```
R5: Rectangle (P1, P2): Pre → Rectangle
      exteriorDoor
```

whereas the windows are covered by rule R6, where again the third precondition is *Rectangle.OuterFace = true*:

```
R6: Rectangle (P1, P2): Pre → Rectangle
      window
```

The following rule replaces a non terminal rectangle by a terminal one, copying all attributes:

```
R7: Rectangle → rectangle
```

The following constraint is added to the store:

```
C71: equals(Rectangle.Geom,
           rectangle.Geom)
```

Finally, a rule generates an initial *Box* from the start symbol *S*, by providing a 3D point *P*. The box is defined by two opposite points, the origin  $(0, 0, 0)$ <sup>c</sup> and *P*, as described above:

**R8:**  $S(P) \rightarrow Box$

The attributes of *Box* are initialized accordingly, and the values  $Box.F_i.OuterFace = true$  and  $Box.F_i.VerticalSeparatingFace = false$  are set for all faces  $F_i$ ,  $1 \leq i \leq 6$ . The attribute *Box.Type* is set to the value ‘Building’.

To generate an indoor model by applying the rules R1 to R8, only a small set of observations is required. The outer hull of a building is represented by three values (length, width, height), and for each splitting step only the split direction and one value are necessary: the storey height or the room length or depth. For each door or window, only two points denoting its position relative to the wall are necessary. For the operational formalization and processing of the grammar rules, the Java-based *XGep* tool (SCHMITTWILKEN et al. 2009), which has been developed at the Institute for Geodesy and Geoinformation, is suitable. The sequence of grammar rule calls, including the required parameter values, can be represented in an XML structure which is immediately processed by *XGep*.

If an indoor model, e.g., a CAD (Computer Aided Design) model, is already available, a conversion tool can be developed that generates the XML structure, which is processed by the *XGep* tool and initiates the sequence of rule calls. If the structure of the indoor model corresponds to the model generated by the grammar (box-like structure), this conversion can be done automatically. Hence, a CAD model can be converted in a model the consistency of which is guaranteed. Likewise, 2D floor plans can be used to activate corresponding grammar rule calls for splitting storey boxes, yielding an indoor model for the corresponding storey.

#### 5.4 Examples

The stepwise generation of a building with interior structures by applying rules R1 to R8 is exemplified in Fig. 4. From the start symbol *S* and parameter value  $P = (10, 14, 6)$ , a *Box* with

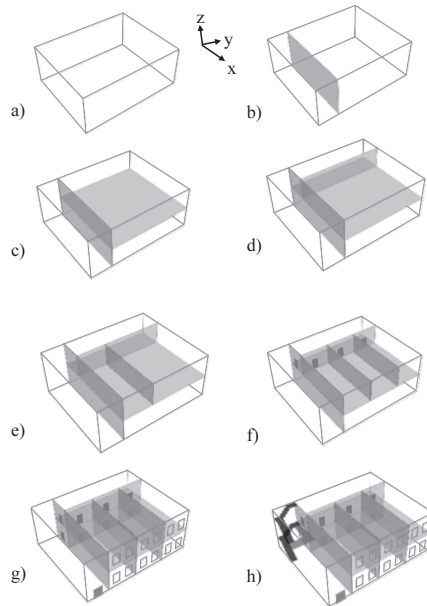


**Fig. 4:** Stepwise generation of a building with interior structures by applications of grammar rules. The stairs in h) can be obtained by additional grammar rules provided by SCHMITTWILKEN et al. (2007).

corresponding lengths of its sides and six faces is derived (a) by rule R8. Applying R1 (*Direction* = ‘*y*’, *Ratio* = 0.15, *Type*<sub>1</sub> = ‘Staircase’, *Type*<sub>2</sub> = ‘BuildingPart’) to *Box*, the structure in Fig. b) results, which consists of *Box*<sup>1</sup> and *Box*<sup>2</sup> with corresponding attribute values. A face (depicted in dark color) is shared by both boxes. Now *Box*<sup>2</sup> is split, by application of rule R1 with *Direction* = ‘*z*’, *Ratio* = 0.5 and *Type*<sub>1</sub> = *Type*<sub>2</sub> = ‘Storey’ (Fig. 4c). Afterwards, the upper storey is split in x-axis direction (Fig. 4d), with *Type*<sub>1</sub> = ‘Floor’ and *Type*<sub>2</sub> = ‘StoreyPart’. The *Box* with *Type* ‘StoreyPart’ again is split in y-direction by Rule R1 (*Type*<sub>1</sub> = ‘Room’ and *Type*<sub>2</sub> = ‘StoreyPart’), yielding the structure in Fig. 4e.

Afterwards, the resulting ‘*StoreyPart*-*Box*’ is split by R1 in two *Rooms* (f). Now, two non-terminal *Rectangles*, namely *Rectangle*<sup>1</sup> and *Rectangle*<sup>2</sup>, are generated by applying rule R3 to the *Box* with type ‘*Floor*’, first with index 4 and second with index 3, according to the naming schema (cf. Fig. 3). In both applications of R3, the *Type* parameter is set to ‘*Wall*’.

By applying rule R4 once to *Rectangle*<sup>1</sup> and three times to *Rectangle*<sup>2</sup>, four internal doors are inserted (Fig. 4f). Note that topology, i. e., the adjacency between the 'floor' Box and the 'Room' Box, for example, is represented explicitly by constraints, particularly by equations. Hence, the reachability relation between rooms can easily be derived by considering these adjacencies and semantics, i. e., a *Door* in a *Rectangle*.

The lower storey is generated in a similar fashion, and windows are inserted by applications of rule R6, in the same way as doors have been inserted by rule R4. Finally, rule R5 inserts an exterior door (Fig. g). The insertion of stairs, as depicted in Fig. h), can be achieved by the grammar presented by SCHMITTWILKEN et al. (2007). Fig. 5 depicts the derivation tree of the rule applications, which corresponds to the generation of the building in the example.

A more detailed view on the constraints is given in Fig. 6, which depicts a slightly modified clipping of the previous example. A door *D* is to be inserted in a wall *W* by rule R6. The scene is represented by the constraints (only the relevant ones are given):

*C*<sup>1</sup>: *equals*(*Box*<sup>1</sup>.*F*<sub>3</sub>, *Box*<sup>2</sup>.*F*<sub>1</sub>)  
*C*<sup>2</sup>: *aggr*(*Box*<sup>1</sup>.*F*<sub>3</sub>, *Box*<sup>21</sup>.*F*<sub>1</sub>, *Box*<sup>22</sup>.*F*<sub>1</sub>)  
*C*<sup>3</sup>: *equals*(*Box*<sup>21</sup>.*F*<sub>1</sub>, *W*.*Geom*)

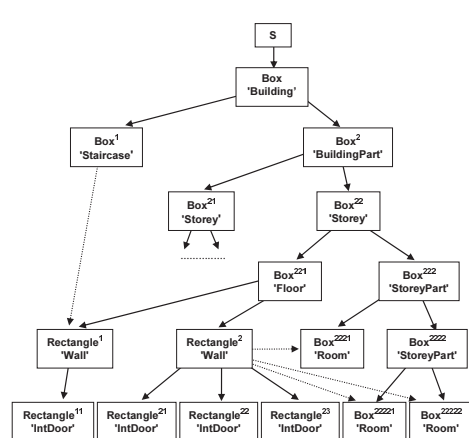


**Fig. 5:** Derivation tree for the generation of the building in Fig. 4. Bold arrows: rule applications; dotted arrows: relations derived from the constraints. The step of replacing a non terminal by a corresponding terminal is omitted.

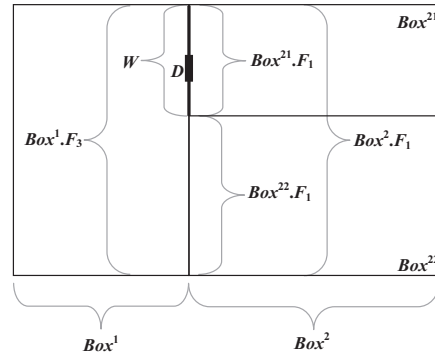


**Fig. 6:** Indoor scene where a door *D* is inserted in a wall *W* (view from above). From the constraints, it can be deduced that *W* and hence *D* are in the boundary of both *Box*<sup>1</sup> and *Box*<sup>21</sup>.

From *C*<sup>1</sup>, *C*<sup>2</sup> and *C*<sup>3</sup> it can be deduced that *W* is part of the boundary of *Box*<sup>1</sup> as well as of *Box*<sup>21</sup> (*C*<sup>3</sup> only), hence the door *D* can be inserted, which connects both rooms represented by *Box*<sup>1</sup> and *Box*<sup>21</sup>, and the constraint

*C*<sup>4</sup>: *inside*(*D*.*Geom*, *W*.*Geom*)

is added to the store.

## 5.5 Extension to Extruded Simple Polygons

The concepts introduced so far aim at generating box-shaped rooms and interior structures from box-shaped building hulls. However, in reality buildings and rooms often have a more irregular, typically L-, T- or X-shaped, structure. We now sketch how to generalize our data types as well as our rules to cope with such irregular shapes. Nearly all buildings and interior structures can be represented by polygonal footprints with right angles, where the floors are horizontal and the walls are vertical. Such structures are called *prisms* in our paper. Our prisms are special cases of general prisms, since all side surfaces are vertical and all angles are 90°.

For adapting our concept to prisms, only a few local changes of the rules are required. Since each prism can be generated by successively splitting boxes in both directions, we

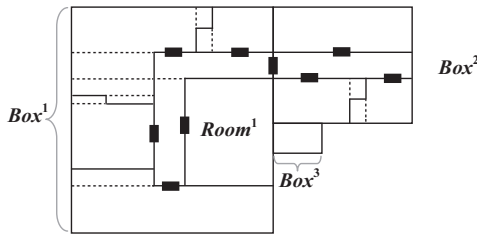


**Fig. 7:** Irregularly shaped footprint of an L-shaped building, which has been generated by splitting boxes and merging boxes belonging to the same room (separated by dotted lines).

only need to extend our approach by an aggregation concept for boxes that defines which boxes belong to the same feature (building, storey, room, ...). This aggregation can be represented by additional constraints. Depending on those constraints it can be determined whether a side of a box is a wall or just a separation between boxes of the same object; in that case, it is labeled as ‘invisible’. Fig. 7 gives an example: We start with three boxes forming a L-shaped building with a protrusion. By splitting boxes (application of a modified rule R1) a polygonal footprint is generated. *Room<sup>1</sup>*, for example, is generated by splitting *Box<sup>1</sup>* two times in different directions. The dotted lines indicate that different boxes belong to the same feature (room). The detailed design of rules for generating complex prism structures will be the topic of a subsequent paper. A further extension of the approach to extruded polygons with arbitrary angles can be achieved by additional rules which modify walls locally by applying rotations; the (local) topology has to be updated consistently.

## 5.6 Derivation of Route Graphs

Based on the building model and the constraints generated by the grammar, the method which derives a route graph  $RG = (Nd, Ed)$  automatically that represents the reachability inside a building is straightforward. In that graph,  $Nd$  is a set of nodes and  $Ed$  a set of un-directed edges. In pseudo code notation, the method to derive the route graph is as follows:

**Input:** A derivation tree generated by the grammar

**Output:** A route graph  $RG = (Nd, Ed)$  representing reachability

1.  $Nd = \emptyset; Ed = \emptyset$ :
2. For each terminal *room*, *hall* or *staircase* generated by the grammar, a node is added to  $Nd$ .
3. For each terminal *internalDoor*:
  - a. get the related *wall* rectangle terminal *w* (using constraint *inside*)
  - b. get the two *room/hall/staircase* terminals *b<sub>1</sub>* and *b<sub>2</sub>* related to *w*, by analyzing the constraint store
  - c. add an edge relating the nodes corresponding to *b<sub>1</sub>* and *b<sub>2</sub>* to the set  $Ed$
4. Add an additional node representing the space outside the building to  $Nd$ , at least one for each *externalDoor*, and add corresponding edges to  $Ed$ . The nodes may be connected to the outdoor network.

To extend the method to planning of escape routes, additional edges and nodes have to be considered. Escape routes using windows near ground can be incorporated, since those windows can be detected by using the three-dimensional geometry provided by the model. Those cases can be treated similar to exterior doors, by providing an additional node outside the building which is connected with the corresponding node representing the room. This will be the topic of a subsequent paper.

## 6 Conclusions

In this paper, we have introduced a grammar which generates buildings and their interior structures. It requires only a small set of observations. In contrast to earlier grammar approaches, e. g., MÜLLER et al. (2006), our grammar generates buildings which are geometric-topologically consistent. This is due to the explicit representation of topology: the adjacency between solids, viz. rooms, floors or staircases, is represented explicitly by constraints stating the identity of shared faces, and that adjacency representation is maintained when solids or faces are split. Hence,

the topology can be generated on demand. Consistency between geometry and topology is assured by using the model introduced by GRÖGER & PLÜMER (2010) where consistency is guaranteed by formal proofs. Once the correct topology is given, the derivation of a route graph which represents the reachability relation inside and outside the building and is suitable for indoor navigation is straightforward. This is due to the correct topology and the representation of semantics as provided by *City-GML*. The semantic information is generated by the grammar, simultaneously to the derivation of geometry and topology. A concept to deal with more complex building hulls and interior structures has been presented; its implementation requires only local modifications and extensions of the grammar rules. This will be elaborated in detail as the next step.

A further step will be the addition of rules which allow for the generation of more features inside and outside buildings, like balconies, pillars and furniture. Stairs can be incorporated by importing the grammar of SCHMITZWILKEN et al. (2007), and a more precise geometrical description of edges by using skeleton algorithms, as proposed by LEE & ZLATANOVA (2009) or MEIJERS et al. (2005).

An interesting and relevant extension of the concept will be the incorporation of *escape routes* as a special case of indoor route planning. The problem of automatically deriving route graphs suitable for finding optimal escape routes in the case of an emergency is much more difficult than ordinary indoor route planning. In an emergency case, the options to leave a building are much more multifaceted: Emergency exits or fire escapes which are usually closed may be used, or balconies or windows at or near ground level. Even balconies or windows far beyond ground level are suitable, when fire ladders or other rescue facilities, e.g., extension masts or rescue nets, are provided. In addition, persons may be evacuated from roofs by helicopters. Hence, the interface between indoor and outdoor is crucial for the derivation of escape routes. A more sophisticated notion of neighborhood between reachable spaces is required to cope with such cases. This extension requires in addition the enrichment of the generated model, since the roof type, for example, must be con-

sidered as well as the terrain surrounding a building.

## Acknowledgements

The authors appreciate the helpful and detailed comments given by the anonymous reviewers. We thank Jan Prinz for proof-reading and improving the English language and style of this text and Gerrit Kowatsch for assistance in preparing the illustrations.

## References

- ALBLAS, H. & MELICHAR, B. (eds.), 1991: Attribute Grammars, Applications and Systems. – Int. Summer School SAGA, Lecture Notes in Computer Science **545**, Springer, Berlin.
- ANAGNOSTOPOULOS, C., TSETOS, V., KIKIRAS, P. & HADJIEFTHYMADES, S., 2005: OntoNav: A semantic indoor navigation system. – 1st Workshop on Semantics in Mobile Environments (SME'05) in conjunction with the 6th Int. Conf. on Mobile Data Management (MDM'05).
- BECKER, T., NAGEL, C. & KOLBE, T.H., 2009: A Multilayered Space-Event Model for Navigation in Indoor Spaces. – 3D Geo-Information Sciences, Lecture Notes in Geoinformation and Cartography, Springer, Berlin, 61–78.
- BOOCHE, G., RUMBAUGH, J. & JACOBSON, I., 2005: Unified Modeling Language User Guide. – Addison-Wesley Longman.
- BRENNER, C. & RIPPERDA, N., 2006: Extraction of Facades Using RJMCMC and Constraint Equations. – Int. Archives of Photogrammetry, Remote Sensing and Spatial Information Sciences **36** (3): 165–170.
- CHALMET, L.G., FRANCIS, R.L. & SAUNDERS, P.B., 1982: Network Models for Building Evacuation. – Management Science **28** (1): 86–105.
- CHOMSKY, N., 1959: On Certain Formal Properties of Grammars. – Information and Control **2**: 137–167.
- DIJKSTRA, E.W., 1959: A note on two problems in connexion with graphs. – Numerische Mathematik **1**: 269–271.
- DÖRSCHLAG, D., GRÖGER, G. & PLÜMER, L., 2008: Über die schrittweise Erstellung und Verfeinerung von Modellhypthesen für Gebäude. – Photogrammetrie – Fernerkundung – Geoinformation **3/2008**: 157–164.

- EGENHOFER, M.J., 1991: Reasoning about binary topological relations. – *Advances in Spatial Databases. Lecture Notes in Computer Science* **525**: 143–160, Springer, Berlin.
- EGENHOFER, M.J. & FRANZOSA, R.D., 1991: Point-Set Topological Spatial Relations. – *Int. Journal of Geographical Information Science* **5** (2): 161–174.
- EGENHOFER, M.J. & HERRING, J.R., 1991: Categorizing binary topological relationships between regions, lines and points in geographic databases. – Technical Report, Department of Surveying Engineering, University of Maine, Orono, ME.
- GRÖGER, G., 2006: Konsistente Modellierung virtueller Städte und Regionen. – Habilitation Thesis, University of Bonn.
- GRÖGER, G., KOLBE, T.H., Czerwinski, A. & NAGEL, C., 2008: OpenGIS City Geography Markup Language (CityGML) Encoding Standard. – Version 1.0.0. OGC Doc. No. 08-007r1.
- GRÖGER, G. & PLÜMER, L., 2009: Updating 3D City Models – how to preserve geometric-topological consistency. – 17th ACM SIGSPATIAL Int. Conf. on Advances in Geographic Information Systems (ACM SIGSPATIAL GIS 2009), ACM Press, New York, 536–539.
- GRÖGER, G. & PLÜMER, L., 2010: How to Achieve Consistency for 3D City Models. – *Geoinformatica* (Online First) DOI: 10.1007/s10707-009-0091-6.
- GUPTILL, S.C. & MORRISON, J.L., 1995: Elements of Spatial Data Quality. – Elsevier, Oxford.
- HATCHER, A., 2001: Algebraic topology. – Cambridge University Press, Cambridge.
- HOPPE, B. & TARDOS, E., 1995: The Quickest Transhipment Problem. – 6. ACM-SIAM Symp. on Discrete Algorithms (SODA), 422–441.
- ISO TC 211, 2002: ISO 10113:2002: Geographic information – Quality principles. – International Organization for Standardization.
- KOLBE, T.H., GRÖGER, G. & PLÜMER, L., 2005: CityGML – Interoperable Access to 3D City Models – Geo-information for Disaster Management. 1st Int. Symposium on Geo-information for Disaster Management, Springer, Berlin, 883–899.
- KOLBE, T.H., GRÖGER, G. & PLÜMER, L., 2008: CityGML – 3D City Models for Emergency Response. – Geospatial information technology for emergency response, International Society for Photogrammetry and Remote Sensing book series **6**: 257–274, Taylor & Francis, London.
- LAKE, R., BURGRAF, D., TRNINIC, M. & RAE, L., 2004: Geography Mark-Up Language: Foundation for the Geo Web. – John Wiley & Sons, Chichester.
- LEE, J., 2001: A 3D Data Model for Representing Topological Relationships between Entities in Build Environments. – Ph.D. Dissertation, Department of Geography, Ohio State University.
- LEE, J. & KWAN, M.P., 2005: A combinatorial data model for representing topological relations among 3D geographical features in micro-spatial environments. – *Int. Journal of Geographical Information Science* **19** (10): 1039–1056.
- LEE, J. & ZLATANOVA, S., 2009: A 3D data model and topological analyses for emergency response in urban areas. – *Geospatial information technology for emergency response*, ISPRS book series, Taylor & Francis, London, 143–168.
- LORENZ, B., OHLBACH, H.J. & STOFFEL, E.P., 2006: A Hybrid Spatial Model for Representing Indoor Environments. – *Web and Wireless Geographical Information Systems, Lecture Notes in Computer Science* **4295**: 102–112, Springer, Berlin.
- MEIJERS, M., ZLATANOVA, S. & PFEIFER, N., 2005: 3D geoinformation indoors: structuring for evacuation. – 1<sup>st</sup> Int. ISPRS/EuroSDR/DGPF-Workshop on Next Generation 3D City Models, EuroSDR, 11–16.
- MÜLLER, P., WONKA, P., HAEGLER, S., ULMER, A. & VAN GOOL, L., 2006: Procedural Modeling of Buildings. – *ACM SIGGRAPH 2006 / ACM Transactions on Graphics (TOG)* ACM Press, 614–623.
- MÜLLER, P., ZENG, G., WONKA, P. & VAN GOOL, L., 2007: Image-based Procedural Modeling of Facades. – *ACM SIGGRAPH 2007 / ACM Transactions on Graphics*, ACM Press, New York, 85–93.
- NORVIG, P. & RUSSELL, S., 2003: Artificial Intelligence – A Modern Approach. – Pearson Education, Inc., New Jersey.
- PU, S. & ZLATANOVA, S., 2005: Evacuation route calculation of inner buildings. – *Geo-information for Disaster Management*. 1st International Symposium on Geo-information for Disaster Management, Springer, Berlin, 1143–1161.
- SCHMITTWILKEN, J., DÖRSCHLAG, D. & PLÜMER, L., 2009: Attribute Grammar for 3D City Models. – *Urban and Regional Data Management. UDMS Annual 2009*, CRC Press, Taylor & Francis Group, 49–58.
- SCHMITTWILKEN, J., SAATKAMP, J., FÖRSTNER, W., KOLBE, T.H. & PLÜMER, L., 2007: A Semantic Model of Stairs in Building Collars. – *Photogrammetrie – Fernerkundung – Geoinformation* **6/2007**: 415–428.
- STINY, G. & GIPS, J., 1972: Shape Grammars and the Generative Specification of Painting and Sculpture. – *IFIP Congress '71 2 – Applications*, 1460–1465.
- UEDA, K., 1985: Guarded Horn Clauses. – *Logic Programming '85, Lecture Notes in Computer Science* **221**: 168–179, Springer, Berlin.

- VAN TREECK, C. & RANK, E., 2004: Analysis of building structure and topology based on Graph Theory. – 10<sup>th</sup> Int. Conf. on Computing in Civil and Building Engineering.
- WONKA, P., WIMMER, M. & WILLIAM, F.S., 2003: Instant Architecture. – ACM Transactions on Graphics **22** (4): 669–677.
- ZLATANOVA, S., 2000: 3D GIS for urban development. – ITC Dissertation **69**, International Institute for Aerospace Survey and Earth Sciences, Enschede, the Netherlands.

Address of the Authors:

Priv.-Doz. Dr. rer. nat. GERHARD GRÖGER and Prof. Dr. rer. nat. LUTZ PLÜMER, University of Bonn, Institute for Geodesy and Geoinformation, Meckenheimer Allee 172, D-53115 Bonn, Tel.: +49-228-7317-64, -50, Fax: -53, e-mail: groeger@igg.uni-bonn.de, pluemer@igg.uni-bonn.de

Manuskript eingereicht: November 2009

Angenommen: März 2010

## Berichte von Veranstaltungen

### 3D – State of the Art: Workshop 3D – Stadtmodelle vom 9.–10. Nov. 2009 in Bonn

Am 9. und 10. November 2009 veranstaltete der/die erste gemeinsame Arbeitskreis/Kommission der DGfK (Deutsche Gesellschaft für Kartographie) und der DGPF unter Leitung von BETTINA PETZOLD (Wuppertal) und EKKEHARD MATTHIAS (Hamburg) einen Workshop rund um das Thema 3D-Stadtmodelle. Mit 23 Vorträgen an zwei Tagen war das Programm nicht nur vielfältig sondern auch sehr anspruchsvoll. Das große Interesse an den Themen zeigte sich auch anhand der Beteiligung: mehr als 100 Teilnehmer waren angereist.

#### Erfassung von 3D-Daten

J. SAILE (Stuttgart) schilderte, wie aus photogrammetrischen Daten und aus airborne LiDAR-Daten 3D-Gebäudemodelle abgeleitet und die Modelle geprüft werden können. Im Anschluss berichteten K. NELLESSEN (Düsseldorf) und R. REICHERT (Remscheid) über die organisatorischen und praktischen Herausforderungen der Bildaufnahme mit Hilfe von unbemannten Flugobjekten. Unterstützt wurde dieser Vortrag durch eine Live-Vorführung eines Kleinstfluggerätes.

#### Verarbeitungssoftware

Prof. Dr. V. COORS (Stuttgart) lichtete den Dschungel der 3D-Software und stellte die verschiedenen Prinzipien zu Ersterfassung, Modellierung, Datenmanagement und Datenbereitstellung vor. Damit steht eine Übersicht der gängigen Werkzeuge zur Verfügung.

#### Standards

U. GRUBER (Recklinghausen) griff das Thema CityGML auf, ein Standard, der inzwischen weltweit verabredet ist und zunehmend Verbreitung findet. Er referierte über erweiterte Datenmodellierungen, die über das CityGML-Standardangebot hinausgehen, um beispielsweise weitere Attribute und Datentypen abzubilden. Auch zukünftige CityGML-Inhalte

wie Brücken, unterirdische Räume und Versorgungsleitungen wurden vorgestellt.

#### Datenmanagement

Qualitätsmanagement und Aktualisierung von 3D-Daten waren zwei der am meisten gewünschten Themen. Diesem Wunsch wurde mit mehreren Vorträgen Rechnung getragen. Prof. Dr. V. COORS (Stuttgart) stellte die Prüfung auf verschiedene Fehler von Gebäudemodellen vor und gab Anregungen und Hilfen zur Behebung dieser Fehler. I. RIDDER und T. JUNG (Bochum) erläuterten ihre Strategien zur Fortführung von 3D-Stadtmodellen mit Hilfe von ALK und ALKIS. H.-U. MOHL (Stuttgart) und Dr.-Ing. R. THIELE (Siegburg) präsentieren ihre Lösung für die Verwaltung verschiedener Gebäudevarianten sowohl in zeitlicher Perspektive (Historisierung) als im Rahmen von Wettbewerben, bei denen mehrere Modelle an einem Ort gleichzeitig zu verwalten sind (Versionierung).

#### Webservices

Da das Thema 3D auch im Internet immer bedeutender wird, waren auch im Rahmen des Workshops entsprechende Vorträge vorgesehen. So sprach Prof. Dr. J. DÖLLNER über das Zusammenspiel verschiedener OGC-konformer Web-Komponenten und ergänzte dies durch eine genauere Betrachtung der Möglichkeiten des Web Perspective Viewing Service – WPVS. L. ROSS setzte die Diskussion dieser technischen Ansätze unter dem Blickwinkel von E-Government-Anwendungen am Beispiel Berlins fort, erläuterte aber auch die wesentlichen Hemmnisse der Umsetzung. Prof. Dr. A. ZIPE (Heidelberg) berichtete über seine Erfahrungen mit GDI-Komponenten in 3D auf der Basis von OpenGIS-Diensten am Beispiel von Open Street Map.

#### Anwendungen

Der Vortragsblock der Anwendungen nahm den Teilnehmerwünschen entsprechend den größten Raum ein. So schilderte F. BILDSTEIN (Bremen) das Potenzial von 3D-Stadtmodellen für Simulation und Training in verschiede-

nen Situationen wie zum Beispiel im ÖPNV (öffentlicher Personennahverkehr), bei Kurieren, Fahrschulen, Polizei und zur Rettung. G. LUDES (Dorsten) zeigte Solarpotenzialanalyse auf Basis eines vorhandenen 3D-Stadtmodells, d. h. anders als der bekannte Ansatz auf Basis von Laserdaten. Dafür bekam er auf der Internsolar 2009 den ersten Preis. Den Bedarf für die Integration von Lärm Daten und 3D-Stadtmodellen begründete Prof. Dr. J. SCHIEWE (Hamburg) und leitete die Anforderungen an 3D-Analyse- und Visualisierungsfunktionen her. Eine nur scheinbar exotische Anwendung stellte Dr. M. SCHLUSE (Aachen) mit dem virtuellen Wald vor. Ziel dieses Projektes ist die georeferenzierte Baumernte und damit verbunden die Erhöhung der Umweltverträglichkeit. Frau Prof. Dr. M. MÜLLER (Dresden) erläuterte die Zuhörer in den Untergrund, zeigte Anwendungen zur Kontrolle des Baumschutzes und stellte dabei ihre umfangreiche Bibliothek von Leitungselementen vor. Frau A. PREDEL (Dresden) gab einen Statusbericht zum 3D Stadtmodell von Dresden und Herr Dr. W. BECKRÖGE erläuterte den Stand der 3D-Modelle für die Kulturhauptstadt Ruhrgebiet 2010. Der letzte Anwendungsvortrag hatte seinen Schwerpunkt in der Wirtschaftsförderung. Frau K. TEICHMANN (Berlin) erläuterte den Teilnehmern den Berliner Ansatz, wie Firmen bei der Ansiedlung unterstützt werden und dabei das 3D-Stadtmodell Hilfe und Unterstützung bietet.

## Ausland

Der Blick über die Grenzen Deutschlands hinweg war den Veranstaltern ein besonderes Anliegen. Darum wurden zwei Länder ausgesucht, die als Nachbarn über ihre 3D-Ansätze berichteten. Prof. L. BODUM (Aalborg, DK) stellte die dänische Vorgehensweise vor, die von einem Zusammenschluss dänischer Kommunen und Universitäten 2007 geprägt ist. W. MEIER (Basel, CH) erläuterte die Planungen der Schweiz zu einem 3D-Kataster und E. SCHMASSMANN (Wabern, CH) schilderte anschaulich den Ansatz des Schweizer Bundesamtes für Landestopographie hinsichtlich eines flächendeckenden 3D-Landschaftsmodeles inklusive Gebäude in LoD2 (Level of Detail 2).

Der Universitätsclub Bonn bot als Veranstaltungsort eine gute Umgebung, in der sich die Teilnehmer offensichtlich wohlfühlten. Ein besonderer Dank geht an das vor Ort unterstützende Team um Dr.-Ing. C. AVERDUNG (Siegburg).

Der Termin für den nächsten Workshop steht bereits fest: er wird am 8. und 9. November 2010 wieder im Universitätsclub Bonn stattfinden. Der Arbeitskreis erarbeitet zurzeit das Programm, das mit Spannung erwartet werden darf. Weitere Informationen findet man unter [www.3d-stadtmodelle.org](http://www.3d-stadtmodelle.org).

BETTINA PETZOLD, Wuppertal  
Ekkehard Matthias, Hamburg

## 9. Oldenburger 3D-Tage über Optische 3D-Messtechnik – Photogrammetrie – Laserscanning vom 3.–4. Februar 2010

Die schon inzwischen 9. Tagung für „Optische 3D-Messtechnik – Photogrammetrie – Laserscanning“ (Oldenburger 3D-Tage) fand vom 3.–4. Februar 2010 in Oldenburg statt. Zur Veranstaltung hatte Prof. Dr. THOMAS LUHMANN vom Institut für Angewandte Photogrammetrie und Geoinformatik (IAPG) der Jade Hochschule eingeladen. Die Tagung wurde wie in den Jahren zuvor von einer Fachausstellung mit 21 Ausstellern begleitet. Die 250 angereisten Teilnehmer aus fünf Ländern konnten sich über insgesamt 62 Fachvorträge freuen.

Die einleitenden Worte sprach Prof. LUHMANN inkl. einem Rückblick auf die acht vergangenen Veranstaltungen. Die anschließenden Grußworte wurden von Dr. ELMAR SCHREIBER, Präsident der neu gegründeten Jade Hochschule, sowie von Dr. HANS SCHROEDER vom Ministerium für Wissenschaft und Kultur gehalten. Dr. SCHROEDER betonte, dass das Ministerium auch weiterhin das wissenschaftliche Feld der optischen 3D-Messtechnik, Photogrammetrie und des Laserscannings unterstützen werde.

Die Tagung gliederte sich in insgesamt 15 Sitzungen zu den Themen Laserscanning – Anwendungen, Photogrammetrie, Prüfung und Kalibrierung, Bewegungsmessung, Dy-



Einblick in die Fachausstellung der 9. Oldenburger 3D-Tage (Foto: Piet Meyer, IAPG Oldenburg)

namische Optische 3D-Messtechnik, Positionsbestimmung, Prüfung und Kalibrierung von terrestrischen Laserscannern, Sensoren und Systeme, Auswertestrategien, Registrierungsverfahren, sowie Oberflächenerfassung,

wovon jeweils zwei Sitzungen parallel abgehalten wurden. Der Eröffnungsvortrag wurde von Prof. MICHAEL SCHENK vom Fraunhofer-Institut für Fabrikbetrieb und -automatisierung in Magdeburg über „Virtuell-interaktive



Eröffnungsvortrag von Prof. Michael Schenk vom Fraunhofer-Institut für Fabrikbetrieb und -automatisierung in Magdeburg (Foto: Piet Meyer, IAPG Oldenburg)

3D-Stadtmodelle“ gehalten. Insbesondere wurde über den synthetischen Modellcharakter der reinen Geometriemodelle referiert, und wie sie in der virtuellen Realität lebendig gemacht werden können.

Die erste Parallelsitzung wurde zum Thema „Laserscanning – Anwendungen“ abgehalten. Die Leitung übernahm Prof. NEITZEL vom i3mainz. Unter diesem Schwerpunkt wurde den Teilnehmern ein breites Feld an Praxisbeispielen angeboten. So gab es Vorträge über die 3D-Erfassung und Modellierung des Bismarck-Denkmales in Hamburg (T. KERSTEN), über Laserscanning eines Brunnens in der archäologischen Zone in Köln (C. FLEISCHER) sowie über die virtuelle Rekonstruktion des Almqah-Tempels von Yeha in Äthiopien (K. MECHELKE). Es wurde auch über Möglichkeiten des 3D-Laserscannings in Lehre und Forschung (J.-M. BROSER) referiert.

Die gleichzeitig stattfindende Sitzung über „Photogrammetrie“ wurde von Prof. PRZYBILLA von der Hochschule Bochum geleitet. Der erste Vortrag handelte von stereoskopischer Vermessung eines Spinnennetzes der Schwarzen Witwe (C. WULFF). Die Ergebnisse dieser Auswertung wurden einem Künstler als Grundlage für eine Installation zur Verfügung gestellt. Als Nächstes wurde vom Institut Seefahrt Leer (J. GÖKEN) über den Einsatz einer speziellen photogrammetrischen Messanlage für dynamische Vermessungen von Schiffsbewegungen und Deformationen berichtet. Anschließend standen Vorträge über photogrammetrische Bildsequenzanalysen von Kopfimpaktorversuchen in der Fahrzeugsicherheit (K. HUCKE) und über Kalibrierung von Zoom- und Shift-Tilt-Objektiven (J. PIECHEL) auf dem Programm. Den Abschluss bildete ein Referat über das „ANDROMEDA-Projekt“ des Landes Thüringen (B. TEICHERT).

Im einzigen nicht parallel stattfindenden Sitzungsblock, der Studentensession der Jade Hochschule unter der Leitung von Prof. LUHMANN, referierten ausschließlich Oldenburger Studierende des Masterstudiengangs Geodäsie und Geoinformatik. Zu Beginn gab es einen Vortrag zur 3D-Erfassung der Kirche Bad Zwischenahn mit Photogrammetrie und Laserscanning (T. KRAUSE). Das zweite Thema war die „Geometrische Kalibrierung von Thermografiekameras“ (J. KIRK). Des Weiteren

wurde den Teilnehmern ein Einblick in die Systementwicklung eines photogrammetrischen 3D-Körperscanners (F. GRUNDMANN) gewährt.

Der Nachmittag stand mit dem Motto „Prüfung und Kalibrierung“ unter der Leitung von Prof. STAIGER sowie in der Parallelsession „Dynamische Prozesse – Bewegungsmessung“ unter der Sitzungsleitung von Dr. RAGUSE. In beiden Sitzungen wurden jeweils vier Vorträge präsentiert. Im Bereich der „Prüfung und Kalibrierung“ gab es zunächst einen Erfahrungsbericht über die Anwendungen der Richtlinie VDI/VDE 2634 Blatt 3 (A. BARTELT). Danach wurde den Hörern die Nützlichkeit schneller TLS-Feldprüfverfahren (B. SIEGRIST) sowie der Genauigkeitsvergleich verschiedener Zielmarkendesigns (F. KERN) nähergebracht. Einen Abschluss fand die Sitzung mit einem Referat über Untersuchungen zur photogrammetrischen Erfassung von Punktwolken mit dem System PhotoModeler Scanner (H.-J. PRZYBILLA).

Im Bereich „Dynamische Prozesse – Bewegungsmessung“ wurde der Auftakt durch einen englischsprachigen Vortrag gegeben. Das Thema war „Spatio-temporal 3D Pose Estimation and Tracking of Human Body Parts in an Industrial Environment“ (M. HAHN). Darauf folgend wurde den Zuhörern ein Einblick in den medizinischen Anwendungsbereich gegeben. Konkret wurde über eine Analyse von Gangparametern für die Dokumentation des Therapiefortschritts bzw. -erfolgs bei der Gangtherapie von Schlaganfallpatienten (J. RADMER) referiert. Die zwei letzten Vortragenden in dieser Session berichteten über Lösungen zur Fahrwerksmessung in der KFZ-Werkstatt (S. ABRAHAM) sowie über Vermessung von Form und Deformation von frei fliegenden Vögeln über Methoden des optischen Flusses (A. FRIEDL).

Die Vortragsreihe des ersten Konferenzta ges fand ihren Abschluss zum einen durch ein Herstellerforum. Auf diesem stellten verschiedene Hersteller unter der Leitung von Prof. KERN neueste Entwicklungen der Hard- und Software für die 3D-Objekterfassung und Rekonstruktion vor. Es wurden Lösungen im Bereich der Auswertestrategie sowie die neuesten Geräte der unterschiedlichen Hersteller präsentiert.

Der parallel stattfindende Themenblock geleitet von Prof. LUHMANN fasste die Ergebnisse des Oldenburger Forschungsschwerpunkts „Dynamische Optische 3D-Messtechnik“ zusammen. Als Erstes wurde über die Aufnahme synchroner Stereobildsequenzen mithilfe einer Einzelbildkamera mit optischer Stereostrahlteilung (J. OHM) referiert. Im zweiten Vortrag wurde über den Einsatz der Stereobildsequenzen mit Störobjekten für die Erfassung und Auswertung von dynamisch verformten 3D-Freiformflächen (B. HERD) berichtet. Einen interessanten Einblick in die Mikroskopie gewährte der nächste Vortragende (M. SCHELLENBERG), der über Lösungen mit Mikrospiegelarrays für eine zeitaufgelöste, konfokale 3D-Mikroskopie sprach. Ein englischsprachiger Vortrag mit dem Thema „Real Time Visualization of Megavoxel Data in Confocal Microscopy“ (E. PEEV) schloss diese Vortragsrunde ab.

Einen netten Abschluss des Tages bildete die Abendveranstaltung in der Weser-Ems-Halle in Oldenburg mit dem traditionellem Grünkohlessen und einem kulturellen Höhepunkt. Der glänzende Auftritt einer Oldenburger Theater-Gruppe (Variete In der Bar zum Krokodil) hat mit ihrem Charme und pikantem Witz alle Teilnehmer der Konferenz köstlich unterhalten. Bis in den frühen Morgen wurden fachliche und weniger fachliche Diskussionen geführt.

Der zweite Konferenztag beinhaltete acht Sitzungsblöcke, von denen immer zwei parallel stattfanden. Der Auftakt erfolgte durch ein weiteres Herstellerforum. Im Block „Dynamische Prozesse - Positionsbestimmung“ unter der Leitung von Dr. WIGGENHAGEN beschäftigten sich die Teilnehmer mit Themen wie Visuelle Positions- und Bewegungsbestimmung eines autonomen Systems (T. LINKUGEL), automatisch generierte Merkmalskarten für Fahrerassistenzsysteme (S. HOFMANN) und deren Untersuchung, sowie mit Ground Truthing von monokolaren Entfernungsschätzungen mittels eines Mehrzeilen-Laserscanners (M. HAHN). Zum Abschluss dieser Runde wurde über ein Mehrkamerasytem referiert (R. SCHÜTZE), das die exakte Positionsbestimmung von beweglichen Effektoren erlaubt.

Prof. STAIGER leitete eine Sitzung des Arbeitskreises „Prüfung und Kalibrierung von terrestrischen Laserscannern“. Im Themenblock „Sensoren und Systeme“ unter dem Vorsitz von Dr. RIEKE-ZAPP bekamen die Teilnehmer sowohl einen Einblick in den Anwendungsbereich und das Potential bildgebender Tachymeter (T. VICOVAC) als auch in die Automatisierung von Fertigungsprozessen großvolumiger Bauteile (M. HERRMANN). Von der Leibniz Universität Hannover (R. SCHMIDT) kam ein Vortrag über „Gig3D“- ein optisches Hochgeschwindigkeits-Messsystem, das bei dreidimensionaler Beobachtung und Analyse



Variete In der Bar zum Krokodil (Foto: Piet Meyer, IAPG Oldenburg)

hochdynamischer Vorgänge eingesetzt wird. Der letzte Vortrag dieser Runde berichtete von „go!CART“ – dem UAV Programm der Metropolregion Bremen-Oldenburg (T. PULS). Der Konferenznachmittag beinhaltete vier Themenblöcke mit insgesamt 15 Vorträgen. Unter der Leitung von Prof. BOOCHS von i3mainz wurde über verschiedene Auswertestrategien referiert. Man beschäftigte sich unter anderem mit dem Least-squares Matching mit erweiterten geometrischen Funktionen (F. BETHMANN), photogrammetrischer Bestimmung von statischen und dynamischen Verformungsstrukturen von Einzelbäumen (A. BIENERT), sowie mit verbesserter Kartenqualität durch Thin Plate Splines und Hough-Transformation (D. BORRMANN). Ein Vortrag über Echtzeit und Embedded-Algorithmen sowie Sensorsysteme für eine dynamische Waldinventur (A. ZIEGLER) bildete den Abschluss dieser Runde.

Zeitgleich fand ein weiterer Block zum Thema „Sensoren und Systeme“ unter der Leitung von Prof. NEU statt. Der erste Vortrag gab den Hörern einen Einblick in die Genauigkeit und Registrierdauer in der klinischen HNO Navigation (T. KRÜGER). Der nächste Vortragende (K. SCHÄDLER) befasste sich mit dem Thema „Depth from Focus in der Produktionspraxis“. Den Ausklang fand dieser Block mit zwei Themen, die Probleme bei Glasfaserbewehrung in Beton (I. FOCKE) sowie Entfernungsmeßung von Time of Flight (ToF)-Kameras unter dem Einfluss der Lichtquellengeometrie (S. NESER) behandelten.

Die Sitzungen „Laserscanning – Registrierungsverfahren“ unter der Leitung von Prof. KERSTEN (HCU Hamburg) und „Oberflächen erfassung“ mit Prof. TEICHERT (HTW Dresden) schlossen die 9. Oldenburger 3D-Tage ab. Die zwei einführenden Vorträge im ersten The-

menblock informierten die Teilnehmer unter anderem über die Untersuchung von Registrierungsverfahren hinsichtlich des Einsatzes in der Deformationsmessung mit terrestrischen Laserscannern (W. MORDWINZEW und Ch. LERCHE) sowie über die Registrierung von Punktwolken auf der Grundlage von Objektprimitiven (M. LICHTENSTEIN). Zum Abschluss wurde den Hörern ein englischsprachiges Referat mit dem Thema „Co-registration of terrestrial laser scans and close range digital images using scale invariant feature detection“ (S. SHAHZAD) geboten.

Im Sitzungsblock über die Oberflächenerfassung referierten sowohl Redner aus der Industrie als auch aus dem wissenschaftlichen Bereich. Der erste Vortrag handelte von Reflexionsmesstechnik im Fahrzeugbau (B. THIELBEER). Danach erfuhrten die Teilnehmer mehr zum Inhalt „Reflexionen über Spiegel“ (T. SCHRAMM). Die letzten beiden Referate beleuchteten das Problem der Hochgeschwindigkeitsprojektion von Speckle-Mustern für eine strukturierte Beleuchtung (M. SCHAFFER) sowie die Problemlösung für das Erfassen von Abstandsänderungen mithilfe eines oszillierenden Fasersensors (M. SCHULZ).

Zusammenfassend lässt sich sagen, dass die 9. Oldenburger 3D-Tage den Teilnehmern eine interessante und informative Mischung aus den Bereichen Wissenschaft, Technik und Anwendung geboten haben. Durch das breite, interdisziplinäre Spektrum der Vorträge wurde die Stellung der Oldenburger 3D-Tage als feste Größe im Veranstaltungskalender gestärkt. Auf die Fortsetzung der Veranstaltung im Jahr 2011 freut sich eine immer größer werdende Community.

MAGDALENA DANNENBERG, Bochum

## Hochschulnachrichten

### Technische Universität Dresden

Prof. Dr.-Ing. THOMAS LUHMANN (Jade Hochschule Oldenburg, Institut für Angewandte Photogrammetrie und Geoinformatik) habilitierte sich am 8. Januar 2010 an der Technischen Universität Dresden, Fakultät Forst-, Geo- und Hydrowissenschaften, für das Fachgebiet Photogrammetrie mit der Arbeit „Erweiterte Verfahren zur geometrischen Kamerakalibrierung in der Nahbereichsphotogrammetrie“.

Habilitationsskommission: Prof. Dr. HANS-GERD MAAS (TU Dresden), Prof. Dr. CHRISTIAN HEIPKE (Leibniz Universität Hannover) und Prof. Dr. RALF REULKE (Humboldt Universität Berlin)

#### Kurzfassung

Die vorliegende Arbeit gibt einen Überblick über Verfahren der photogrammetrischen Kamerakalibrierung in der Nahbereichsphotogrammetrie. Im Gegensatz zur Luftbildphotogrammetrie zeichnet sich die Nahbereichsphotogrammetrie durch komplexere und nicht standardisierte Aufnahmesituationen, höchste Genauigkeitsforderungen (im industriellen Bereich), eine Vielzahl von Aufnahmesystemen, verschiedenste Umgebungsparameter und Anforderungen an Echtzeit-, Online- oder Offlineauswertungen aus.

Kamerakalibrierung ist eine der Kernfragen der Photogrammetrie und stets mit der Frage der erzielbaren Messgenauigkeit verbunden. Durch die übliche Integration von Objektvermessung und simultaner Kalibrierung im Rahmen der Bündelausgleichung sind beide Bereiche stark miteinander korreliert. Es liegt daher nahe, die Güte einer Kamerakalibrierung mit unabhängigen Referenzgrößen im Objektraum zu verifizieren. Dieser Ansatz liegt der vorliegenden Arbeit zu Grunde.

Die Definition des Begriffes Kamerakalibrierung, die Einführung wichtiger Parameter und Qualitätsmerkmale, die prinzipiellen Methoden zur Kalibrierung und übergreifende

Systemaspekte bilden den Schwerpunkt des ersten Kapitels. Die langjährige Tradition der photogrammetrischen Kalibrierung hat ihre Basis in einer möglichst exakten, aber gleichzeitig mathematisch überschaubaren Modellierung der optischen Abbildung. Dieses Vorgehen ist auch heute noch üblich und verschafft der photogrammetrischen Kameramodellierung einen signifikanten Genauigkeitsvorsprung im Vergleich zu alternativen Modellen, wie sie zum Beispiel im Bereich Computer Vision entwickelt werden.

Die Abhängigkeit der Kamerakalibrierung von der anwendungsbezogenen oder messsystembedingten Aufnahmesituation wird in Kap. 2 aufgegriffen. Hier wird insbesondere betont, dass die Möglichkeiten zur Simultan-Kalibrierung des Aufnahmesystems beschränkt sind, wenn Online-Messsysteme eingesetzt werden. Des Weiteren wird ein allgemeines schematisches Modell der Einflussgrößen auf die Kalibrierung und damit für die erreichbare Leistungsfähigkeit eines Systems aufgestellt, das die Komplexität der photogrammetrischen Messtechnik im Allgemeinen und der Kamerakalibrierung im Besonderen herausstellt.

Die physikalischen Grundlagen der Kamerakalibrierung werden in Kap. 3 soweit vertieft, wie sie für das Verständnis der optischen und mathematischen Zusammenhänge erforderlich sind. Ausgehend von Definitionen aus der Wellenoptik werden geometrisch orientierte Aspekte der optischen Abbildung diskutiert. Die Definition des Projektionszentrums, wichtiger Bildbezugspunkte sowie der aus der Optik bekannten Abbildungsfehler sind für die exakte Modellierung der photogrammetrischen Abbildung unerlässlich. Der Abschnitt gibt weiterhin Hinweise für erweiterte Abbildungsmodelle, etwa im Bereich der Farbabbildung, der Strahlverfolgung durch ein Objektiv oder die Einführung eines objektseitigen Projektionszentrums.

In Kap. 4 folgt die Zusammenstellung der photogrammetrischen Standardverfahren zur Kamerakalibrierung. Diese sind seit Jahren in der Praxis eingeführt und haben sich für eine

Vielzahl unterschiedlicher Aufnahmesysteme und Sensoren bewährt. Gleichwohl bilden sie in der Regel nur die Abbildungsvorgänge ab, die in qualitativ hochwertigen Objektiven und Kameras bei hinreichender Messgenauigkeit vorkommen.

Erweiterte Modelle der Kamerakalibrierung und der mathematischen Abbildung werden in Kap. 5 diskutiert. Sie umfassen zunächst erweiterte wellenlängenabhängige Abbildungsmodelle, z. B. durch Berücksichtigung der chromatischen Aberration oder beim Strahlverlauf durch verschiedene optische Medien. Die Modellierung des Bildsensors in Form flächenhaft wirkender Korrekturmodelle eröffnet ein neues Feld von Kalibrieransätzen, in denen im Extremfall eine Richtungskorrektur für jedes einzelne Pixel ermittelt werden kann. Schließlich wird das physische Kamerasystem (Gehäuse und Objektiv) näher betrachtet, da es während der Bildaufnahme von äußeren Einflüssen beeinträchtigt werden kann, z. B. in Form mechanischer oder thermischer Deformationen oder durch Schwerkrafteinflüsse. Zu den erweiterten Kameramodellen zählen weiterhin veränderte Abbildungsmodelle, wenn besondere Objektivformen oder alternative Strahlengänge durch zusätzliche optische Komponenten (z. B. Spiegel oder Prismen) im Aufnahmesystem eingesetzt werden.

Die in Kap. 5 vorgestellten Erweiterungen der Standardverfahren sind zum Teil von hohem praktischen Wert, etwa zur Einführung bildvarianter Kameramodelle, zur Beschreibung von Sensordeformationen für Aufnahmesysteme mit geringerer mechanischer Stabilität (Consumerkameras) oder zur Optimierung der Messgenauigkeit bei hochwertigen Systemen. Die einzelnen Modellansätze sind dabei unterschiedlich tief ausgeführt, da sie nur zum Teil vom Autor und seiner Arbeitsgruppe umgesetzt worden sind und durch eigene Erfahrungen und Beispiele untermauert werden können. Dort, wo eigene Entwicklungen einen wesentlichen Beitrag zur Modellbildung und deren Überprüfung bilden, wird vertieft auf die Materie eingegangen und es werden fallweise praktische Auswertereispiele diskutiert.

In Kap. 6 werden anhand zweier umfangreicher Versuchsserien bisher unveröffentlichte

Untersuchungen vorgestellt. Ziel ist jeweils die systematische Variation von Aufnahmesystemen und Modellparametern, wobei die jeweiligen Auswirkungen auf die statistische Präzision und die Genauigkeit im Objektraum verifiziert werden. Hierbei treten teils überraschende Detailergebnisse zutage, es werden aber auch Potenziale erweiterter Modellansätze sichtbar. Durch die hier zugrunde gelegte Bestimmung der Längenmessabweichung gelingt es, unabhängig von statistischen Optimierungen und inneren Genauigkeitsangaben eine fundierte Aussage zur Qualität einer Kamerakalibrierung in Kombination mit der dreidimensionalen Objektrekonstruktion zu machen. Die derzeitige Grenze der Leistungsfähigkeit digitaler photogrammetrischer Messsysteme im Nahbereich kann mit einer Längenmessabweichung angegeben werden, die um ca. Faktor 4 größer als die mittlere Standardabweichung (RMS 1 Sigma) der Objektkoordinaten ist.

Das in einer Vielzahl von Publikationen über Jahrzehnte diskutierte Thema der photogrammetrischen Kamerakalibrierung kann hier dennoch nicht allumfassend dargestellt werden. Es bleiben einige Randgebiete und alternative Konzepte, deren Wirkung und Anwendbarkeit noch zukünftig geklärt werden müssen. Darüber hinaus bleibt eine Reihe offener Fragen, die an dieser Stelle ebenfalls nicht abschließend geklärt werden und Raum lassen für weitere Untersuchungen. Dazu gehören Ansätze zur Kalibrierung jeder einzelnen Pixelposition im Bildsensor oder zur Berücksichtigung kompletter Abbildungsstrahlengänge, wie sie die technische Optik beim Design von Objektiven schon lange verwendet. Denkbar sind auch Kalibrierungsansätze, die den Objektraum in Form von Voxel-Korrekturmodellen beschreiben und damit zu einer Optimierung der photogrammetrischen Messgenauigkeit im gesamten Messvolumen beitragen könnten. Schließlich ist noch weitgehend ungeklärt, inwieweit eine Kombination von radiometrischer und geometrischer Kameramodellierung sinnvoll sein kann, die simultan in einem gemeinsamen Rechenprozess analog zur Bündelausgleichung bestimmt werden könnte.

Das in der Arbeit skizzierte allgemeine Kalibrierungsmodell stellt den Versuch dar, alle

an der photogrammetrischen Messung beteiligten Komponenten und Umgebungsparameter zusammenzufassen und zu strukturieren. Dieses Modell zeigt prinzipiell auf, an welchen Schnittstellen Wechselwirkungen einzelner Einflussgrößen zu erwarten sind. Viele dieser Einflussgrößen sind bisher nicht weiter in ein mathematisches Modell der Kalibrierung eingeflossen, so dass systematische Modellbildungen und Untersuchungen in Zukunft erforderlich sein werden, um den gesamten Prozess der hochgenauen photogrammetrischen Messtechnik im Nahbereich besser zu verstehen und die Leistungsfähigkeit von Sensoren und Verfahren weiter zu steigern.

Die Habilitationsschrift ist in digitaler Form bei der Deutschen Geodätischen Kommission, Reihe C, Nr. 645, erschienen.

### **Westfälische Wilhelms-Universität Münster**

Herr Dipl.-Geogr. KARL-PETER KRÜGER legte am 14. Juli 2009 am Institut für Geographie der Westfälischen Wilhelms-Universität Münster mit der Arbeit „*Der Landschaftswandel in der türkischen Euphratregion – Eine multitemporale, multisensorale Fernerkundungsanalyse anhand von Fallbeispielen in den Provinzen Gaziantep und Urfa*“ die Dissertationsprüfung zum Dr. rer. nat. ab. Prüfungskommission: Prof. Dr. PAUL REUBER, Prof. Dr. ANTONIO KRÜGER, Prof. Dr. GERALD WOOD, Prof. Dr. HEINZ HEINEBERG und Dekan – Prof. Dr. HANS KERP

#### **Kurzfassung**

Die Dissertationsschrift beschäftigt sich mit einer Untersuchungsregion, die politischgeographisch und wirtschaftsgeographisch von großer Brisanz und Interesse ist. Es handelt sich um Südostanatolien, einen Landstrich, der innerhalb der Türkei die Grenzregion zu den Nachbarstaaten des Nahen und Mittleren

Ostens bildet. Innerhalb dieser Region realisiert die Türkei seit Jahrzehnten ein sehr ehrgeiziges Bewässerungsprojekt, dessen Rückgrat eine Kette von Großstaudämmen darstellt, zu denen auch der international bekannte Ataturk-Staudamm gehört.

Die Problematik des sehr restriktiven Umgangs mit raumbezogenen Informationen nimmt die Dissertation methodisch und inhaltlich ins Visier, indem sie versucht, einerseits im Rückgriff auf Fernerkundungsdaten die raumbezogenen Grundlagen zu erarbeiten, die Wissenschaftlern für ihre Analysen in der Form nicht zur Verfügung stehen, andererseits ist es ihr Ziel, mit einer Auswertung dieser Daten erste inhaltliche Aussagen über länger angelegte Wandlungsprozesse in der Kulturlandschaft zu dokumentieren.

Von ihrem Charakter her ist die Dissertation entsprechend hybrid und im Schnittfeld von Humangeographie und Geoinformatik angesiedelt. Der Erkenntnisgewinn zielt einerseits auf den methodisch-instrumentellen Fortschritt, in dem sie fragt, wie mit vorhandenen Fernerkundungsdaten geographisch-kartographische Grundlageninformationen für einen ansonsten politisch eher abgeschotteten Untersuchungsraum zur Verfügung gestellt werden können. Andererseits erarbeitet sie mit diesem Material erste Module einer deskriptiv angelegten Analyse des historischen Wandels von Siedlungs- und Agrarlandschaften im Untersuchungsgebiet. Dieser hybride Ansatz stellt eine große Stärke und einen wichtigen Innovationsschritt der Arbeit dar.

Bezüglich des agrarstrukturellen Wandels des Südostanatolienprojektes gehen die Ergebnisse in die Richtung, dass sich bisher kein eindeutiger Trend in Richtung Bewässerungsmaßnahmen und Einsatz von agroindustriellen Produktionsmethoden für das Projekt belegen lässt.

Die Dissertation ist im MIAMI-Publikationsserver der Universitätsbibliothek publiziert: [miami.uni-muenster.de](http://miami.uni-muenster.de)

## Buchbesprechung

**DIERK HOBBIE, 2010: Die Entwicklung photogrammetrischer Verfahren und Instrumente bei Carl Zeiss in Oberkochen. Deutsche Geodätische Kommission (DGK), Reihe E Heft Nr. 30, 144 S., München**

Diese Dokumentation kommt nüchtern daher, jedoch verbirgt sich hinter ihrem schlichten Titel ein regelrechter Thriller: Die Anfänge von CARL ZEISS in Oberkochen liegen im Juni 1945, als nach der Katastrophe des Weltkrieges die „erste Garnitur“ der Zeissianer auf amerikanischen Armeelastwagen von Jena nach Heidenheim an der Brenz deportiert wurde. Die folgenden 50 Jahre der Firma sind voller Dynamik und Dramatik, eine Zeitspanne, geprägt durch große technische und politische Veränderungen. Vom Beginn auf niedrigstem Niveau, etwa Wiederaufnahme von Luftbildumzeichnern und Stereoskopen (z. B. Taschenstereoskop TS4, von dem insgesamt 80.000 Stück verkauft wurden), über Weiterentwicklung noch aus Jena stammender Vorkriegs-Produktionslinien, wie Luftbildkameras, STEREOPLANIGRAPH oder Entzerrungsgerät SEG, schloss CARL ZEISS Oberkochen in den 70er Jahren zur Weltspitze auf (z. B. Vorstellung vom PLANIMAT und insbesondere vom analytischen Plotter PLANICOMP C100 beim ISP-Kongress in Helsinki 1976). Der Thriller, die Erfolgsgeschichte, endet leider ohne Happy End insofern, als sich die Firma CARL ZEISS nach der Wiedervereinigung 1990 sukzessive aus der Photogrammetrie zurückzog, nicht ohne langfristig vergebliche Versuche, mit Partnern stabile Kooperationen aufzubauen. Am 30.9.2002 gingen die 40 % Anteile an der Firma Z/I IMAGING von ZEISS an INTERGRAPH, und dies markiert das Ende.

Der Text ist – um im Bild zu bleiben – mit Herzblut geschrieben. DIERK HOBBIE kam 1968, gerade 25 Jahre alt, als frischgebackener Diplomingenieur von der damaligen TH Hannover direkt nach Oberkochen und wurde dort später nach der Leitung der „Entwicklung“ mit der Leitung des Projektbereichs „Photogrammetrie“ und dann sogar mit der des gesamten Projektbereichs „Vermessung“ betraut.

Seine 47 aufgeführten Publikationen dokumentieren seine Beiträge vor allem zur Herstellung von Entzerrungen und Orthophotos sowie zu „seinem“ Planicomp, ehe er ab 1990 auch übergeordnete Themen aufgreift, wie Gedanken zur Zukunft von ZEISS in Jena und in Oberkochen sowie zum Berufsbild des Geodäten.

Die vorliegende, insgesamt 144 Seiten (einschließlich 19 Seiten Literatur) umfassende Dokumentation behandelt schwerpunktmäßig auf etwa 100 Seiten Luftbildaufnahme und Luftbildauswertung; hinzu kommen Kapitel über Vorgeschichte und den Wiederbeginn in Oberkochen, über terrestrische Photogrammetrie, Sonderanwendungen sowie Fernerkundung und Aufklärung. Der Text endet mit „Photogrammetrie – Entwicklung und ihre Mitarbeiter“, wo DIERK HOBBIE in aller Kürze, aber dennoch detailliert Statistiken liefert zu Produktion, zu Patenten und Publikationen und vor allem die vielen wissenschaftlichen Mitarbeiter nennt, welche in den 80er und 90er Jahren ihren Beitrag zur erfolgreichen Oberkochener Produktpalette geleistet hatten.

Auch die Kapitel über Entwicklung von Verfahren und Instrumenten vermitteln den Eindruck, dass es dem Autor um eine möglichst vollständige Dokumentation geht, von Bleistiftspitzmaschinen für Zeichentische bis hin zu Stereoauswertungsgeräten 1. Ordnung, welche an aufwändiger feinmechanischer Kunst Planetarien nicht nachstehen. Auch werden Produkte aufgeführt, die aus unterschiedlichen Gründen nicht in Serie gingen. Vieles ist dokumentiert, was sonst mittelfristig verloren wäre, wie die Zahl der ausgelieferten Exemplare: Z. B. gingen insgesamt 1.300 analytische Plotter aus Oberkochen in alle Welt. Ein PLANICOMP C100 (1976) bestand nur noch aus 460 „gefertigten Einzelteilen“, ein PLANIMAT D2 (1967) aus 1.700 und ein STEREOPLANIGRAPH C8 (1952) aus 5.000. Solche Zahlen veranschaulichen den dramatischen Wandel in der Feinwerktechnik, der anschließend mit rein digitalen Verfahren zu einem Paradigmenwechsel wurde. Aufstieg und Fall der photogrammetrischen Produktion in Ober-

kochen wird von DIERK HOBBIE nicht nur sachkundig, sondern auch immer sachlich und fair gegenüber „Mitbewerbern“ dargestellt.

Eine weitergehende Analyse der Fakten führt zu einer Reihe grundsätzlicher Erkenntnisse: Die photogrammetrische Disziplin wurde von der Industrie (hier der Firma CARL ZEISS Oberkochen) enorm mitgeprägt. Die enge Verbindung zu universitärer Forschung und die Durchlässigkeit für Wissenschaftler in beide Richtungen führten zu nachhaltiger Synergie. Hochschulinstitute allein sind langfristig nicht geeignet, Produkte zu vermarkten. Andererseits sind Firmen allein nicht geeignet, neue wissenschaftliche Erkenntnisse zu suchen. Die Marktfähigkeit eines Produkts richtig einzuschätzen, erfordert große Erfahrung sowie genaue Kenntnis der Kundenbedürfnisse und der technischen Möglichkeiten. Häufig wird eine Produktpalette anzubieten sein: Oberklasse (luxuriöse Allesköninger), Mittelklasse („Arbeitspferde“) und abgespecktes Basismodell (als „Unterkasse“ würde es nicht gut ankommen). Diese Dreiteilung gilt für Automobile und Staubsauger ebenso wie für Stereoplotter. Es gibt Sackgassen (z.B. Stereoplotter mit optischer Projektion in den 60er Jahren) und zu bestimmten Zeiten Entwicklungssprünge (z.B. digitale Orthophotos

in den 90er Jahren). Die Entwicklung der vergangenen 50 Jahre ist indes geprägt durch immer *schnellere* Veränderung von Markt einerseits und Produkten andererseits.

Die Schrift, erschienen als Heft Nr. 30 in der Reihe E der DGK („Geschichte und Entwicklung der Geodäsie“) ist komplementär zur Schrift von HORST SCHÖLER, welcher 2006 in Heft Nr. 27 die Aktivitäten im Jenaer Zeiss Werk zusammenstellte. Ergänzt durch die von RUDOLF SCHUMANN geschriebene und 1986 von KLAUS SZANGOLIES im Band XVIII des Jenaer KOMPENDIUM PHOTOGRAFMETRIE herausgegebene Darstellung der Jenaer Vorkriegsentwicklungen liegt damit der weitaus wichtigste Teil der photogrammetrischen Industrieproduktion in Deutschland hervorragend dokumentiert vor. Zusammen mit Heft 6/2009 der Zeitschrift „Photogrammetrie – Fernerkundung – Geoinformation“, in welchem JÖRG ALBERTZ einen historischen Rückblick auf „100 Jahre Deutsche Gesellschaft für Photogrammetrie, Fernerkundung und Geoinformation e.V.“ liefert, besitzen die Photogrammeter damit ein Kompendium ihrer Geschichte, um welches uns viele andere Fachrichtungen beiderseits werden.

HANS-PETER BÄHR, Karlsruhe

## Veranstaltungskalender

### 2010

8.–10. Juni: **58. Deutscher Kartographentag** in Berlin/Potsdam. [dkt2010.dgfk.net/](http://dkt2010.dgfk.net/)

9.–10. Juni: **6. Hamburger Forum für Geomatik** – Aktuelle Entwicklungen aus Forschung und Praxis in **Hamburg-Veddel**. [www.geomatik-hamburg.de/forum-geomatik/2010/](http://www.geomatik-hamburg.de/forum-geomatik/2010/)

10.–11. Juni: **6. GIS-Ausbildungstagung 2010 in Potsdam**. [gis.gfz-potsdam.de](http://gis.gfz-potsdam.de)

12.–14. Juni: ISDE 2010 **Digital Earth Summit** „Digital Earth in the Service of Society“:

**Sharing Information, Building Knowledge** in **Nessebar**, Bulgaria. [www.cartography-gis.com/digitalearth/](http://www.cartography-gis.com/digitalearth/)

16.–18. Juni: **GIS/SIT 2010** – Schweizer Forum für Geoinformation an der Universität **Zürich-Irchel**, Schweiz. [www.gis-sit.ch/](http://www.gis-sit.ch/)

16.–18. Juni: **ISPRS Commission I Symposium “Image Data Acquisition – Sensors & Platforms”** in **Calgary**, Kanada. [www.geocnf.ca](http://www.geocnf.ca)

16.–18. Juni: **IEEE Conference on Computer Vision and Pattern Recognition** in **San Francisco**, USA. [www.cvpr2010.org/](http://www.cvpr2010.org/)

- 22.–24. Juni: ISPRS Commission V Symposium “Close-Range Sensing: Analysis & Applications” in Newcastle upon Tyne, Großbritannien. [www.isprs-newcastle2010.org/](http://www.isprs-newcastle2010.org/)
29. Juni–2. Juli: **GEOBIA 2010 – GEOgraphic Object-Based Image Analysis** in Ghent, Belgien. [geobia.ugent.be](http://geobia.ugent.be)
- 1.–3. Juli: **30. Wissenschaftlich-technische Jahrestagung der DGPF** im Rahmen der Dreiländertagung in Wien, Österreich. [www.dgpf.de/neu/jahrestagung/informationen.htm](http://www.dgpf.de/neu/jahrestagung/informationen.htm)
- 5.–7. Juli: ISPRS Commission VII Symposium “100 Years ISPRS – Advancing Remote Sensing Science” in Wien, Österreich. [www.isprs100vienna.org/](http://www.isprs100vienna.org/)
- 6.–9. Juli: **GI\_Forum2010:** Symposium & Exhibit “Applied Geoinformatics” in Salzburg, Österreich. [www.gi-forum.org/](http://www.gi-forum.org/)
- 7.–9. Juli: **AGIT 2010 Symposium und Fachmesse für Angewandte Geoinformatik** in Salzburg, Österreich. [www.agit.at/](http://www.agit.at/)
- 20.–23. Juli: ISARA 9<sup>th</sup> International Symposium on Spatial Accuracy Assessment in Natural Resources & Environmental Sciences in Leicester, Großbritannien. [www.le.ac.uk/geography/accuracy/index.html](http://www.le.ac.uk/geography/accuracy/index.html)
- 1.–5. August: **SPIE Optical Engineering + Applications** in San Diego, USA. [spie.org/optical-engineering.xml](http://spie.org/optical-engineering.xml)
- 9.–13. August: ISPRS Commission VIII Symposium “Remote Sensing Applications & Policies” in Kyoto, Japan. [www.isprscm8.org/](http://www.isprscm8.org/)
- 1.–3. September: ISPRS Commission III Symposium “Photogrammetric Computer Vision & Image Analysis” in Paris, Frankreich. [pcv2010.ign.fr/](http://pcv2010.ign.fr/)
- 1.–5. September: **7<sup>th</sup> ICA Mountain Cartography Workshop** in Borsa, Rumänien. [www.mountaincartography.org/activities/workshops/](http://www.mountaincartography.org/activities/workshops/)
- 5.–11. September: **European Conference on Computer Vision in Heraklion**, Kreta, Griechenland, [www.ics.forth.gr/eccv2010](http://www.ics.forth.gr/eccv2010)
- 14.–17. September: **GIScience 2010 – 6<sup>th</sup> International Conference on Geographic Information Science** in Zürich, Schweiz. [www.giscience2010.org/](http://www.giscience2010.org/)
- 20.–23. September: **SPIE Remote Sensing** in Toulouse, Frankreich. [spie.org/remote-sensing-europe.xml](http://spie.org/remote-sensing-europe.xml)
- 22.–24. September: **DAGM 2010 – 32<sup>nd</sup> Annual Pattern Recognition Symposium** in Darmstadt. [www.dagm2010.org/](http://www.dagm2010.org/)
- 5.–7. Oktober: **INTERGEO®** – Kongress und Fachmesse für Geodäsie, Geoinformation und Landmanagement in Köln. [www.intergeo.de/de/deutsch/index.php](http://www.intergeo.de/de/deutsch/index.php)
- 11.–13. Oktober: ISPRS WG I/4 Workshop on Modeling of Optical Airborne & Space Borne Sensors in Istanbul, Türkei.
- 27.–29. Oktober: **12. Seminar “GIS & Internet”** – Integration von GIS-Funktionalitäten in Lösungen an der UniBw München in Neubiberg. Infos: [www.agis.unibw.de/gis&internet/](http://www.agis.unibw.de/gis&internet/)
- 8.–9. November: **Workshop 3D-Stadtmodelle in Bonn** (Universitätsclub). [3d-stadtmodelle.org](http://3d-stadtmodelle.org)
- 16.–18. November: ISPRS Commission IV Symposium “Geodatabases & Digital Mapping” in Orlando, USA. [www.commission4.isprs.org/](http://www.commission4.isprs.org/)
- ## 2011
- 13.–19. Februar: **16. Internationale Geodätische Woche** in Obergurgl, Tirol, Österreich. Infos: [geodaetischewoche@uibk.ac.at](mailto:geodaetischewoche@uibk.ac.at) oder [geodesie.uibk.ac.at/obergurgl.html](http://geodesie.uibk.ac.at/obergurgl.html)
- 11.–13. April: **JURSE 2011** – Joint Urban Remote Sensing Event (URBAN 2011 + URS 2011) in München. [www.jurse2011.tum.de](http://www.jurse2011.tum.de)
- 13.–15. April: **EOGC 2011** – 3rd Conference on Earth Observation for Global Changes in München. [www.eogc2011.tum.de](http://www.eogc2011.tum.de)

## Neuerscheinungen

HOBbie, D. 2010. Die Entwicklung photogrammetrischer Verfahren und Instrumente bei Carl Zeiss in Oberkochen. Deutsche Geodätische Kommission (DGK), Reihe E Heft Nr. 30, 144 S., ISBN 978-3-7696-9673-8, München.

SANDAU, R. (Ed.) 2010. Digital Airborne Camera – Introduction and Technology. Original

German edition published by Wichmann Verlag, 2005, XII, 343 p., 215 illus., Hardcover, ISBN: 978-1-4020-8877-3, Springer.

SANDAU, R., ROESER, H.-P. & VALENZUELA, A. (Eds.) 2010. Small Satellite Missions for Earth Observation – New Developments and Trends. X, 450 p., 150 illus., Hardcover, ISBN: 978-3-642-03500-5, Springer.

## Zum Titelbild

### Quadcopter-Demonstration beim Workshop 3D-Stadtmodelle in Bonn

Das Titelbild zeigt einen Quadcopter der Fa. Rotorscope während eines Demonstrationsfluges beim Workshop 3D-Stadtmodelle im November in Bonn (siehe auch Bericht in diesem Heft). Die Kamera-Aufnahmen wurden direkt auf den Beamer geleitet, so dass sich das Publikum während der Aufnahmen auf der großen Leinwand selbst betrachten konnte.

Bei der Texturierung von Gebäudemodellen mit so genannten „echten Texturen“ bereiten Hindernisse wie Bäume, Autos, Elemente der Stadtmöbelung, etc. immer wieder Probleme, wenn die Bilder vom Boden aus aufgenommen werden. Bei engen Gassen kann zudem kein günstiger Aufnahmewinkel eingehalten werden, die Aufnahmen müssen steil nach oben erfolgen. Bei Luftbildschrägaufnahmen geschieht genau das Gegenteil, der Aufnahmewinkel ist sehr steil nach unten gerichtet, so dass Details oft nicht mehr erkennbar sind. Der optimale Aufnahmestandpunkt liegt daher oft „irgendwo“ in der Mitte! Um wenige Meter oberhalb des Bodens Aufnahmen machen zu können, wird seit einiger Zeit der Einsatz unbemannter Fluggeräte (unman-



Quadcopter während eines Demonstrationsfluges beim Workshop 3D-Stadtmodelle in Bonn (Foto: B.J. Horst)

ned aerial vehicles – UAV) getestet. Sie ermöglichen die gewünschten Fassadenaufnahmen in optimaler Höhe. In bebauten Stadtgebieten sind dabei einige Herausforderungen zu meistern, wie eine ungenaue GPS-Orientierung, böige Windverhältnisse, wechselnde Lichtverhältnisse und eine enge Bebauung. Zur Sicherheit des Flugkörpers kommen daher

oft zusätzliche Abstandhaltesysteme zum Einsatz.

BETTINA PETZOLD

Stadt Wuppertal, Ressort Vermessung, Katasteramt und Geodaten, Johannes-Rau-Platz 1, 42275 Wuppertal, bettina.petzold@stadt.wuppertal.de

EKKEHARD MATTHIAS

Landesbetrieb Geoinformation und Vermessung Hamburg, Sachsenkamp 4, 20097 Hamburg, ekkehard.matthias@gv.hamburg.de

## Korporative Mitglieder

### Firmen

- AEROWEST GmbH
- AICON 3D Systems GmbH
- aphos Leipzig AG
- Applanix Corporation
- Becker GeoInfo GmbH
- Bernhard Harzer Verlag GmbH
- Blom Deutschland GmbH
- Brockmann Consult
- bsf swissphoto
- Büro Immekus
- CGI Systems GmbH
- con terra GmbH
- Creaso GmbH
- DEFINIENS AG
- DELPHI IMM GmbH
- Deutsches Bergbau-Museum
- EFTAS Fernerkundung Technologietransfer GmbH
- ESG Elektroniksystem- und Logistik-GmbH
- ESRI Geoinformatik GmbH
- EUROPEAN SPACE IMAGING
- Eurosense GmbH
- fokus GmbH
- fpi Fuchs Ingenieure GmbH
- g.on experience gmbh
- GAF GmbH
- GeoCad GmbH
- GeoCart Herten GmbH
- GeoContent GmbH
- Geoinform. & Photogr. Engin. Dr. Kruck & Co. GbR
- geoplana Ingenieurgesellschaft mbH
- GEOSYSTEMS GmbH
- GGS – Büro für Geotechnik, Geoinformatik, Service
- Hansa Luftbild AG
- IGI – Ingenieur-Gesellschaft für Interfaces mbH
- ILV Ing.-büro für Luftbildausw. und Vermessung
- Imetric 3D GmbH
- INVERS – Industrievermessung & Systeme
- J. Linsinger ZT-GmbH
- Jena-Optronik GmbH
- KAZ Bildmess GmbH
- Leica Geosystems GmbH
- Luftbild Brandenburg GmbH Planer + Ingenieure
- Luftbilddatenbank-Würzburg
- Messbildstelle GmbH
- Microsoft Photogrammetry
- MILAN Geoservice GmbH
- PHOENICS GmbH
- PMS – Photo Mess Systeme AG
- RWE Power AG, Geobasisdaten/Photogrammetrie
- technet GmbH
- TERRA-Bildmessflug GmbH & Co.
- TerraVista Umweltdaten GmbH
- TRIGIS Vermessung + Geoinformatik GmbH
- Trimble Germany GmbH
- trimetric 3D Service GmbH, Garbsen
- Wichmann, VDE Verlag GmbH
- Z/I Imaging Ltd.

**Behörden**

Amt für Geoinformationswesen der Bundeswehr  
Bayerische Landesanstalt für Wald und Forstwirtschaft  
Bundesamt für Kartographie und Geodäsie  
Bundesmin. für Ernäh., Landw. u. Verbraucherschutz  
DB Netz AG  
Hess. LA für Bodenmanagement und Geoinformation  
Innenministerium NRW, Gruppe Vermessungswesen  
Inst. für Umwelt- und Zukunftsforschung  
LA für Geoinformation u. Landentw., Baden-Württem.  
LA für Vermessung und Geoinformation, Bayern  
LB Geoinformation und Vermessung, Hamburg  
LB f. Küstenschutz, Nationalpark u. Meeres schutz, SH  
Landesvermessung und Geobasisinformation Nieders.  
Märkischer Kreis, Vermessungs- und Katasteramt  
Regierungspräs. Tübingen, Abt. 8 Forstdirektion  
Regionalverband Ruhr  
Staatsbetrieb Sachsenforst Pirna  
Stadt Bocholt, Fachbereich 31  
Stadt Düsseldorf, Vermessungs- und Katasteramt  
Stadt Köln, Amt für Liegensch., Verm. und Kataster  
Stadt Wuppertal, Verm., Katasteramt und Geodaten  
Thüringer LA für Vermessung und Geoinformation

**Hochschulen**

BTU Cottbus, Lehrstuhl für Vermessungskunde  
FH Frankfurt a.M., FB 1, Studiengang Geoinformation  
FH Mainz, Inst. f. Raumbez. Inform.- und Messtechn.

FH Oldenburg, Inst. für Angew. Photogr. und Geoinf.  
HCU HafenCity Universität Hamburg, Geomatik  
HFT Stuttgart, Vermessung und Geoinformatik  
HS Bochum, FB Vermessung und Geoinformatik  
HS Karlsruhe, FB Geoinformationswesen  
HTW Dresden, FB Vermessungswesen/Kartographie  
Ruhr-Uni Bochum, Geographisches Institut  
RWTH Aachen, Geodätisches Institut  
TU Bergak. Freiberg, Inst. f. Markscheid. u. Geodäsie  
TU Bergak. Freiberg, Inst. für Geologie, RSG  
TU Berlin, Computer Vision & Remote Sensing  
TU Braunschweig, Inst. für Geodäsie und Photogr.  
TU Clausthal, Inst. für Geotechnik und Markscheidew.  
TU Darmstadt, Inst. für Photogrammetrie und Kartogr.  
TU Dresden, Inst. für Photogrammetrie und Fernerk.  
TU München, FG Photogrammetrie und Fernerk.  
TU Wien, Inst. für Photogrammetrie und Fernerk.  
Uni Bonn, Inst. für Photogrammetrie  
Uni Göttingen, Inst. für Waldinv. und Waldwachstum  
LUH Hannover, Inst. für Kartogr. und Geoinformatik  
LUH Hannover, Inst. für Photogrammetrie und GeoInf.  
Uni Heidelberg, IWR Interdis. Zentr. f. Wiss. Rechnen  
Uni Karlsruhe, Inst. für Photogrammetrie und Fernerk.  
Uni Kassel, FB Ökologische Agrarwissenschaften  
Uni Kiel, Geographisches Institut  
Uni Stuttgart, Inst. für Photogrammetrie  
Uni Würzburg, Geographisches Institut  
Uni zu Köln, Geographisches Institut

Gesellschafter-Geschäftsführer einer „kleinen“ GmbH (5 Mitarbeiter), der Inhaber und Verkäufer hält 52,5% der Anteile – keine Klauseln im Ges.-Vertrag, die einem Verkauf entgegenstehen könnten – möchte seine gesamten Anteile aus privaten Gründen veräußern.

Die Firma ist gut am Markt platziert, schuldenfrei und könnte Ihr Portfolio (NKF, Fachkataster, etc.) sicher gut ergänzen. Der geschützte Markennahme kann ebenfalls übernommen werden. Inhalte des Leistungsspektrums liegen hauptsächlich in der Photogrammetrie, der Geoinformatik (alle marktüblichen GI-Systeme im Einsatz), Digitalisierungen und der digitalen Kartographie sowie der konventionellen Vermessung. Diese Dienstleistungen beziehen sich hauptsächlich auf die Erstellung von Fachkatastern (Grün, Baum, Versiegelung, Strasse, Winterdienste, Friedhof, etc.) sowohl für die öffentliche Hand als auch für die freie Wirtschaft. Übergangsphase oder länger kann begleitet werden. Beste Kontakte vorhanden. Produktionsstandort ist ausschließlich Deutschland.

Seriöse Interessenten melden sich bitte unter **Chiffre RSH 2010031**  
an den Verlag: E. Schweizerbart'sche Verlagsbuchhandlung (Nägele u. Obermiller),  
Johannesstraße 3A, 70176 Stuttgart